NEW MATERIALS FOR MAGNETIC COOLING BELOW 1°K

by

Yingchieh Hsu

Submitted in partial fulfillment
of the requirements for the degree of
Doctor of Philosophy

Department of Physics,
Faculty of Pure and Applied Science,
The University of Ottawa,
Ottawa, Canada.

1968

ABSTRACT

A few natural minerals containing transition elements as impurities were investigated for their cooling properties by adiabatic demagnetization. Considering the lowest temperatures attained and the length of the warm-up times under a known constant heat leak, pink and white calcites, magnesite, brown apatite and fluorite were found promising for obtaining temperatures below $0.1^{\circ}K$. Beryl has a large heat capacity but a higher final temperature.

A series of carbonate minerals, pink and white calcites, magnesite and dolomite were chosen for further studies. The impurity responsible for the paramagnetism of these samples was identified to be Mn^{2+} by means of ESR analysis. The other important transition element impurity, Fe^{2+}, could not be detected even at helium temperature by ESR at X-band frequencies but is thought to cause the extra broadening observed for the Mn^{2+} lines. The ESR spin-Hamiltonian parameters obtained were found in agreement with the published values. The sign of D, the second order of the axial field splitting constant, was determined to be negative for Mn^{2+} in both magnesite and dolomite.

A simplified technique for calibrating carbon resistance thermometers below $1^{\circ}K$ was developed and is described. A method for eliminating galvanometer "double-kick" in a d.c. magnetic susceptibility bridge was developed and is described.

Entropy diagrams below $1^{o}K$ obtained by a series of adiabatic demagnetizations gave the following results: a value of about $0.05^{o}K$ was the characteristic temperature estimated for the pink and the white calcites and the magnesite, and of about $0.1^{o}K$ for the dolomite, in fair agreement with the values predictable from the ESR data for Mn^{2+}. As for the constant in the "high temperature" tail of the specific heat, cT^{2}/R, the agreement with the ESR was good below $0.4^{o}K$ with values of 6×10^{-3} $(^{o}K)^{2}$ for the pink and the white calcites and the magnesite, and 22×10^{-3} $(^{o}K)^{2}$ for the dolomite. Above $0.4^{o}K$, contributions to the specific heat from the interactions between Mn^{2+} and Fe^{2+}, from Fe^{2+} and from the lattice gave a much higher value to the constants.

The static magnetic susceptibility was measured from 4.2 to $0.06^{o}K$ and gave the following Curie constant values: 0.44×10^{-3} for the pink calcite, 0.27×10^{-3} for the magnesite and 0.05×10^{-3} for the dolomite in emu/cm^{3}, at high temperature, all the samples being polycrystalline. The pink calcite and the dolomite obey Curie's law down to $\sim 0.8^{o}K$ and the magnesite to $\sim 0.3^{o}K$. From what was observed the magnetic ordering temperatures for these samples must be much below $0.06^{o}K$.

Measurements of the thermal conductivity is reported for the polycrystalline pink calcite, magnesite and dolomite, and for the single crystals of white calcite and iceland spar between 4 and $0.2^{o}K$. The thermal conductivity of the iceland

spar, measured for comparison purpose only, is about 15 times better than that of CrK alum as reported elsewhere, whereas that of the single crystal of white calcite is about 2 times higher. The polycrystalline samples are poor from this point of view.

As cooling agents, these natural minerals are valuable and provide readily lower temperatures than hydrated manganous salts. Synthetic minerals of this class containing up to 0.4% of Mn^{2+}, if they could be obtained in single crystal form, should prove very useful in adiabatic demagnetization.

to my parents

ACKNOWLEDGMENTS

I would like to express my gratitude to the individuals and institutions that have aided me in completing this work.

Dr. G. Lamarche, my supervisor, for his guidance, stimulating and valuable discussions, help in preparing the manuscript, and aid in financial support from his N. R. C. research grants.

Dr. A. Manoogian for his suggestion of looking for samples in the naturally occuring minerals, help in ESR experiments, and valuable discussions.

Dr. J. Ancsin of N. R. C. for his helpful advice in preparing a carbon thermometer for the preliminary experiments, and a valuable discussion on the problem of galvanometer "double-kick".

Drs. J. R. Morton and L. Vannotti of N. R. C. for their assistance in taking some helium temperature ESR spectra using their spectrometer.

Mr. A. Danilov for making some helpful comments.

Mr. B. W. Chan for assistance in taking ESR spectra and in doing some calculations.

The Physics Department Workshop staff and especially Mr. R. Hart for making a good vacuum chamber, Mr. D. Kingswell for making a goniometer type of sample holder and Mr. N. Goodchild for obtaining two miniature bevel gears used in

the sample holder.

My wife for her help in preparing the manuscript, part of typing, and for her encouragement and patience.

Mr. R. Filion for help in tracing some graphs and in doing some calculations.

Department Of Geology, University Of Ottawa for allowing me to use the facilities in preparing samples and especially Dr. R. Kretz for his useful discussion on the stein test scheme in identifying samples.

The Geological Survey Of Canada For Providing Specimens From The National Mineral Collection for donating samples and especially Mr. R. Steacy for his assistance.

The Analytical Chemistry And Spectrochemistry Sections, Mineral Sciences Division, Mines Branch, Department Of Energy, Mines And Resources, Canada for the chemical analyses and especially Dr. A. H. Gillieson and Mr. D. Chavelte for their help.

Mr. T. T. Chen of Geology Department, Carleton University for doing X-ray analysis used to identify structures of the samples studied.

The Ontario Department of University Affairs for awarding me Ontario Research Fellowships.

STATEMENT OF ORIGINALITY

So far as the author is aware the following parts of the present work are claimed to be orginal.

1. Cooling below $1^{o}K$ by adiabatic demagnetization using white and pink calcites, magnesite, dolomite, brown and greenish brown apatites, fluorite and beryl.

2. Determination of S/R-T diagrams of pink and white calcites, magnesite and dolomite down to $0.06^{o}K$.

3. Measurements of static magnetic susceptibilities of polycrystalline pink calcite, magnesite and dolomite down to $0.06^{o}K$.

4. Measurements of thermal conductivities of polycrystalline pink calcite, magnesite and dolomite, and single crystals of white calcite and iceland spar between 4 and $0.2^{o}K$.

5. Determination of the sign of D, the second order of the axial field splitting constant of Mn^{2+} in single crystals of magnesite and dolomite.

6. Interpretation of broadening of Mn^{2+} linewidth in calcites.

7. ESR of Mn^{2+} in pink calcites.

8. Modified techniques in calibrating Speer carbon thermometers and in measuring thermal conductivities below $1^{o}K$.

9. Elimination of galvanometer "double-kick" in a d.c. magnetic susceptibility bridge.

TABLE OF CONTENTS

LIST OF FIGURES

LIST OF TABLES

CHAPTER I

INTRODUCTION

1. Introductory Remarks

This study is an extension of a search for suitable paramagnetic substances for magnetic cooling below $1^{o}K$ and thermometry in the low temperature range.

The method of adiabatic demagnetization (AD) to obtain temperatures below $1^{o}K$ was first suggested by Debye[1] and Giauque[2] independently around 1926. The first experiments with this method were carried out in 1933[3] and since then magnetic cooling has become an established cryogenic technique, both for studying the properties of the paramagnetic salts used as cooling agents and for carrying out experiments on other substances in this new temperature region. This method is based on the change in entropy of an assembly of magnetic dipoles during the adiabatic removal of an externally applied magnetic field.

The paramagnetic salts commonly used for this purpose, such as chromium potassium alum $\{CrK(SO_4)_2.12H_2O\}$, ferric ammonium alum $\{FeNH_4(SO_4)_2.12H_2O\}$ etc. have certain disadvantages, in that:

1) they have a tendency to loose part of their waters of crystallization with resultant modification of magnetic properties,

2) they have a low thermal conductivity at very low temperatures, and

3) they are not very suitable for machining and making a good thermal contact to cool other materials.

There might be some materials having good magnetic properties for cooling process and having none of the drawbacks mentioned above. The ideal substances should have the following properties:

1) a very high physical stability and enough hardness, so that a sample can be prepared in any desirable shape and can be polished into smooth surfaces to allow a good thermal contact, without shattering even if a reasonable pressure is applied,

2) very high chemical stabilities:

a) insoluble in water and in most other common solvents, and

b) either containing no water of crystallization so that reproducible results may be easily obtained, or retaining it well,

3) a high magnetic entropy, i.e. the resultant angular momentum quantum number should be large at the initial temperature before demagnetization so that the change of

1) they have a tendency to loose part of their waters of crystallization with resultant modification of magnetic properties,

2) they have a low thermal conductivity at very low temperatures, and

3) they are not very suitable for machining and making a good thermal contact to cool other materials.

There might be some materials having good magnetic properties for cooling process and having none of the drawbacks mentioned above. The ideal substances should have the following properties:

1) a very high physical stability and enough hardness, so that a sample can be prepared in any desirable shape and can be polished into smooth surfaces to allow a good thermal contact, without shattering even if a reasonable pressure is applied,

2) very high chemical stabilities:

a) insoluble in water and in most other common solvents, and

b) either containing no water of crystallization so that reproducible results may be easily obtained, or retaining it well,

3) a high magnetic entropy, i.e. the resultant angular momentum quantum number should be large at the initial temperature before demagnetization so that the change of

the entropy can be large,

4) a high Curie constant C because the change of entropy upon magnetization is proportional to the magnetic susceptibility χ (susceptibility is defined as a ratio of the magnetization M to the magnetic field H, i.e. $\chi \equiv M/H$). In this case, a strong cooling power can be obtained,

5) a high Debye temperature so that they will have a small lattice specific heat at low temperatures, and

6) a high heat capacity at very low temperatures, and following Curie's law down to the milli-degree range.

2. Historical

The search for non-hydrated paramagnetic materials was initiated by Daunt and co-workers about 15 years ago. So far only a few substances have been found suitable for cooling process down to around $0.1^{\circ}K$. These substances together with the lowest attained temperatures T_f and the high temperature specific heat constants CT^2/R are given in Table I-1*. Unfortunately, only incomplete data have been published.

Among these materials listed in Table I-1, synthetic ruby not only was considered as a possible thermometric substance[11] for He^3 refrigerator but has been used as such for

---

*Hereafter the Roman character represents a chapter number and the Arabic character represents a number of events.

TABLE I-1

PUBLISHED NON-HYDRATED MATERIALS
FOR MAGNETIC COOLING BELOW 1°K

Substance	T_f (°K)	CT^2/R $(°K)^2$	Ref.
Ferric acetonylacetonate $(C_5H_7O_2)_3Fe$	0.4	~520 $\times 10^{-3}$	4,85
Ammonium hexafluoro-chromite $(NH_4)_3CrF_6$	0.1	23.2×10^{-3}	5
Synthetic ruby (Al_2O_3:0.6%Cr^{3+})	0.3	~1 $\times 10^{-3}$	6,85
Th-2.3%Er	0.07	-	7
Cu-La:Er	0.03†	-	8
MgO:0.1%Mn^{2+}	0.04	6×10^{-3}	9,10

†T_f of this substance is unknown but the magnetic susceptibility was measured to 0.03°K.

quite a while. In general, the thermal conductivity of non-metallic substance is usually poorer than that of metallic materials. In order to improve this, paramagnetic metallic alloys were suggested and investigated [7,8]. However, with a metal there is an added difficulty that one might expect eddy-current heating when demagnetizing; this problem was in great part solved since in some cases the residual resistivity is high.

In our laboratory Walsh[9] suggested in his thesis

that cubic crystal of MgO or CaF_2 doped with about 0.2% of Mn^{2+} would give a good cooling and a reasonable specific heat in the temperature range of 0.01 to 0.5°K. He also pointed out that the thermal conductivity of these materials would be favorable. The cooling was verified and the specific heat was measured later by Ancsin[10].

3. The Present Work

As the materials used by Walsh and Ancsin are not readily available and are expensive, it was thought desirable to look for more readily available and cheap materials to continue this type of investigation. Naturally occurring minerals appeared to furnish a wide variety of host crystals containing numerous types of paramagnetic ions. Obviously there are some drawbacks here, as even the best specimens are not likely to be perfect single crystals and certainly will contain more impurities than is desirable. But it was believed that enough information could be gathered from these minerals to guide the composition of future possible artificial minerals if the cooling properties discovered warranted their preparations.

At first a large number of minerals were considered (see Chapter II) and it was found that some of them were capable of cooling down to a few hundredths of a degree. A list of some of the interesting ones is given in Table II-1.

Among those, a series of common carbonates, calcite, magnesite and dolomite, were chosen for further studies.

To learn as much as possible about the properties of these substances as cooling agents, the zero magnetic field energy levels of paramagnetic ions in crystals were investigated by means of electron spin resonance (ESR) (see Chapter IV). From this knowledge, one can then attempt to predict the low temperature behavior. To verify these predictions, the magnetic entropies and susceptibilities of these materials were investigated experimentally over as wide a range as possible (see Chapter VI). In order to assess their usefulness, their thermal conductivities were also measured (see Chapter VII).

For the duration of low temperature experimental work, secondary thermometers were employed to measure the temperatures. These thermometers were calibrated Speer carbon resistors. A rather simplified technique was developed to calibrate these resistors (see Chapter V).

CHAPTER II

A PRELIMINARY INVESTIGATION OF SOME MINERALS FOR MAGNETIC COOLING BELOW 1°K

1. Introduction

To assess the usefulness of some minerals for cooling below 1°K, adiabatic demagnetization experiments on the following samples were performed: *

polycrystals: grayish white magnesite, pink calcite, green fluorite, and grayish dolomite,

single crystals: white calcite, brown apatite, greenish brown apatite, pale blue beryl, brown MgO:Mn^{2+}, and yellow MgO:Mn^{2+} & Fe^{3+}.

The MgO samples were used just for the purpose of comparison (the brown MgO was the same sample used by Ancsin[10]). These minerals were chosen for the following reasons:

a) they were available and the cooling properties of some of these materials were roughly evaluated from the published ESR data.

---

*The source of the samples is given in Appendix A.

b) they have reasonable hardness.

c) they showed reasonably large intensities and widths of lines in ESR spectra.

The investigation includes performing adiabatic demagnetization, and measuring the lowest temperature attained and warm-up time. From these results, it was possible to single out the most promising minerals for further investigations.

A conventional cryostat for adiabatic demagnetization was used. The samples were shaped into blocks and one surface in each block was polished in order to make a good thermal contact with a sample holder. On this holder, a Speer carbon resistor thermometer was soldered for monitoring temperatures. The apparatus used for the adiabatic demagnetization was basically similar to the one described by Ancsin[10]. Here, only the details pertinent to the experimental chamber and sample mounting will be illustrated. Also, the experimental procedure will be described.

2. Experimental

1) Preparation of Samples

All the samples were shaped into blocks, about 1"x5/8"x3/8" in size, by using a 12" diamond wheel. The biggest surface in a block, which was used for making contact with copper specimen holder, was finally polished

with grit No. 600-RA carborundum (silicon carbide grain)* on a piece of frost glass. The polished surfaces for two kinds of apatite single crystal were parallel to their hexagonal axes. In the case of white calcite and MgO samples, their natural cleavage planes were used for thermal contacts.

2) Preparation of Thermometer and Specimen Holder

A Speer 1002, 1/2 W. resistor of 220 ohms nominal resistance was specially treated by grinding off most of the insulating layer and fitting it loosely in a thin wall copper tube of the same length. Some GE 9555 baking varnish was put homogeneously on the resistor and the assembly was baked at 140°C for about 2½ hours. The body of the resistor assembly was then soldered on a thin copper plate, 1½"x7/16". This copper plate was used as a sample holder.

3) Experimental Chamber and Mounting of Specimen

The experimental chamber showing the details of mounting of specimen is sketched in Fig. 11-1. Two blocks of samples were glued on a copper strip with Dow Corning silicone grease and tightened up with a piece of No. 40 nylon sewing threads. The assembly was then suspended from a stainless steel support as shown in Fig. 11-1. CrK alum

---

*A product of Canadian Carborundum Co. Ltd., Niagara Falls, Canada.

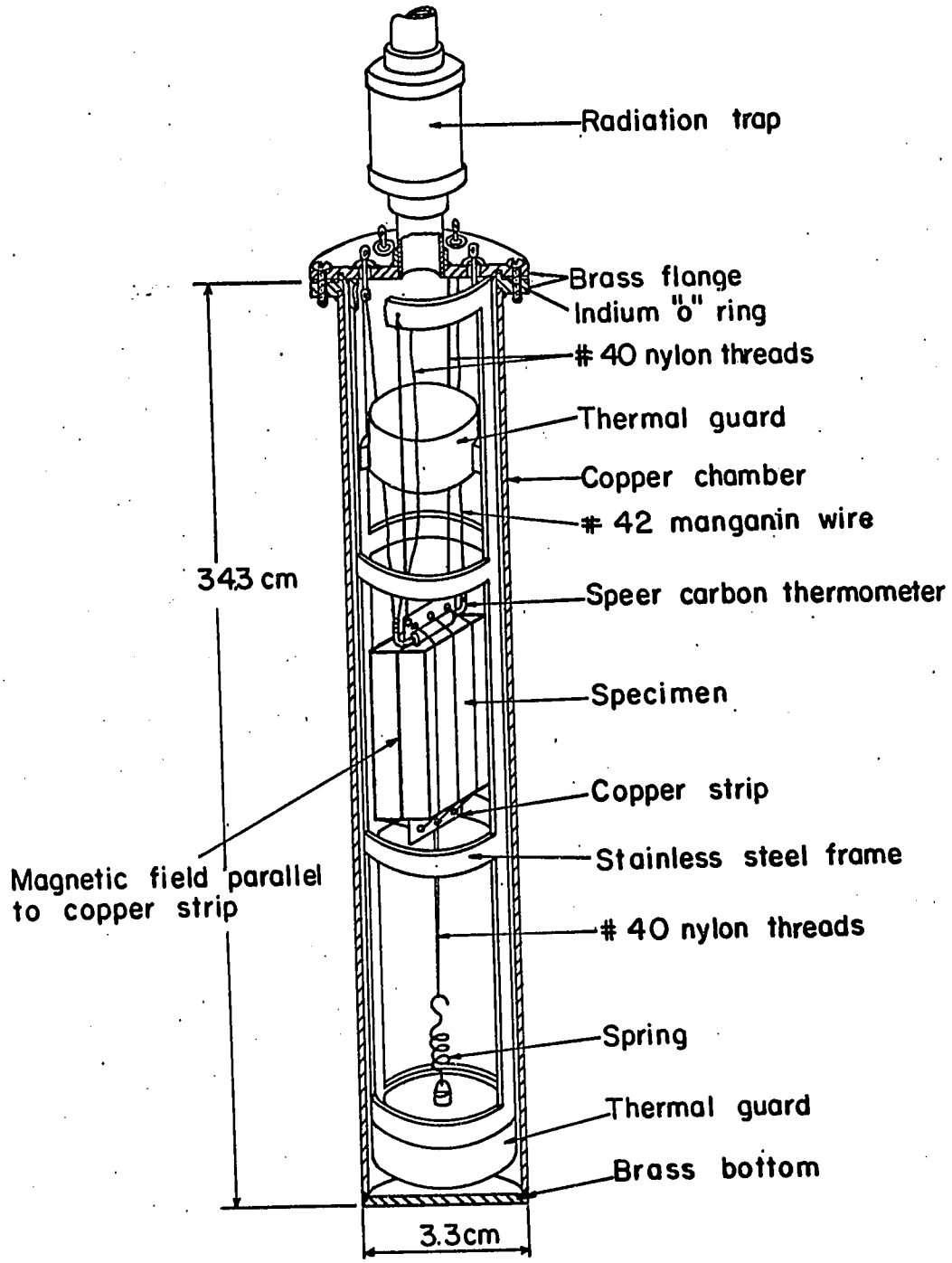

Fig. II-1 The AD experimental chamber and the sample mounting.

thermal guards were employed for reducing heat leak both through nylon threads and through residual exchange gas. These guards consisted of two pill boxes filled with di-iso-butyl phthalate $\{C_6H_4\text{-}1,2\text{-}[COOCH_2CH(CH_3)_2]_2\}$ mixed CrK alum powder and they were mounted on the stainless steel support above and below the specimen some distance away, as shown in Fig. II-1.

4) Experimental Procedure

The procedure followed for doing adiabatic demagnetization is described step by step as follows, where times and quantities indicated are typical and approximate:

a) 5 cm Hg of helium-4 exchange gas was introduced into the experimental chamber for heat conduction between sample and chamber wall.

b) 1.5 cm Hg of air was left in the liquid helium dewar jacket space for conduction. The helium dewar was opened to the atmosphere through a vent in the system.

c) The outer dewar vessel was filled with liquid nitrogen. After 1½ hours, the sample was cooled down to the liquid nitrogen temperature, $77^{\circ}K$.

d) The liquid helium dewar jacket space was evacuated for 10 minutes.

e) Liquid helium-4 was then transferred slowly and at the same time some helium gas in the chamber was pumped out. Only 0.5 mm Hg of exchange gas was left for

conduction at this stage. The transfer lasted three quarters of an hour.

f) The liquid helium bath was then pumped and the vapor pressure was set with the aid of a pressure regulator. The carbon thermometer was calibrated against the vapor pressure of helium-4 using the 1958 He^4 temperature scale. The lowest temperature of the helium bath attained by pumping was 1.3°K. Between 4.2 and 1.3°K, a dozen temperature-resistance calibration points were recorded. This required one hour.

g) The sample was then magnetized with a field of 18 kilo-gauss and 10 minutes was allowed to remove heat of magnetization.

h) The field was left on for 2 or 3 hours while the exchange gas was removed.

i) When the pressure in the experimental chamber reached a few 10^{-5} mm Hg, the sample was demagnetized to zero field. This demagnetization spread over a 15 min. period.

j) The temperature was measured at regular intervals from the time the magnet was rolled away until the specimen was warmed back to the bath temperature.

3. Result and Discussion

The adiabatic demagnetization results, together with some descriptions of the minerals, are summarized in

TABLE II-1

DESCRIPTION OF SOME MINERALS AND THEIR AD RESULTS

SAMPLES	COLOUR & HARDNESS	SYMMETRY	MASS-gms	IMPURITY PARAMAG.ION	LOWEST T. ATT'ND WARM-UP TIME
Magnesite ($MgCO_3$)	grayish white $3\frac{1}{2}$ - 5	$\bar{3}\frac{2}{m}$	16.8	0.10% Mn^{2+} ± 50%	0.03°K - 0.35°K 48 min.
Calcite ($CaCO_3$)	pink 3	$\bar{3}\frac{2}{m}$	20.3	0.13% Mn^{2+}	0.08°K - 0.35°K 103 min.
Calcite* ($CaCO_3$)	white 5	$\bar{3}\frac{2}{m}$	18.4	0.06% Mn^{2+}	0.29°K - 1.3°K 14 min.
Apatite* $\{Ca_5(F, Cl, OH)(PO_4)\}$	brown 5	$\frac{6}{m}$	20.4	0.18% Mn^{2+} small Fe^{3+}	0.05°K - 0.37°K 50 min.
Apatite* $\{Ca_5(F, Cl, OH)(PO_4)\}$	green & brown 5	$\frac{6}{m}$	21.8	0.12% Mn^{2+} small Fe^{3+}	0.1°K - 0.35°K 30 min.
Fluorite (CaF_2)	green 4	$\frac{4}{m}\bar{3}\frac{2}{m}$	30.2	0.05% Mn^{2+}	0.09°K - 0.7°K 42 min.
Beryl $\{Be_3Al_2(Si_6O_{18})\}$	pale blue $7\frac{1}{2}$ - 8	$6/m^2/m^2/m$	20.0	0.07% Mn^{2+} 0.04% Cu^{2+}	0.26°K - 0.38°K 47 min.
Dolomite ($CaMgCO_3$)	grayish white $3\frac{1}{2}$ - 4	$\bar{3}$	21.4	0.06% Mn^{2+}	0.09°K - 0.35°K 6 min.
MgO*	brown	Cub. Oct.	21.0	0.10% Mn^{2+}	0.04°K - 0.35°K†
MgO*	yellow	Cub. Oct.	5.3	0.02% Mn^{2+} 0.2% Fe^{3+}	0.52°K
$FeNH_4$ ALUM	brown	Cub. Oct.	1.3		0.08°K - 0.35°K 193 min.

x the chemical analysis is described in Appendix A.

* single crystal, magnetized as follows:
(a) Hexagonal axes of apatites were perpendicular to magnetic field.
(b) Cleavage planes of calcite and MgO were parallel to the magnetic field.

† without heat guards.

Table II-1. The heat leak to the samples in these experiments was estimated from a measurement with a small quantity of ferric ammonium alum to be of the order of 100 ergs/min using a well calibrated Speer carbon thermometer (see Chapter V). Part of the AD result of this ferric ammonium alum is also listed in Table II-1 for the purpose of comparison with other materials.

The results of spectrochemical semi-quantitative analysis of these minerals are given in Appendix A. According to these results, these minerals are chemically and magnetically impure. However, it appears that the ion responsible for the paramagnetism is primarily the Mn^{2+} in the most of these minerals. On the other hand, iron is the main other magnetic impurity in most minerals. Although the ESR signals of Fe^{+} and Fe^{2+} were not observed at X-Band even at helium temperature, the iron has some influence on Mn^{2+} as is discussed later in Chapters IV and VI.

The absolute temperatures were roughly estimated according to a R vs T curve of another Speer resistor with the same nominal value. This Speer resistor (R_3) was calibrated at a later time and it shall be stated in Chapter V.

It has been pointed out on a theoretical basis[9] and verified experimentally[10] that MgO:0.1%Mn^{2+} is a suitable cooling agent. From Table II-1 we see that magnesite, pink

calcite, apatite and fluorite are also of interest in this respect. Beryl did not reach the temperature below 0.1°K but its heat capacity was tremendously large. It took about 47 minutes to warm up by only 0.1°K in the same temperature range as that of other samples. What is responsible for the paramagnetism of beryl is still not known. However, we could make an assumption from its ESR spectra that the paramagnetism might arise from Cu^{2+} ions. Yellow MgO did not attain a very low temperature. In this regard we can not make a final comment because a large enough sample was not available.

As far as specific heat and low final temperature are concerned, pink calcite, magnesite and brown apatite are the most promising substances for magnetic cooling below 1°K or even below 0.1°K. They compare favorably with ferric ammonium alum.

For further study, a series of carbonates, pink and white calcites, magnesite and dolomite, were chosen. Brown apatite was finally rejected because it contains more than one type of magnetic ion and an evaluation of its thermodynamic properties at 1°K would be difficult and unreliable.

CHAPTER III

IDENTIFICATION OF THE SAMPLES

1. Introduction

Calcite, magnesite and dolomite are common minerals. Calcite is found in the form of both single and polycrystals. But magnesite and dolomite are found mostly in polycrystalline form. Single crystals of magnesite and dolomite are very rare. In order to have more information on these carbonates for future references, crystallography, physical and chemical properties, and distinction of them are summarized from several mineralogy books.[12-16]

Spectrochemical semi-quantitative analysis was made on transparent calcite (iceland spar), white calcite, pink granular calcite (pink calcite), grayish white magnesite (magnesite), grayish white granular dolomite (dolomite) and brown $MgO:Mn^{2+}$. The result of this analysis is given in Appendix A. This type of analysis was made for the purpose of detecting the impurities and their weight percentages. The accuracy is rather poor; that is, about 50%. Besides, the amount of the impurity is variable with different parts of material even if it is taken from the same

piece of the mineral. Spectrochemical quantitative analysis for determining the percentage ratio of Ca:Mg on these samples was also made. This is just to identify these samples, since these carbonates have the same calcite structure and they look quite similar. The results are also given in Appendix A.

To complete and verify the identification, both X-rays and stain techniques were utilized.

2. Description of Samples

1) Calcite ($CaCO_3$)

A. Crystallography, Structure and Habit

Hexagonal. $\bar{3}2/m$. The crystal habit is extremely varied and some 300 different forms have been reported. There are three important habits: (1) short to long prisms, (2) rhombohedra, and (3) scalenohedra. Repeated parallel twinning is common.

Calcite structure; see Fig. III-1. This structure resembles that of halite with planar CO_3 groups taking the place of Cl ions. The CO_3 groups are arranged in parallel position normal to the three-fold axis [0001], which corresponds to a cube diagonal or [111] direction of cleavage rhombohedron.

Crystals and crystal aggregates, coarse granular to impalpable, stalactitic, nodular, encrusting, and as a component of shells.

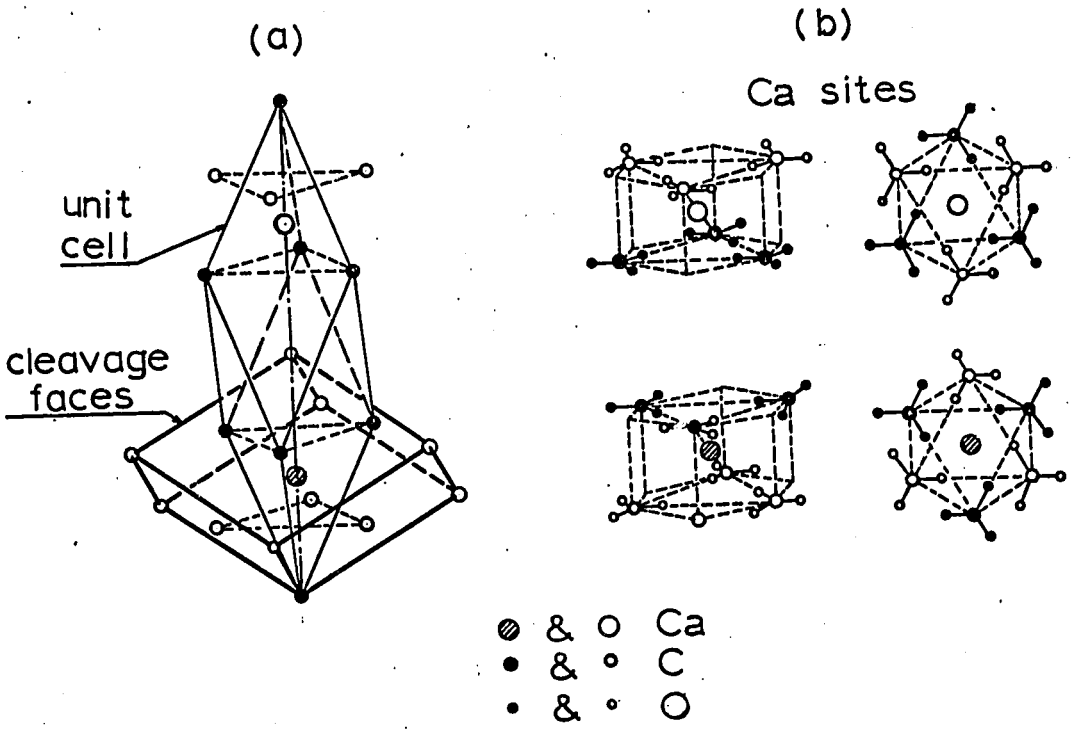

Fig. III-1 The true unit cell and the cleavage unit cell of calcite.

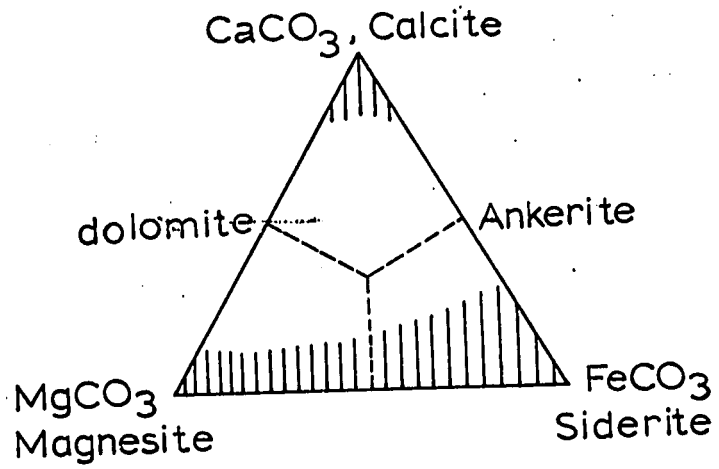

Fig. III-2. Compositional variation diagram of some carbonates.

B. Physical Properties

Perfect rhombohedral cleavage ($10\bar{1}1$). Parting on ($01\bar{1}2$) and sometimes on (0001). Conchoidal fracture. Brittle.

Hardness 3 [approximately 2.7 on (0001) and 3.5 on ($10\bar{1}1$)]. Density 2.71.

Colorless and transparent or white when purer; colors varying widely with substitution: yellow, brown, pink, blue, lavender, greenish (due to chlorite), gray, reddish brown (due to hematite). White to grayish streaks.

Sometimes fluorescent or phosphorescent under electromagnetic radiation (X-rays, ultraviolet, sunlight). Often thermoluminescent. Infusible.

C. Distinctive Properties and Tests

Cleavage, crystals, hardness. Soluble in cold dilute HCl with effervescence. Tests for calcium.

D. Confused with: Dolomite, Aragonite

E. Chemistry

Calcite is the thermodynamically stable form of calcium carbonate at all pressures. Calcite may be pure $CaCO_3$, but often contains other metals in substitution for Ca, see Fig. III-2. Minor substitution of Mg occurs in calcite, but tendency to form the ordered phase dolomite is very great in keeping with the large difference (26.5%) in ionic radii between Ca and Mg. Fe^{2+} substitute for Ca

to a somewhat greater extent (21.7% difference in ionic radii) and the ordered phase ankerite is less common. Mn^{2+} substitutes extensively for Ca (14.3% difference in radii), and the disordered phase shows extensive solubility. Zn and Co have been found as substitution for Ca to a minor extent.

2) Magnesite ($MgCO_3$)

A. Crystallograph, Structure and Habit

Hexagonal. $\bar{3}2/m$. Crystals rare.

Isostructural with calcite, see Fig. III-1.

Usually massive, also granular, compact, earthy, fibrous.

B. Physical Properties

Perfect rhombohedral cleavage ($10\bar{1}1$). Conchoidal fracture. Brittle.

Hardness 4. Density 3.00.

Vitreous to earthy luster. Translucent to transparent. Colorless, white grayish white, yellowish to brown. Streak white.

Sometimes shows green or blue fluorescence or phosphorescence in ultraviolet light. Triboluminescent. Infusible.

C. Distinctive Properties and Tests

Chalky or porcelain-like appearance. Effervesces in hot hydrochloric acid.

D. Chemistry

In $MgCO_3$, Fe^{2+} may substitute for Mg and a complete series extends to siderite ($FeCO_3$) Mn and Ca substitute for Mg up to about Mn:(Mg, etc.)=1:9.3 and Ca:(Mg, etc.)=1:8.9,Co substitute for Mg with Co:(Mg,Fe)=1:15. Ni is sometimes present in very small amounts. The compact massive types of magnesite often contain SiO_2 (opal) or magnesium silicates as impurities.

3) Dolomite $\{CaMg(CO_3)_2\}$

A. Crystallography, Structure and Habit

Hexagonal. $\bar{3}$. Crystals usually rhombohedra or prisms, often with curved faces. Repeated parallel twinning.

Isostructure with calcite, see Fig. III-1. The Ca and Mg atoms of dolomite alternate in Ca sites of Calcite.

Massive, granular, and as crystals.

B. Physical Properties

Perfect rhombohedral cleavage $(10\bar{1}1)$. Parting parallel to $(02\bar{2}1)$. Subconchoidal fracture. Brittle.

Hardness 3.5-4. Density 2.85.

Luster vitreous to pearly. Colorless and transparent or white in pure dolomite but sometimes gray or greenish, becoming yellowish brown or brown with increasing content of Fe^{2+}; also pink, rose or flesh-red, especially in varieties containing much Mn^{2+}. Translucent. Streak white.

May fluoresce under ultraviolet light. May be thermoluminescent. Infusible.

C. Distinctive Properties and Tests

Cleavage. Effervesces in hot dilute HCl.

D. Confused with: Calcite.

E. Chemistry

Fe^{2+} and to less extent Mn^{2+}, Co^{2+}, Pb, and Zn substitute for Mg. Fe^{2+} and Mn^{2+} apparently also can substitute in part for Ca. Ca also can substitute for Mg (these cations are structurally non-equivalent in dolomite) up to a maximum of about Ca:Mg=1:5 in the Mg positions, and Mg similarly can substitute for Ca up to a maximum of about Mg:Ca=1:20 in the Ca positions. In the case of Fe^{2+}, a series extends from the end-member $CaMg(CO_3)_2$ up to $Ca(Fe^{2+},Mg)(CO_3)_2$ with Mg:(Fe,Mn)=1:2.6 at least. Fe^{2+} and Mn^{2+} apparently may substitute for both Ca and Mg, but, according to literature[17] Mg is more often substituted by Fe^{2+}, Mn^{2+} etc. than Ca.

4) The crystal constants of the three carbonates are shown in Table III-1.[16]

3. Identification of the Carbonate Samples

1) Warnes' Staining Scheme

Carbonate minerals are notoriously difficult or even impossible to differentiate by the inspection or

TABLE III-1

THE CRYSTAL CONSTANTS OF CALCITE, MAGNESITE AND DOLOMITE

Crystal	Unit Cell		Cleavage Rhombohedron		Hexagonal Pseudo-Cell		Symmetry
	a_o	α	a'_o	α'	a''_o	c''_o	
Calcite	6.361A	46°06'	6.412A	101°55'	4.981A	17.020A	$\bar{3}$ 2/m
Magnesite	5.61	48°12'	6.064	102°58'	4.581	14.840	$\bar{3}$ 2/m
Dolomite	6.050	46°54'	6.19	102°47'	4.815	16.119	$\bar{3}$

simple methods described in Section 2 unless X-ray method is employed. But we do not use X-ray method to determine a bulky material, because it takes a long time to do it, since the amount of sample used in this method is very limited. Fortunately, there is a straightforward, positive and fairly new staining method, which is called Warnes' staining scheme[18], available for the identification of the major anhydrous carbonate in fragments and section of rocks. This staining method was employed to identify the samples used for both ESR and AD experiments. After the staining test was made on these fragments, a small specimen was taken from each fragment for X-ray test. This test was made for the purpose of checking if their structures were changed for containing various impurities.

2) X-ray Method

The samples of calcite, magnesite and dolomite

were structurally confirmed by means of X-ray powder method. The results were identified with the standard pictures of calcite, magnesite and dolomite.

4. Conclusions

We have given here a summary of the main properties and habits of the class of minerals we are interested in. The samples used in this work were properly identified using the information given in this Chapter. It is realized that there is a wide variety of these carbonates occurring naturally and it is only a few of them which are of interest for cooling. In fact if such cooling agents are to be of practical value either a source of reasonably homogeneous mineral will have to be found or else batches of such minerals would have to be synthesized according to the composition we shall specify as a result of our study.

CHAPTER IV

ELECTRON SPIN RESONANCE STUDY OF Mn^{2+} IN NATURAL CRYSTALS OF CALCITE, MAGNESITE AND DOLOMITE

1. Introduction

ESR spectroscopy has proved to be a powerful technique for studying a system containing unpaired electron spins. The ESR technique and its theories have been developed by a large number of authors. This technique was employed in our case to identify the origin of the paramagnetic properties of the samples and to evaluate the spin-Hamiltonian parameters of Mn^{2+} in these carbonate samples.

The ESR of Mn^{2+} in these carbonates has been investigated by several authors (references given later). However, in this study we are interested in knowing if the values of the spin-Hamiltonian parameters have changed in the case of different samples from different areas and of samples containing more concentrated Mn^{2+} ions and other impurity ions. It is also of interest to study what the influence the Fe^{2+} ions may have on the Mn^{2+} ions in this environment.

From the measured spin-Hamiltonian parameters, it is possible to evaluate the "high temperature" specific heat constants which are due to crystalline field and hyperfine splittings. The "high temperature" specific heat constants will then be useful in evaluating other interactions which will be discussed later in Chapter VI. From the knowledge of zero magnetic field energy levels, an attempt was made to predict the characteristic temperatures.

2. Literature Survey

1) Mn^{2+} in Calcite

ESR absorption of approximately 0.06 wt. % in single crystals of calcite has been studied by several groups. Hurd, Sack and Hershberger (HSH)[19] were the first to investigate Mn^{2+} in calcite using an axial trigonal symmetry for the crystalline field. Their results were recalculated by Zaripov, Murtazin and Stepanov (ZMS)[20], carrying out their calculations to the second order in fine structure interaction and to the fourth order in the hyperfine structure, by means of perturbation theory. HSH reported that the fine structure lines of Mn^{2+} in calcite were split into doublets in some orientations. According to their observations, the doublet separations depended upon the orientation of the applied magnetic field with respect to the crystal directions, the splitting being

most pronounced at about 60^{o} with respect to the trigonal c axis, and decreasing to zero at 0^{o} and 90^{o}. Furthermore, it was noted that the strong fine-structure lines split into wider doublets than the weak ones. This effect was explained independently by Kikuchi[21] and McConnell[22]. They pointed out that the additional splittings could be accounted for in terms of cubic field effects some ten times weaker than those due to the axial field. The unit cell in calcite lattice contains two Ca^{2+} ions, but the cubic field axes at the two Ca^{2+} ions will not coincide[23]. Thus, for a general orientation of the calcite crystal relative to the external magnetic field, there would be two types of Mn^{2+} ions (which presumably replaced a small number of Ca^{2+} ions far removed from another), and two sets of energy levels corresponding to the two possible orientations of the cubic field axes relative to the external field. This explanation was further confirmed,[24,25] by adding a cubic field term to the Hamiltonian.

As regards to the weak lines in the main ESR spectra of Mn^{2+} in calcite, their explanation was made by Matarrese[26]. They were identified as belonging to the forbidden hyperfine transitions. The detailed study of these transitions to the third order was made by Ursu et al[27]. Besides the forbidden hyperfine transitions, there were also forbidden electronic transitions corresponding

to $\Delta M = \pm 2$ found at $4.2^{\circ}K$[26], where M is the electronic magnetic quantum number. The spectrum, consisting of 24 lines, of these transitions was centered at half the field of the main spectrum. It has not been found theoretically possible to fit the observed line positions satisfactorily.

From the differences in intensities of the lines of the ESR spectrum at $4.2^{\circ}K$, it was determined that the second order axial field splitting constant D is negative. From a knowledge of the relative signs of D, A, and a - F, where A is the hyperfine splitting constant, a the cubic field splitting constant and F the fourth order of the axial field splitting constant, A is negative and a - F is positive. An interesting feature of the low-temperature spectrum was that the lines in the middle of the spectrum appear to saturate less readily than the lines at either end. In addition, the g-factor becomes anisotropic ($g_{\parallel} \approx 2.004$, $g_{\perp} \approx 1.997$) and the numerical values of A and D are slightly greater.

The ESR spin-Hamiltonian parameters for Mn^{2+} in calcite are [20,19,26] $D = -81 \pm 0.2$, $F = 7.704 \pm 0.002$, $A = -93.95 \pm 0.05$, $B = -94.40 \pm 0.05$, $g_{\parallel} = 2.0018 \pm 0.0006$, $g_{\perp} = 2.0013 \pm 0.0006$, where the values of D, F, A and B are in units of gauss.

2) Mn^{2+} in Magnesite and Dolomite

The ESR hyperfine structure spectra of Mn^{2+} in

magnesite and dolomite have been studied both experimentally and theoretically.[28] The values of the parameters of the spin-Hamiltonian describing the position of lines in the spectrum were determined. The spin-Hamiltonian for Mn^{2+} in both magnesite and dolomite was the same as that for Mn^{2+} in calcite described by Ursus et al[27]. These studies were made on single crystals and cleavage cuts of magnesite and dolomite. These crystals contained only a small amount of Mn^{2+} impurity (0.n - 0.00n%). The other impurities in the crystals were unknown.

The values of ESR spin-Hamiltonian parameters of Mn^{2+} in magnesite and dolomite are

Crystal	g	D	a - F	A	B
Magnesite	2.001	±85.5	±12.1	±92.0	±93
Dolomite	2.003	±153.2	±10.4	±93.4	±94.3

where all the values except g are in units of gauss and they have an accuracy of ± 3 gauss.

3. Spin-Hamiltonian

The crystal structures of the three carbonates, calcite, magnesite and dolomite, have a trigonal symmetry. They have already been described in Chapter III. The immediate surrounding of the Mn^{2+} ions which replaced Mg or Ca isomorphously in these substances is an octahedron formed by six oxygen atoms. This octahedron is deformed

along the three-fold axis which coincides with the crystalline c-axis or [111] direction of the crystal. In order to describe the resonance spectra, it is necessary to choose a spin-Hamiltonian which reflects the symmetry of the crystalline field in which the ion is replaced. Since Mn^{2+} ion is in $3d^5$, $^6S_{5/2}$ ground state, the more appropriate spin-Hamiltonian as given by several groups[25,27-30] is

$$\mathcal{H} = g_{||}\beta H_z S_z + g_{\perp}\beta(H_x S_x + H_y S_y) + \frac{a}{6}[S_\xi^4 + S_\eta^4 + S_\zeta^4 - \frac{1}{5}S(S+1)(3S^2+3S-1)] + D[S_z^2 - \frac{1}{3}S(S+1)] + \frac{F}{180}[35S_z^4 - 30S(S+1)S_z^2 + 25S_z^2 - 6S(S+1) + 3S^2(S+1)^2] + AS_zI_z + B(S_xI_x + S_yI_y), \quad \text{(IV.1)}$$

where β is the Bohr magneton,

$g_{||}$ and $g_{\perp}$ are the electronic spectroscopic splitting factors for $\vec{H} \,//\, z$ and $\vec{H} \perp z$ respectively,

D and F are the second and the fourth order of the axial field splitting constants, respectively,

a is the cubic field splitting constant,

A and B are the hyperfine coupling constants parallel and perpendicular to the symmetry z axis respectively,

x,y,z is an orthogonal crystal co-ordinate system,

ξ,η,ζ is an orthogonal, magnetic complex co-ordinate system, the axes of the cubic field interaction,

the z-axis is along the deformation direction which coincides with the [111] direction in the system of co-ordinates ξ, η, ζ, and

S and I are the electronic and nuclear spin operators respectively.

If we do ESR at X-band frequency (about 9.5 GH_z) so that the value of H will be of the order of 3000 gauss, then the first two Zeeman interaction terms denoting the interaction between the external field and the magnetic moment of the electronic spin are the dominant terms in the Hamiltonian. Accordingly, the energy levels can be evaluated by treating the remaining terms as perturbations. The next three terms arise from the crystalline field interactions. The remaining terms are due to the hyperfine structure of the ESR spectrum.

In accordance with the perturbation calculation, the resulting strongly allowed transitions ($\Delta M = \pm 1$, $\Delta m = 0$) can be described in the following forms[28-30]. In these expressions, first order in a and F, and first and second orders in A, B and F are included:

when $\vec{H} // z$, then

$$H_{M,m;M-1,m} = H_o - D(2M-1) - {}^{*}f(M) - Am - \frac{B^2}{2H_o}\left[\frac{35}{4} - m^2 + m(2M-1)\right], \quad \text{(IV.2)}$$

*The sign is wrong in the reference (28).

where $f(5/2) = -f(-3/2) = -\frac{4}{3}(a - F)$

$f(3/2) = -f(-\frac{1}{2}) = \frac{5}{3}(a - F), \quad f(\frac{1}{2}) = 0$;

when $\vec{H} \perp z$, then

$$H_{M,m;M-1,m} = H_o + D(M - \tfrac{1}{2}) + f(M) - \frac{D^2}{8H_o}[2S(S + 1) - 6M(M - 1) - 3] - Bm - \frac{A^2 + B^2}{4H_o}[\frac{35}{4} - m^2 + m(2M - 1)], \qquad (IV.3)$$

where $f(5/2) = -f(-3/2) = \frac{1}{2}(a - F)$,

$f(3/2) = -f(-\frac{1}{2}) = -\frac{5}{8}(a - F), \quad f(\frac{1}{2}) \doteq 0.$

In these expressions, we assumed that the g-factors of Mn^{2+} are isotropic, i.e. $g_{||} = g_{\perp}$, and that $H_o = \frac{h\nu}{g\beta}$ is the resonance condition in the absence of fine and hyperfine structure, where ν is the applied microwave frequency. All the parameters in Eqs. (IV.2) and (IV.3) are expressed in units of gauss. The g-values can be obtained by evaluating H_o from these expressions.

4. The Energy Level Diagram

If we neglect the cubic field interaction, the hyperfine structure and the higher order terms of the axial field splitting, then the energy levels of Mn^{2+} in these carbonates, when $H // z$, can be expressed as[20]

$$E_M = HM + D[M^2 - \tfrac{1}{3}S(S + 1)]. \qquad (IV.4)$$

The energy levels for all the electronic magnetic quantum number M were calculated as function of H and the

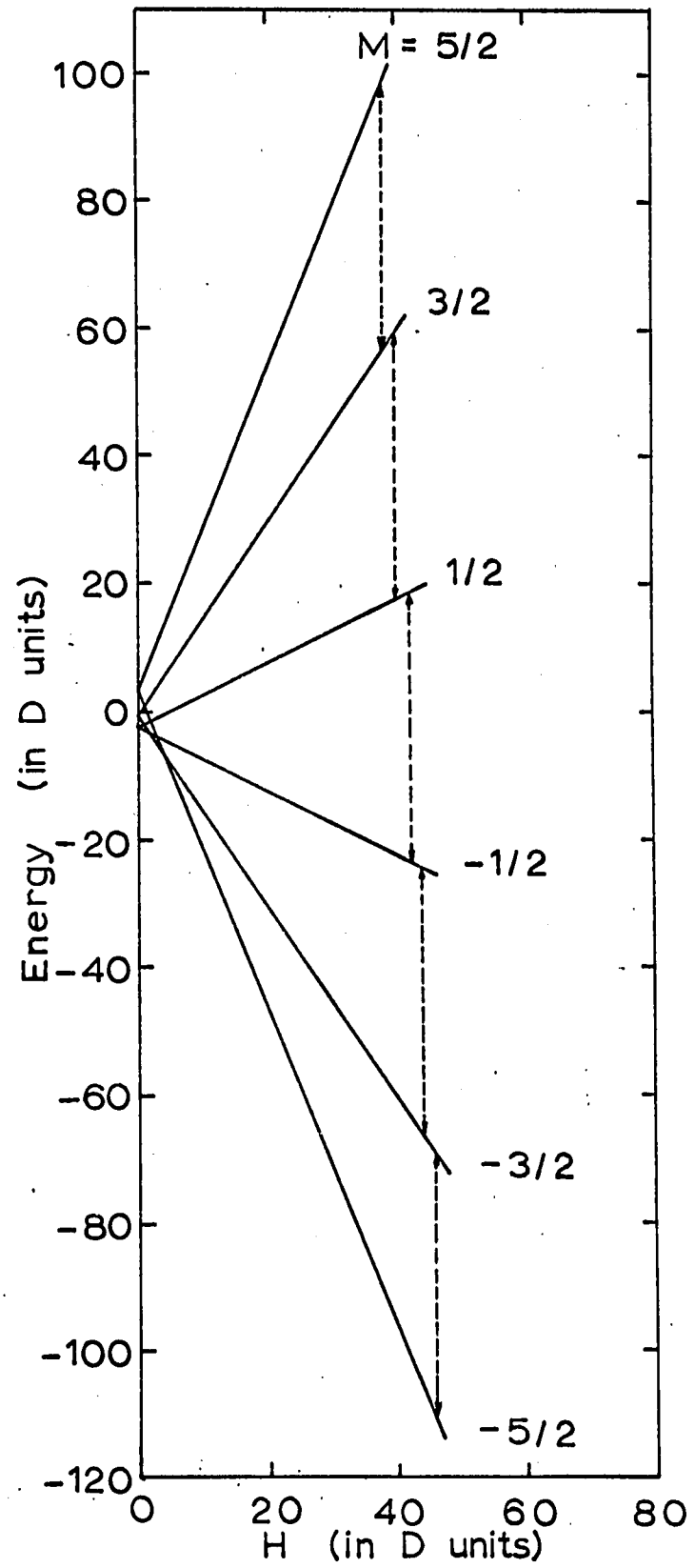

Fig. IV-1. Energy level diagram of Mn^{2+} in calcite, $\overline{H}//z$

result is plotted in Fig. IV-1. In this figure, the vertical transitions indicate the centers of gravity of the hyperfine lines at X-band frequency ($\sim$9.5 GH_z) for calcite. In this plot, D was assumed positive. The sign of D can be obtained from the helium temperature spectrum. Suppose the line intensity of $-3/2 \leftrightarrow -5/2$ transition is smaller than that of $5/2 \leftrightarrow 3/2$ transition at very low temperatures, then D would be negative. In this case, the whole plot will be inverted.

5. Experimental

1) ESR Spectrometer

The ESR experiments were performed with a Hilger & Watts X-band (Microspin Type W903, Instr. No. 178Q) ESR spectrometer with 100-KH_z magnetic-field modulation. A transmission type cylindrical cavity operating in the TE_{011} mode was used for the room temperature experiments. A rectangular cavity operating in the TE_{012} mode, used in conjunction with a metal cryostat, was employed for the helium temperature experiments.

A special goniometer type of sample holder was designed* and made to fit the cylindrical cavity. The sample was placed on the nylon bevel gear and it could be

---

*The design of the goniometer was based on the one designed by Dr. J. R. Morton of National Research Council of Canada. The working drawing is given in Appendix B.

rotated in any orientation with respect to the external magnetic field. The details of the goniometer is given in Appendix B. The accuracy of both dials is about ±2 degrees.

2) Experimental Method

a) At Room Temperature

The crystals were prepared by cleaving them along the natural rhombohedral cleavage planes of calcites, magnesites and dolomites to a size approximately 3 mm on a side, so that the [111] direction (or c-axis) of each crystal could be aligned with an accuracy of ±30 minutes. The crystal was then mounted on a goniometer, using Dow Corning silicone grease, in such a way that its c-axis was parallel to the external magnetic field. The crystal symmetry of these three carbonates demands that one of the magnetic axes should be along [111] direction, and the remaining two in the (111) plane. With the aid of goniometer, an axis was found along which the widest spread of the thirty ESR lines was obtained. We defined this axis as the magnetic z-axis which coincided with the crystal c-axis. This could be confirmed by obtaining the same spectra taken every 10° for a total rotation of the crystal of 180° when the z-axis was oriented perpendicularly to the external magnetic field[19], by means of goniometer and

rotated in any orientation with respect to the external magnetic field. The details of the goniometer is given in Appendix B. The accuracy of both dials is about ±2 degrees.

2) Experimental Method

a) At Room Temperature

The crystals were prepared by cleaving them along the natural rhombohedral cleavage planes of calcites, magnesites and dolomites to a size approximately 3 mm on a side, so that the [111] direction (or c-axis) of each crystal could be aligned with an accuracy of ±30 minutes. The crystal was then mounted on a goniometer, using Dow Corning silicone grease, in such a way that its c-axis was parallel to the external magnetic field. The crystal symmetry of these three carbonates demands that one of the magnetic axes should be along [111] direction, and the remaining two in the (111) plane. With the aid of goniometer, an axis was found along which the widest spread of the thirty ESR lines was obtained. We defined this axis as the magnetic z-axis which coincided with the crystal c-axis. This could be confirmed by obtaining the same spectra taken every 10° for a total rotation of the crystal of 180° when the z-axis was oriented perpendicularly to the external magnetic field[19], by means of goniometer and

stereographic technique*.

The microwave frequency was read directly from the wave meter with the aid of the calibration curve made by Hilger & Watts company. The magnetic field was indicated on the chart recordings at intervals of 5.8716 gauss by a Hilger & Watts proton resonance magnetometer which was calibrated by a Hewlet Packard frequency counter (Model 5245L). The error in locating spectral lines was ±0.5 to 1 gauss depending on the linewidth. The proton probe of the magnetometer and the sample could not be put at the same position, therefore DPPH (g = 2.0036) was employed for the field calibration. The correction to the magnetic field was -1.0 gauss.

b) At Liquid Helium Temperature

In order to determine the sign of D-value on these samples, each sample was mounted on the bottom plate of a rectangular cavity, using Dow Corning silicone grease, in such a way that each c-axis was parallel to the external magnetic field.

---

*The stereographic paper used was printed in Great Britain by John Dickens & Co. Ltd., Northampton.

6. Results and Discussion

At room temperature, all the spectra of these carbonate crystals showed 5 groups of 6 major lines. There were also some small minor lines, with much less intensity, that appeared in the spectra. By studying the angular variation of the spectra in these crystals, we were able to ascertain that the observed spectra were due to Mn^{2+} ions and these minor lines arose from forbidden hyperfine transitions.

By observing the spectra from many crystals of calcite, there was no evidence of 6 groups of 5 lines as reported by Kikuchi and Matarrese [25].

In addition to Mn^{2+} resonance lines, all the samples failed to show ESR signals which would arise from other impurities. As we can see from Appendix A, in general the largest amount of impurities in these carbonate samples consist of iron. Most irons could be assumed as Fe^{2+}, since a) the information given in Chapter III indicates that Fe^{2+} substitutes for Ca or Mg to a large extent; b) Fe^{3+} in these carbonates should be observable at both room and liquid helium temperatures[31]; c) the formation of Fe^{1+} from Fe^{2+} is unusual[32]. However, the resonance due to Fe^{2+} was not observed at X-band frequency suggesting that the initial splitting is much larger than a value of the order of 3000 gauss or that the spin-lattice

relaxation time is very short. According to various reports, both large splitting and short spin-lattice relaxation time are present for ferrous ions in various substances. Therefore, in general, the resonance of Fe^{2+} in a crystal can be observed only at K-band ($\sim$ 24 GHz) or higher frequency and at low temperatures.[33]

Now, let us examine if there is any sign of an interaction between Mn^{2+} and Fe^{2+} ions. The only evidence that can be seen from an ESR absorption line is in the width and the intensity of the Mn^{2+} lines. Consider the Mn^{2+} spectra in both the white and the pink calcites. They are suitable for comparison because they contain about the same amount of Mn^{2+} but different amount of Fe^{2+}. The Mn^{2+} spectra in both the white and the pink calcite crystals at room temperature are given in Fig. IV-2 and Fig. IV-3, respectively. The lines in the white calcite are well resolved with narrow linewidth, while in the pink calcite resolution is poor and lines are wide. We believe that Fe^{2+} ions contribute in broadening the lines as we shall see below.

It was noted[29,34,35] that Mn^{2+} resonance absorption lines are sharp (width of < 10 gauss) and exhibited fine and hyperfine structures in the spectra if the manganous ions are diluted by non-magnetic ions. This is due to the reduction of dipole-dipole interaction between the manganous

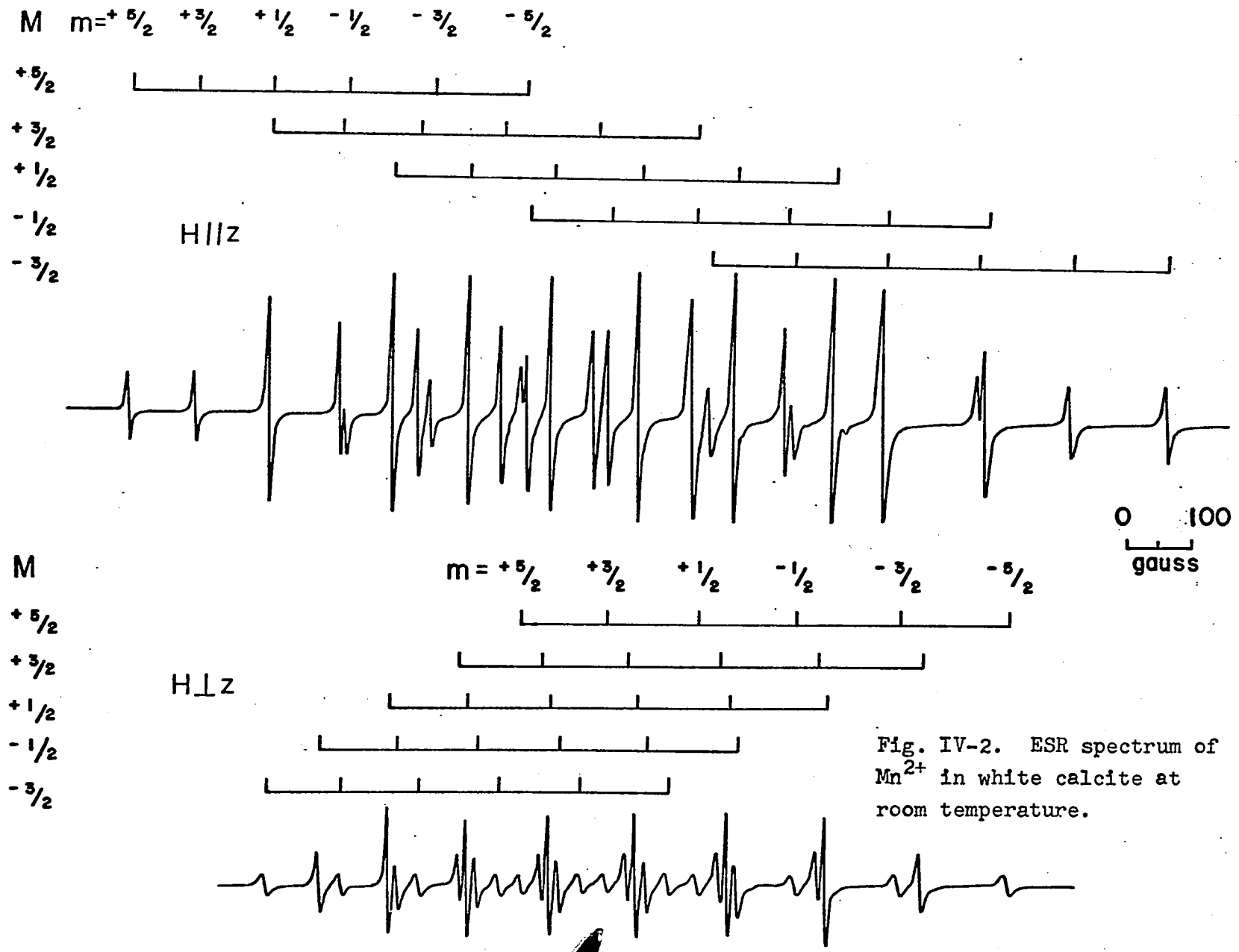

Fig. IV-2. ESR spectrum of Mn^{2+} in white calcite at room temperature.

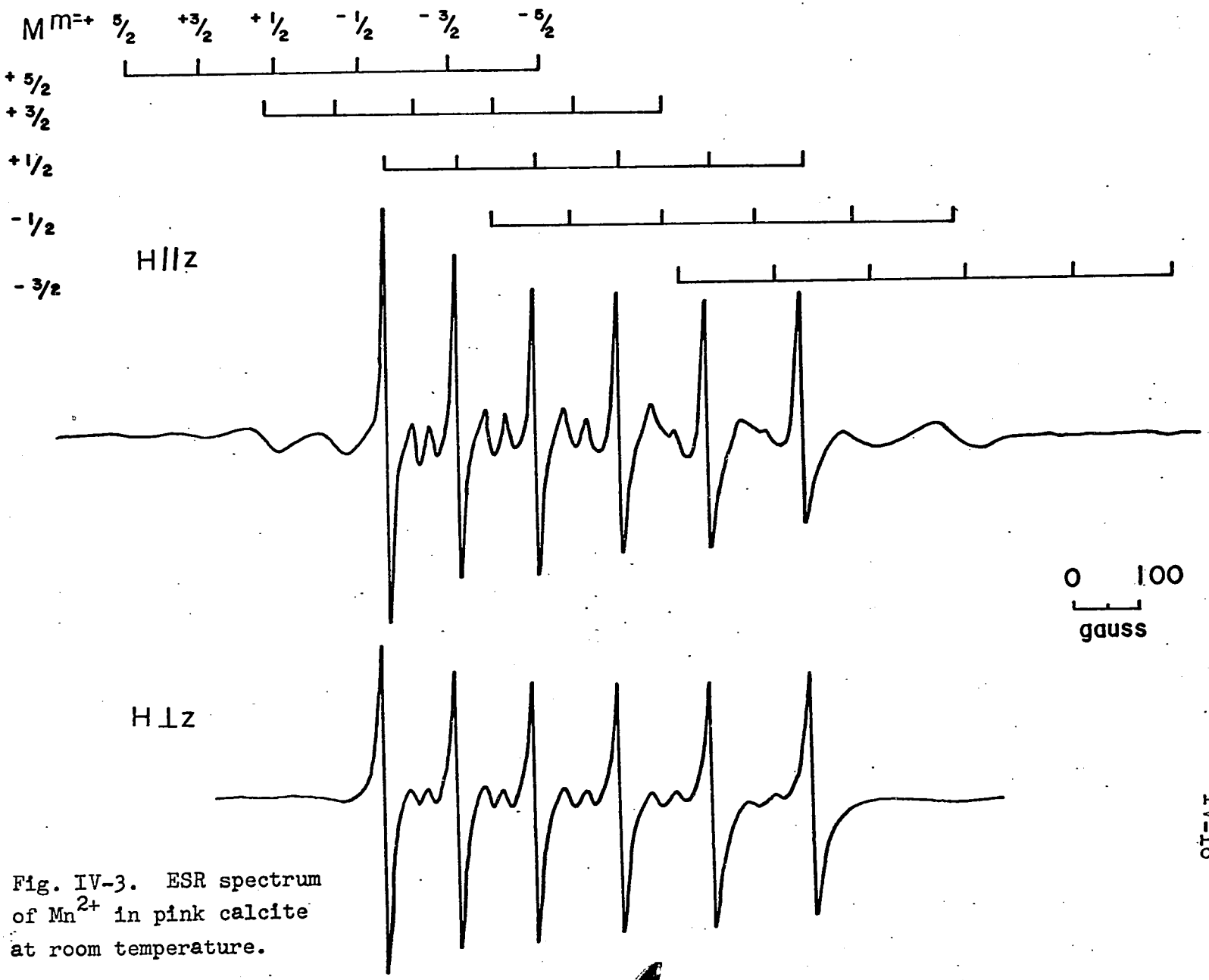

Fig. IV-3. ESR spectrum of Mn^{2+} in pink calcite at room temperature.

ions. In this case, its spin-lattice relaxation time can be expected to be short because it is in S-state. However, in the case of Mn^{2+} ions[35] which were added as an impurity to Tutton salts $\{R(NH_4)_2(SO_4)_2 \cdot 6H_2O\}$ of some sorts of magnetic ions R, such as Fe^{2+}, Ni^{2+} or Co^{2+}, or added to some cupric salts, such as $CuSO_4 \cdot 5H_2O$ or $Cu(NH_4)_2(SO_4)_2 \cdot 6H_2O$, then the observed fine and hyperfine structures of Mn^{2+} were almost the same as those just mentioned in the beginning of this paragraph but their linewidths were somewhat larger. Especially in the case of nickel Tutton salts, the linewidth of Mn^{2+} was found to be around 50 gauss and its intensity was fairly small. This is the case which is similar to the case of Mn^{2+} in pink calcite, as shown in Fig. IV-3. By analogy we are tempted to deduce that the dipole-dipole interaction between Mn^{2+} and Fe^{2+} could be responsible for the broadening of lines.

Because of this broadening, the analysis of Mn^{2+} spectra in this pink calcite was difficult to do. On the other hand, the doublets of the fine structure lines of Mn^{2+} in some orientations, that was reported by HSH[19], were not distinguishable. For reference, the Mn^{2+} linewidths in these carbonate samples are listed in Table IV-1. The spectra for magnesite and dolomite were the same as those

TABLE IV-1

LINEWIDTHS OF Mn^{2+} IN THE CARBONATES

FOR H // z AT ROOM TEMPERATURE

Transition Group	Pink Calcite	White Calcite	Magnesite	Dolomite
5/2 ⟷ 3/2	44*	6.5	14	12
3/2 ⟷ 1/2	32	4.1	9	7
1/2 ⟷ -1/2	6	3	3	3
-1/2 ⟷ -3/2	32	4.7	8	7
-3/2 ⟷ -5/2	43	6.6	14	12

*All the values are in units of gauss.

reported by Vinokurov et al[28], therefore it will not be given here. From Table IV-1 we can see that the Mn^{2+} linewidths in the white calcite are the narrowest, corresponding to the smallest iron concentration.

At liquid helium temperature, all the Mn^{2+} spectra in all the samples exhibited two to three times larger linewidth than those which were observed at room temperature. As an example let us consider the case of pink calcite, its spectrum at helium temperature is shown in Fig. IV-4 in which the linewidth in each line is larger than that shown in Fig. IV-3. What Marshall et al[31] reported that the Mn^{2+} linewidths in calcite became narrower at lower temperatures was not observed in any of our samples.

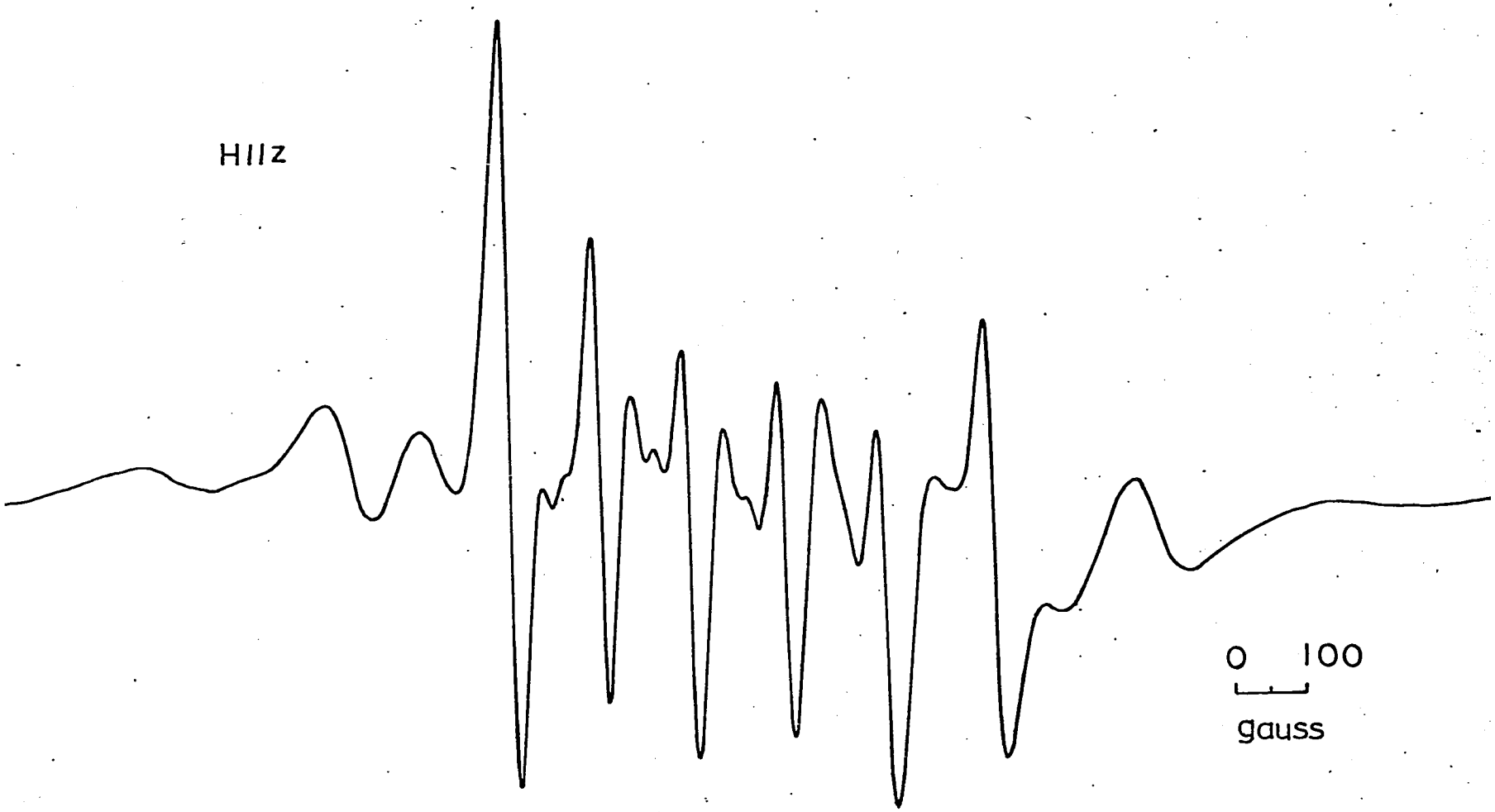

Fig. IV-4. ESR spectrum of Mn^{2+} in pink calcite at liquid helium temperature.

The spin-Hamiltonian parameters for the carbonates were calculated by using Eqs. (IV.2) and (IV.3) simultaneously and are given in Table IV-2. Within the experimental error, most values of the parameters in these carbonates are in agreement with the published ones.

TABLE IV-2

SPIN-HAMILTONIAN PARAMETERS OF Mn^{2+} IN THE CARBONATES

Parameter	Pink Calcite	White Calcite	Magnesite	Dolomite
$g_{\parallel}$	2.0023±0.001	2.0007±0.0005	2.0016±0.001	2.0010±0.001
$g_{\perp}$	2.0042±0.001	2.0006±0.0005	2.0016±0.001	2.0009±0.001
D	-79.5±1	-80.0±0.5	-86.3±1	-148.4±1
a - F	7.8±1	8.0±0.5	13.6±1	10.9±1
A	-94.6±1	-94.2±0.5	-91.5±1	-90.7±1
B	-89.2±1	-93.9±0.5	-96.1±1	-92.4±1

All the values of the parameters except g's are in units of gauss.

In the case of axial and cubic symmetries, Bleaney and Trenam[30] have given formulas for the energy levels due to crystalline field splittings; they are

$$E_{1,2} = \frac{1}{3}D - \frac{1}{2}(a - F) \pm \frac{1}{6}\sqrt{(18D + a - F)^2 + 80a^2}, \quad \text{(IV.5)}$$

$$E_3 = -\frac{2}{3}D + (a - F). \quad \text{(IV.6)}$$

In our case, since the value of a in each sample is very

The spin-Hamiltonian parameters for the carbonates were calculated by using Eqs. (IV.2) and (IV.3) simultaneously and are given in Table IV-2. Within the experimental error, most values of the parameters in these carbonates are in agreement with the published ones.

TABLE IV-2

SPIN-HAMILTONIAN PARAMETERS OF Mn^{2+} IN THE CARBONATES

Parameter	Pink Calcite	White Calcite	Magnesite	Dolomite
$g_{\parallel}$	2.0023±0.001	2.0007±0.0005	2.0016±0.001	2.0010±0.001
$g_{\perp}$	2.0042±0.001	2.0006±0.0005	2.0016±0.001	2.0009±0.001
D	-79.5±1	-80.0±0.5	-86.3±1	-148.4±1
a - F	7.8±1	8.0±0.5	13.6±1	10.9±1
A	-94.6±1	-94.2±0.5	-91.5±1	-90.7±1
B	-89.2±1	-93.9±0.5	-96.1±1	-92.4±1

All the values of the parameters except g's are in units of gauss.

In the case of axial and cubic symmetries, Bleaney and Trenam[30] have given formulas for the energy levels due to crystalline field splittings; they are

$$E_{1,2} = \frac{1}{3}D - \frac{1}{2}(a - F) \pm \frac{1}{6}\sqrt{(18D + a - F)^2 + 80a^2}, \quad \text{(IV.5)}$$

$$E_3 = -\frac{2}{3}D + (a - F). \quad \text{(IV.6)}$$

In our case, since the value of a in each sample is very

small the last term in the square root can be neglected. Eq. (IV.5) can then be written as

$$E_1 = \frac{10}{3}D - \frac{1}{3}(a - F) \text{ and} \qquad \text{(IV.9)}$$

$$E_2 = -\frac{8}{3}D - \frac{2}{3}(a - F). \qquad \text{(IV.10)}$$

Since D is negative for all the samples in the present work, the zero magnetic field energy levels without hyperfine structure consist of 3 Kramers doublets which can be plotted as shown in Fig. IV-5. At temperatures low compared with $\{6D + \frac{1}{3}(a - F)\}/k$, where k is Boltzman constant, this leads to a contribution to the high temperature magnetic specific heat in the zero magnetic field:[30,36]

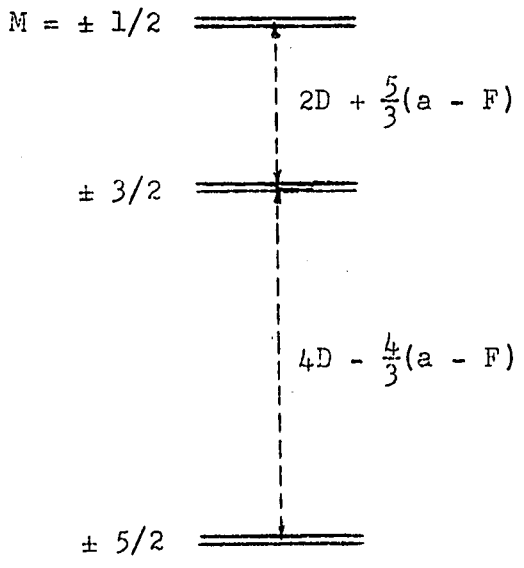

Fig. IV-5. Crystalline field splitting at H = 0.

$$CT^2/R = \frac{1}{45}D^2S(S+1)(2S-1)(2S+3) + \frac{14}{27}F(F-2a) + 2a^2 + \frac{1}{9}(A^2 + 2B^2)S(S+1)I(I+1), \qquad \text{(IV.11)}$$

where the parameters D, F, a, A and B are expressed in ^{o}K. The calculated values of CT^2/R are given in Table IV-3, where the contributions from a and F are neglected.

TABLE IV-3

CALCULATED VALUES OF CT^2/R & Θ

Sample	CT^2/R	Θ
Pink Calcite	$4.8\times10^{-3}\ (^{o}K)^2$	$0.044^{o}K$
White Calcite	4.8	0.044
Magnesite	4.7	0.049
Dolomite	6.3	0.082

From the energy levels we can judge that if the hyperfine structure is large compared to the fine structure, then the former would influence the lowest temperature which could be attained by AD. On the other hand, if the fine structure is large or comparable with the hyperfine structure, then the former is important. In our case, both fine and hyperfine structures are comparable, thus we might assume that the magnetic specific anomaly peak would be around $\{4D - \frac{4}{3}(a - F)\}/k$ which we call the characteristic temperature Θ. The values of Θ for these materials have

been calculated and they are also given in Table IV-3.

According to various reports, e.g. the paper by Bleaney and Ingram[29], the values of spin-Hamiltonian parameters change with temperatures. This is consistent with the report by Kimura and Uryû[37] which states that the symmetry of the surrounding anions which produce the crystalline field may not be the same at different temperatures. In addition to the above, there are always some magnetic interactions that take place. All these factors influence the characteristic temperatures as predicted in Table IV-3.

CHAPTER V

CALIBRATION OF SPEER CARBON RESISTORS AS THERMOMETERS FOR USE BELOW 1°K

1. Introduction

To study the properties of cooling agents below 1°K, the great difficulty is the establishment of a reliable scale of temperature. In this temperature range all the conventional methods fail. The well known and reliable method is the calorimetric method which is commonly used. In this method, the Kelvin definition of thermodynamic temperature, $T = dQ/dS$, is employed from which absolute temperatures may be obtained directly if the change in entropy corresponding to the introduction of a known amount of heat can be determined. Usually the magnetic temperature T^* is chosen as a thermometric parameter, and one may write $T = (dQ/dT^*)/(dS/dT^*)$ or $T = C^*/(dS/dT^*)$ where $C^* = dQ/dT^*$, the specific heat of the paramagnetic sample. The magnetic temperature T^* is defined as a Curie scale of temperature by extrapolating Curie's law from the calibrated helium temperatures into

the demagnetization range. However, this method is long and difficult.

A much easier method, and one which does give comparable if not higher accuracy if done carefully, consists in using a secondary thermometer calibrated with cerium magnesuim nitrate (CMN) below $1^{o}K$. Many authors have used this approach. Resistance thermometers are the most convenient secondary thermometers to use below $1^{o}K$. In this work Speer carbon resistors were chosen, since they are good for thermometry down to about one hundredth of a degree Kelvin. Carbon resistance thermometers provide many practical advantages such as compactness, insensitiveness to magnetic fields, small heat capacity, short thermal relaxation time, and stability under the heating which is sometimes necessary during assembly of apparatus. However, the calibration process is elaborate. Here we describe a simplified technique which we have developed and adopted to calibrate resistors.

The magnetic susceptibility χ of CMN is known to follow Curie's law, i.e. is inversely proportional to the absolute temperature T ($\chi \propto 1/T$), from $4.2^{o}K$ down to $0.006^{o}K$.[38] Thus, to measure temperatures below $1^{o}K$, the susceptibility of CMN is measured from $4.2^{o}K$ down to $1.3^{o}K$ while the salt is kept in equilibrium with a pumped helium-4 bath. The temperature is then obtained by

measuring the vapor pressure of liquid and using available pressure versus temperature tables[39]. From these data a graph of χ vs $1/T$ gives a straight line which can safely be extrapolated below $1^{\circ}K$.

In our case, we used the simplest experimental arrangement which consisted in placing CMN in the center of one of the secondaries of a mutual inductor. The latter consisted of a primary with two secondary coils wound in opposite directions, so that when the salt was not there the emfs induced in both coils on reversing the current in the primary just cancelled each other. With the salt in place a net emf proportional to the susceptibility was measured. In our arrangement a d.c. bridge was set up and the deflection read on a ballistic galvanometer.

The main difficulty in this case usually arises when a metallic specimen chamber is used as opposed to a glass or plastic one. Then the galvanometer experiences a so-called "double-kick". This arises because on reversing the primary a short transient current exists in the secondary circuit that deflects the galvanometer violently on one side then on the other before it starts to move normally. Under such conditions, no reliable readings can be taken. We describe in this Chapter an arrangement of the coil in the mutual inductor and how it should be located on a metal chamber so that the "double-kick" could

be cancelled and a secondary thermometer be reliably and easily calibrated. To study the "double-kick" further, several experiments were carried out, and the details and results are given in Appendix C.

2. Experimental

Fig. V-1 shows the assembly of the copper experimental chamber, the mutual inductor windings and the mounting for the CMN and a Speer carbon thermometer and the salt for cooling by adiabatic demagnetization. Four pieces of single crystals of CMN were shaped, oriented and combined into a 1" sphere. They were so wrapped by a single length of copper "coil foil" (see below) as to insure that both surfaces of each piece of crystal were in thermal contact with the foil (see the side view in Fig. V-1 for details). The areas of thermal contact were coated with Apiezon N grease before assembly to insure a better thermal contact. The whole sphere was then tightened by a piece of No. 40 nylon sewing thread C and it was held tightly in place by a brass spring. Bakelite clamps D, F were used to strengthen the foil support held in the chamber by the same size of nylon threads.

The coil foil B^{41} was constructed by winding tightly a single layer of No. 40 B & S enamelled copper wire on a large drum side by side and a layer of 0.001" Mylar was between them. The resultant coil was coated with a very

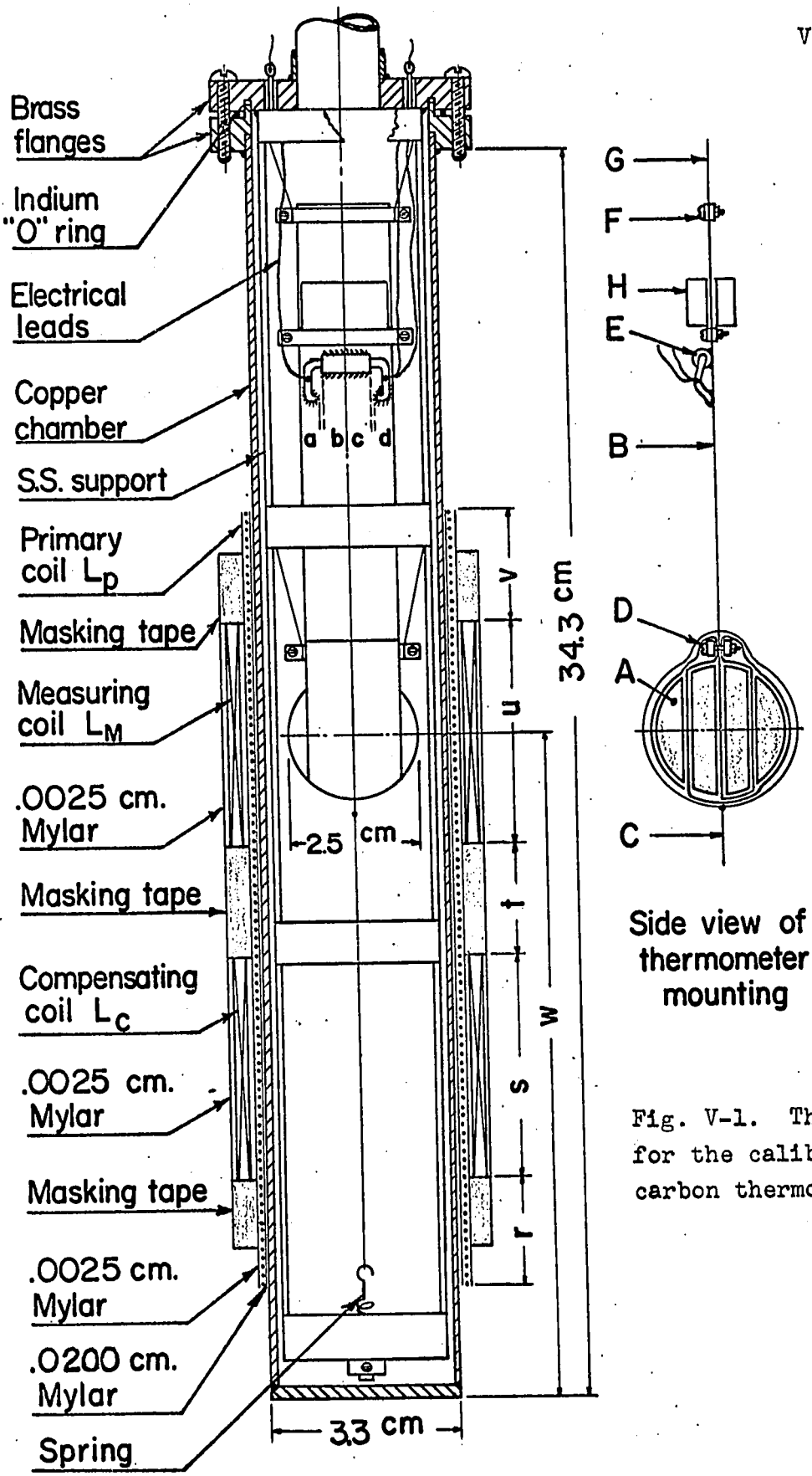

Side view of thermometer mounting

Fig. V-1. The apparatus for the calibration of a carbon thermometer.

thin layer of GE 9555 baking varnish and then baked in an oven at 140°C for about 2½ hours. The varnished coil was cut parallel to the axis of the drum and the Mylar was removed without any difficulty. Thus a foil consisting of parallel and electrically insulated wires held together with varnish was obtained and has been called "coil foil". This forms an ideal support for specimen in AD as it has a good thermal conductance and shows very little eddy-current effects when placed in changing magnetic field. Our method of preparing such foils is somewhat different from that described by Anderson et al[41].

The carbon thermometer E was prepared by grinding off most of the outer insulating layer of a Speer carbon resistor and fitting it loosely in a thin wall copper tube of the same length. (Two carbon thermometers R_2 and R_3 were prepared, for measuring thermal conductivity, by fitting in a special thin wall copper tubes with a fin on each tube; see Fig. VII-1.) Same varnish was put on the resistor and the assembly was also baked at 140°C for 2½ hours. The body and leads of the resistor assembly were then indium soldered onto stripped areas of the coil foil. These areas were stripped to the bare copper after the foil was made. Before the foil was made, these areas were covered with masking tape before applying baking varnish. The indium was applied beforehand on the copper tube and

on the stripped spots of the foil to minimize heating on final soldering. The stripped spots were laterally spaced to avoid short circuits (see the distance left between "a" and "b" and "c" and "d" in Fig. V-1).

Four Speer 1002, ½W., resistors of 220 ohms nominal value were calibrated. The resistance was measured at low temperatures with a three-lead d.c. Wheatstone bridge to an accuracy of 0.1% and with a power dissipation of 10^{-10} W. In the early stages, while calibrating the first thermometer R_1, the mutual inductor was wound as described by Type I in Table V-1, where N_P, N_M and N_C are the number of turns of coils L_P, L_M and L_C respectively, and the other symbols are defined in Fig. V-1. A very large galvanometer

TABLE V-1

THE SPECIFICATION OF TWO TYPES OF MUTUAL INDUCTORS

Type	r	s	t	u	v	w	N_P	N_M	N_M
I	3.5	3.8	4.1	1.3	2.5	11.4	750	8,000	8,600
II	2.0	4.0	2.0	4.0	2.0	22.8	750	13,000	14,000

The dimension of the coils are in units of cm.

"double-kick" was experienced at $4^{\circ}K$. In fact, no measurements could be done with the CMN thermometer above $3^{\circ}K$. For the calibration of other resistors, the winding

scheme given as Type II in Table V-1 was adopted. This time no double-kick was observed on the galvanometer deflections. The calibration of the CMN was done with ease. It was reproducible and no correction was necessary as long as the solder on the resistor was at least 3½" above the center of the measuring coil L_M. In both types of winding, a single layer of Nb wire was used for the primary.

As the experimental time for the whole run was only about 5½ hours with a heat leak of about 100 ergs per minute, and no heater was used to warm up the parts below 1^oK, two different arrangements were devised to cover the whole tmperature range below 1^oK. In the first, the foil was suspended so as to orient the trigonal axis of the CMN in the direction of the magnetizing field, and hence the CMN did not get cooled on demagnetization. The cooling in this case was obtained by attaching some ferric ammonium alum ($FeNH_4$ alum) (about 3~5 grams) on the top of the foil, as shown in Fig. V-1 at K. The alum had no influence on the susceptibility readings. Allowing 1200 seconds for thermal equilibrium to set in[41], the lowest significant temperature readings were then about 0.06^oK. In the second arrangement, the trigonal axis of the CMN sphere was turned by 90^o and the alum was removed. With this arrangement, lower initial temperatures were obtained.

But because of the fast warming up, the calibration was obtained only for temperatures above 0.1°K. The overlapping regions from the runs with different arrangements were always in agreement with one another. The results of the calibrations for all four resistors were plotted in Fig. V-2.

In order to check the reliability of these calibrated thermometers, a small sphere of ferric ammonium alum (1.3 gm) was mounted in the place where CMN once was and it was demagnetized. The susceptibility of the alum measured down to 0.08°K and its magnetic temperatures were calculated. This result was in agreement with the published values within 1%. At the same time the result was used for calculating heat leak of the system according to a published method[42]. The heat leak of this system was about 100 ergs/min.

3. Discussion and Conclusions

No reproducible calibrations were obtained below 0.06°K. This was probably due to lack of adequate thermal equilibrium between the resistor and the CMN, due to the relatively large heat input when measuring their resistances, and due to heat leak because of the surrounding. Besides the irreproducibility below 0.06°K, the resistors also indicated a loss of sensitivity. Harrison[43] has shown that the power dissipated in such thermometer has a large

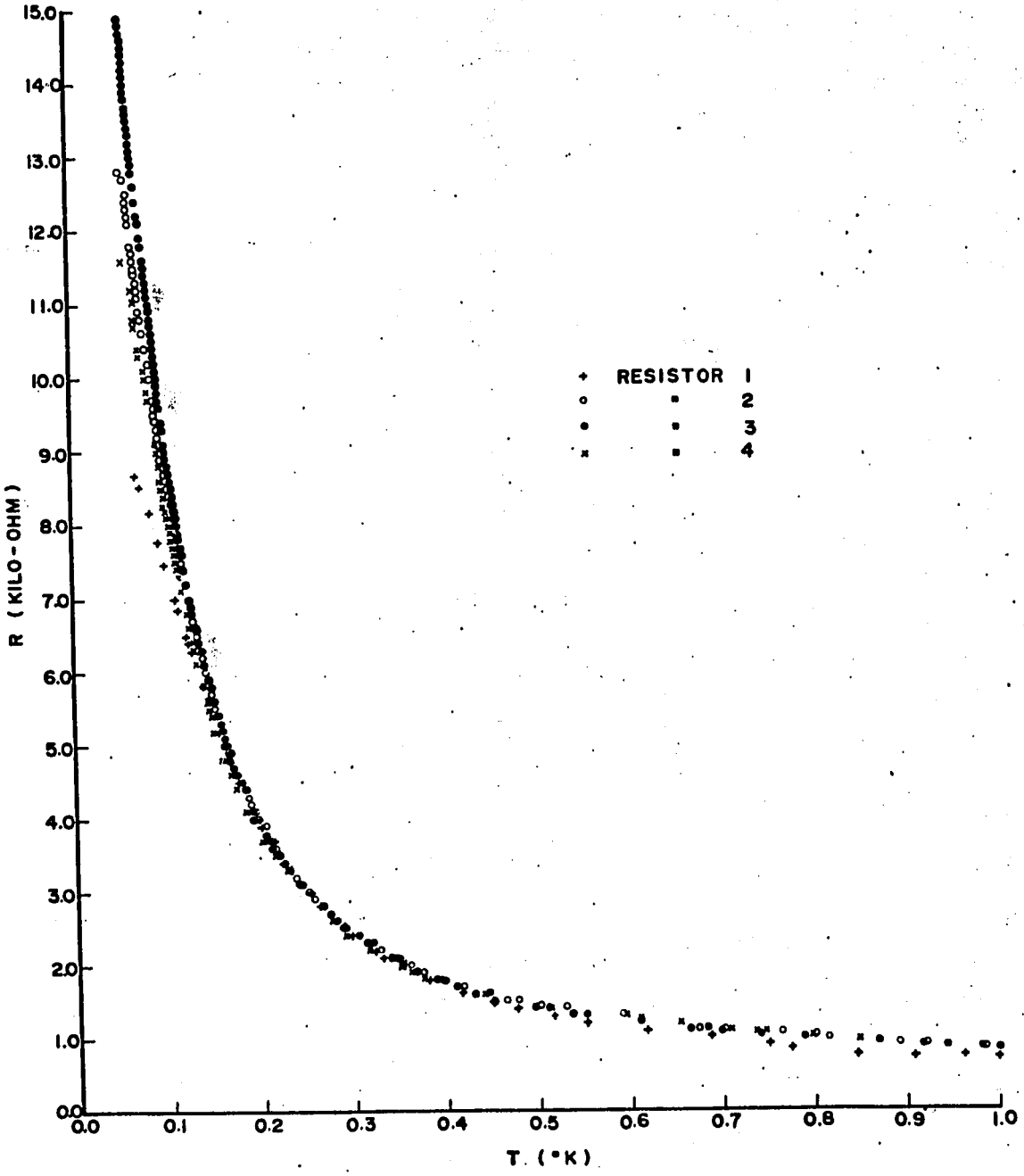

Fig. V-2. Calibration of four Speer 220 Ω resistors below 1°K.

influence on its useful range. He has given the maximum power allowable as a function of temperature. Thus to be able to use our thermometer down to 0.03°K the maximum dissipated power should not exceed 10^{-13}W. This information came to us too late to be put into practice in these calibrations.

Within the experimental error, the resistance was found to vary as 1/T between 4.2 and 1°K. Below 1°K, a plot of R vs 1/T is no longer linear. No one has reported a simple means of fitting this type of data over an extended range below 1°K. Curve fitting has to be supplemented with a correction curve. It was judged simpler to make use of the calibrated points as such and to interpolate graphically to obtain our temperature readings. The results of several independent calibrations on a given thermometer always coincided with an experimental error of ~2%.

After a thermometer has been calibrated in this fashion, it can be left on the coil foil but the CMN removed and replaced by a sphere made up of a different substance. The magnetic susceptibility versus temperature of this new substance can then be measured with the carbon resistor as a thermometer. This technique has been used in measuring the susceptibility of polycrystals of pink calcite, magnesite and dolomite. The detail is given in the next Chapter.

CHAPTER VI

ADIABATIC DEMAGNETIZATION

&

MAGNETIC SUSCEPTIBILITY

1. Introduction

In order to get an estimate of the usefulness of these carbonates as possible cooling agents, we have conducted the following studies:

1) Examination of the "high temperature" specific heat tail in an attempt to discover the splitting responsible for cooling.

2) Comparison of the observed and predicted (from the ESR spin-Hamiltonian parameters) values of the specific heat in the $1/T^2$ region.

3) Estimate of the characteristic temperatures corresponding to the maximum in the specific heat.

4) Investigation of the magnetic susceptibility to determine the temperature range in which Curie's law is obeyed.

5) Attempt to estimate the Curie points.

In principle, the magnetic behavior of a paramagnetic substance below $1^{o}K$ could be calculated if we have a Hamiltonian containing exact energy levels of all ions including dipole-dipole and exchange interactions. We of course do not have this information. Also the impurity renders useless all attempts at making a sufficiently good model of the situation. The knowledge we have of the ESR spin-Hamiltonian parameters may allow us to account for the origin of the $1/T^2$ behavior in the "high temperature" region. The dipole-dipole and exchange effects are then held responsible for the difference in the "high temperature" specific heat between the observed value and the calculated value from the spin-Hamiltonian parameters.

2. Theoretical Aspects

1) The "High Temperature" Contribution of Specific Heat

According to theories[44-46] and observations[45,47], for most of the paramagnetic substances in the "high temperature" region, the Stark effect, hyperfine structure, and magnetic interactions lead to a specific heat of the form b'/T^2, where b' is a constant, provided that they are not too large. In this region the variation of the specific heat with temperature is given by

$$c = b'/T^2 + \gamma T^3 \qquad \text{(VI.1)}$$

where γ is a constant and the last term is a contribution of lattice specific heat which, in general, is appreciable at temperatures above $0.5^{\circ}K$. The lattice specific heat can be neglected if a substance has a high Debye temperature.

To examine $1/T^2$ law, warm-up time after demagnetization can be studied. The result is plotted as $1/T$ vs t, where t is time corresponding to temperature T. If the slope of this curve, $d(\frac{1}{T})/dt$, is constant, then the specific heat of the substance follows $1/T^2$ law. This can be shown as follows. The heat leak $\dot{Q}$ of a cryostat can be expressed as

$$\dot{Q} = c\frac{dT}{dt} = -cT^2\{d(\tfrac{1}{T})/dt\} = -b'\{d(\tfrac{1}{T})/dt\} \qquad \text{(VI.2)}$$

where $b' = cT^2$. Assuming that $\dot{Q}$ is constant, when the slope $d(\frac{1}{T})/dt$ is constant, b' is constant and c is proportional to $1/T^2$. If the slope of the $1/T$ vs t curve is not constant, then the higher order terms in $1/T$ become important. In this case, either the magnetic interactions in the crystal become dominant or the energy level splittings must be very large and b' is no longer only proportional to $1/T^2$, since the higher order terms are no longer negligible.

2) Evaluation of the Specific Heat Constant, $b = \frac{cT^2}{R}$

The specific heat c for the "high temperature" region and for all the temperatures can respectively be

written as

$$\frac{c}{R} = \frac{b}{T^2} \qquad \text{(VI.3)}$$

$$c = T\frac{dS}{dT} \qquad \text{(VI.4)}$$

where S represents the entropy of a substance in this Chapter unless otherwise specified, and b is defined as $b \equiv Rb'$; R is the gas constant. By eliminating c from Eqs. (VI.3) and (VI.4) and integrating, one can obtain

$$\frac{S_i}{R} - \frac{S}{R} = \frac{b}{2T^2} - \frac{b}{2T_i^2} \qquad \text{(VI.5)}$$

where S_i is the initial entropy which is equal to Rln6 for Mn^{2+} ions. If we plot (ln6-S/R) against $1/T^2$, then the slope of the curve is a straight line down to a certain temperature and twice the value of the slope should be equal to b $(= \frac{cT^2}{R})$.

3) Magnetic Susceptibility

Since the principal magnetic susceptibilities can be obtained directly from the spin-Hamiltonian, these susceptibilities in the higher temperature region can be expressed in a convergent power series in 1/T. Van Vleck and Penney[48] have pointed out that the fine structure of the electronic levels leads to a term in $1/T^2$ in the principal susceptibilities, whose magnitude varies with the direction of the applied magnetic field. For a splitting of this type shown to exist in Mn^{2+} in these carbonates,

the principal susceptibilities for an ion with axial symmetry was given by Bleaney[49]:

$$\chi_{\parallel} = \frac{Ng^2\beta^2S(S+1)}{3kT}\left\{1 - \frac{D(2S-1)(2S+3)}{15kT}\right\} \qquad \text{(VI.6)}$$

$$\chi_{\perp} = \frac{Ng^2\beta^2S(S+1)}{3kT}\left\{1 + \frac{D(2S-1)(2S+3)}{30kT}\right\}, \qquad \text{(VI.7)}$$

where $\chi_{\parallel}$ and $\chi_{\perp}$ are, respectively, the magnetic susceptibility χ for the c-axis parallel and perpendicular to the small measuring field, k is Boltzman constant and the other symbols are as defined in Chapter IV. It is seen from these expressions that the hyperfine structure has no first or second order effect on the susceptibility. For the mean or powder susceptibility the second order terms in Eqs. (VI.6) and (VI.7) average to zero, if $g_{\parallel} = g_{\perp} = g$. That is

$$\chi = \frac{C}{T} \qquad \text{(VI.8)}$$

where

$$C = \frac{Ng^2\beta^2S(S+1)}{3k}. \qquad \text{(VI.9)}$$

Since the convergence of the power series in 1/T is favorable in the particular case of S states (g is approximately isotropic), one should expect the mean susceptibility to obey Curie's law down to a certain temperature with substances containing or doped with diluted S-state ions. Below this temperature, deviation from Curie's law may be expected to occur if the magnetic interactions are appreciable compared to kT.

the principal susceptibilities for an ion with axial symmetry was given by Bleaney[49]:

$$\chi_{\parallel} = \frac{Ng^2\beta^2S(S+1)}{3kT}\left\{1 - \frac{D(2S-1)(2S+3)}{15kT}\right\} \qquad \text{(VI.6)}$$

$$\chi_{\perp} = \frac{Ng^2\beta^2S(S+1)}{3kT}\left\{1 + \frac{D(2S-1)(2S+3)}{30kT}\right\}, \qquad \text{(VI.7)}$$

where $\chi_{\parallel}$ and $\chi_{\perp}$ are, respectively, the magnetic susceptibility χ for the c-axis parallel and perpendicular to the small measuring field, k is Boltzman constant and the other symbols are as defined in Chapter IV. It is seen from these expressions that the hyperfine structure has no first or second order effect on the susceptibility. For the mean or powder susceptibility the second order terms in Eqs. (VI.6) and (VI.7) average to zero, if $g_{\parallel} = g_{\perp} = g$. That is

$$\chi = \frac{C}{T} \qquad \text{(VI.8)}$$

where

$$C = \frac{Ng^2\beta^2S(S+1)}{3k}. \qquad \text{(VI.9)}$$

Since the convergence of the power series in 1/T is favorable in the particular case of S states (g is approximately isotropic), one should expect the mean susceptibility to obey Curie's law down to a certain temperature with substances containing or doped with diluted S-state ions. Below this temperature, deviation from Curie's law may be expected to occur if the magnetic interactions are appreciable compared to kT.

3. Experimental

1) Measurement of Warm-up Time

The same cryostat as shown in Fig. II-1 was employed for this purpose, except the thin copper plate for supporting the sample was replaced by a piece of coil foil in order to reduce eddy current when demagnetizing. For increasing the cooling efficiency, a large amount of sample (about 100 gm which is specified in each figure of Figs. VI-1 to 4) was used. On the coil foil, a calibrated Speer carbon thermometer (R_1) was originally soldered and this whole assembly was obtained after the thermometer was calibrated (see Chapter V). The experimental method was similar to that given in Chapter II.

2) Determination of Zero Field S/R vs T Curve

A series of adiabatic demagnetization was performed on samples which were previously used for warm-up time measurements with different initial conditions H/T_i to obtain various final temperatures T. Samples were demagnetized to H = 0. The values of the entropy from the different initial conditions were obtained from Hull-Hull table[50]. Since the demagnetization is an adiabatic process, the entropy is equal to that in zero field .

3) Measurement of the Magnetic Susceptibility

Measurements were made on the polycrystalline pink calcite, magnesite and dolomite. Measurement on the white

calcite was ignored, because a large enough sample was not available.

Samples were prepared in the same way as CMN sample (see Chapter V) and they were mounted in the same place where CMN sphere once was. This was made right after the third carbon thermometer was calibrated.

To measure the susceptibility of these samples the experimental technique used for calibrating the secondary thermometer (see Chapter V) was reversed. After thermal equilibrium was obtained between the sample and the thermometer, the susceptibility was read at various temperatures determined from the calibrated thermometer.

4. Results and Discussion

1) Warm-up Time

Figs. VI-1 to 4 show the results of warm-up time for the pink calcite, the white calcite, the magnesite and the dolomite, respectively. We can see that the "high temperature" contribution of specific heat of the pink calcite follows $1/T^2$ law down to $\sim 0.45^{\circ}K$, the white calcite down to $\sim 0.5^{\circ}K$, the magnesite down to $0.4^{\circ}K$ and the dolomite down to $\sim 0.9^{\circ}K$.

The pink calcite has the longest warm-up time among these samples. This means that it has a large heat capacity which is due to a high concentration of paramagnetic ions in it. The ion concentration shall be discussed in 4(4).

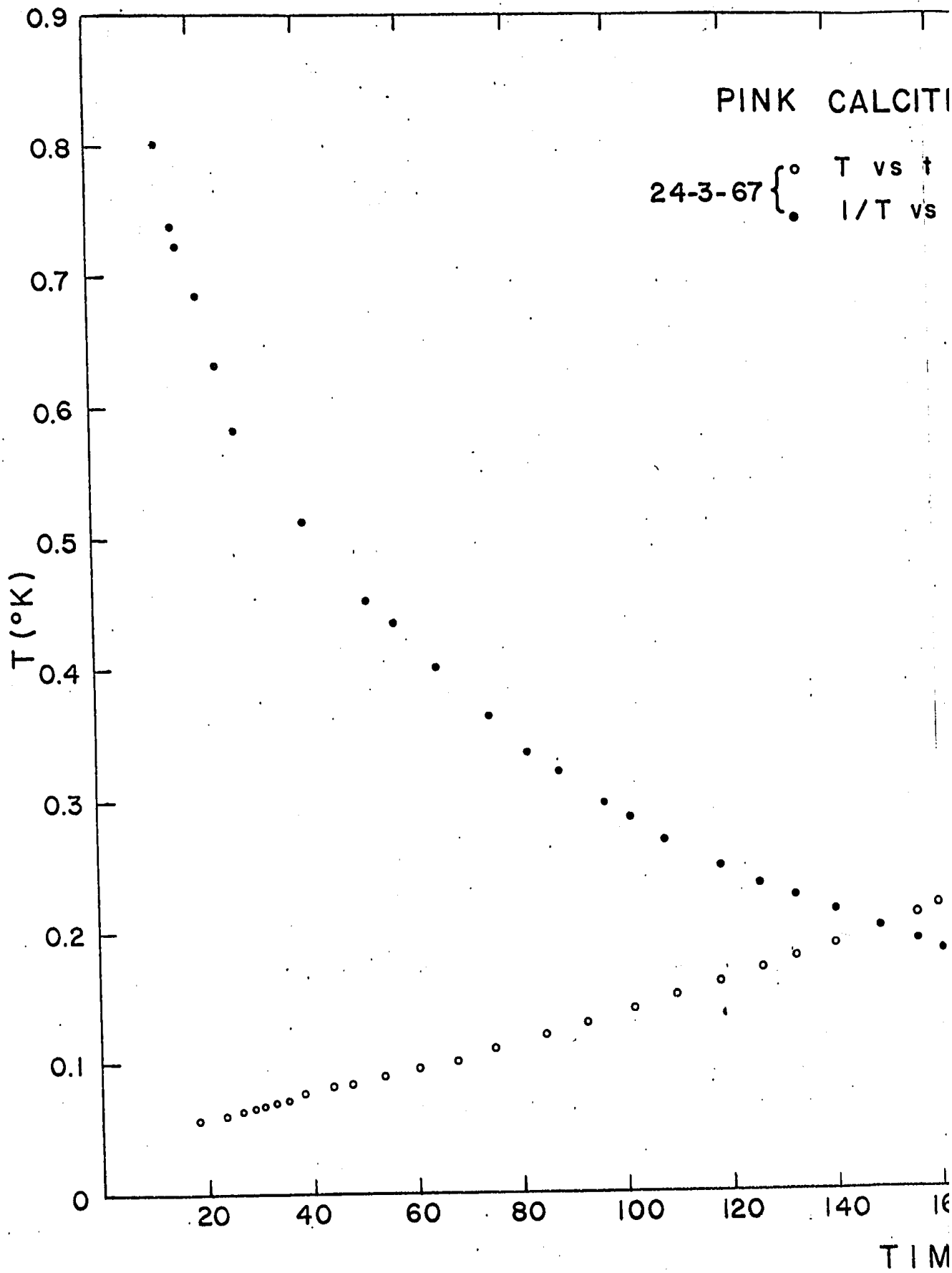

Fig. VI-1. Warm-up time of pink calcite.

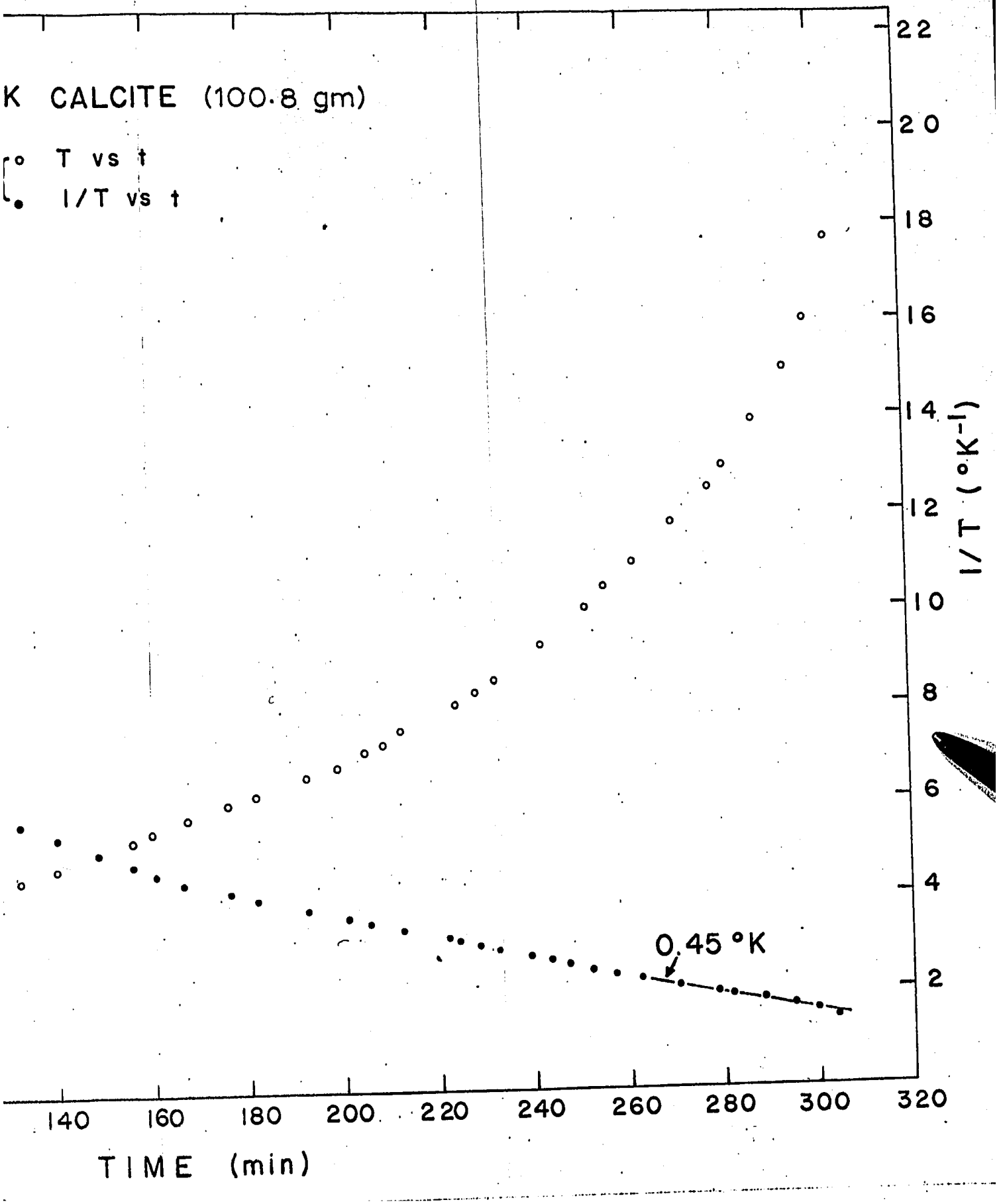
K CALCITE (100.8 gm)
T vs t
1/T vs t
0.45 °K
22
20
18
16
14
12
10
8
6
4
2
1/T (°K-1)
140
160
180
200
220
240
260
280
300
320
TIME (min)

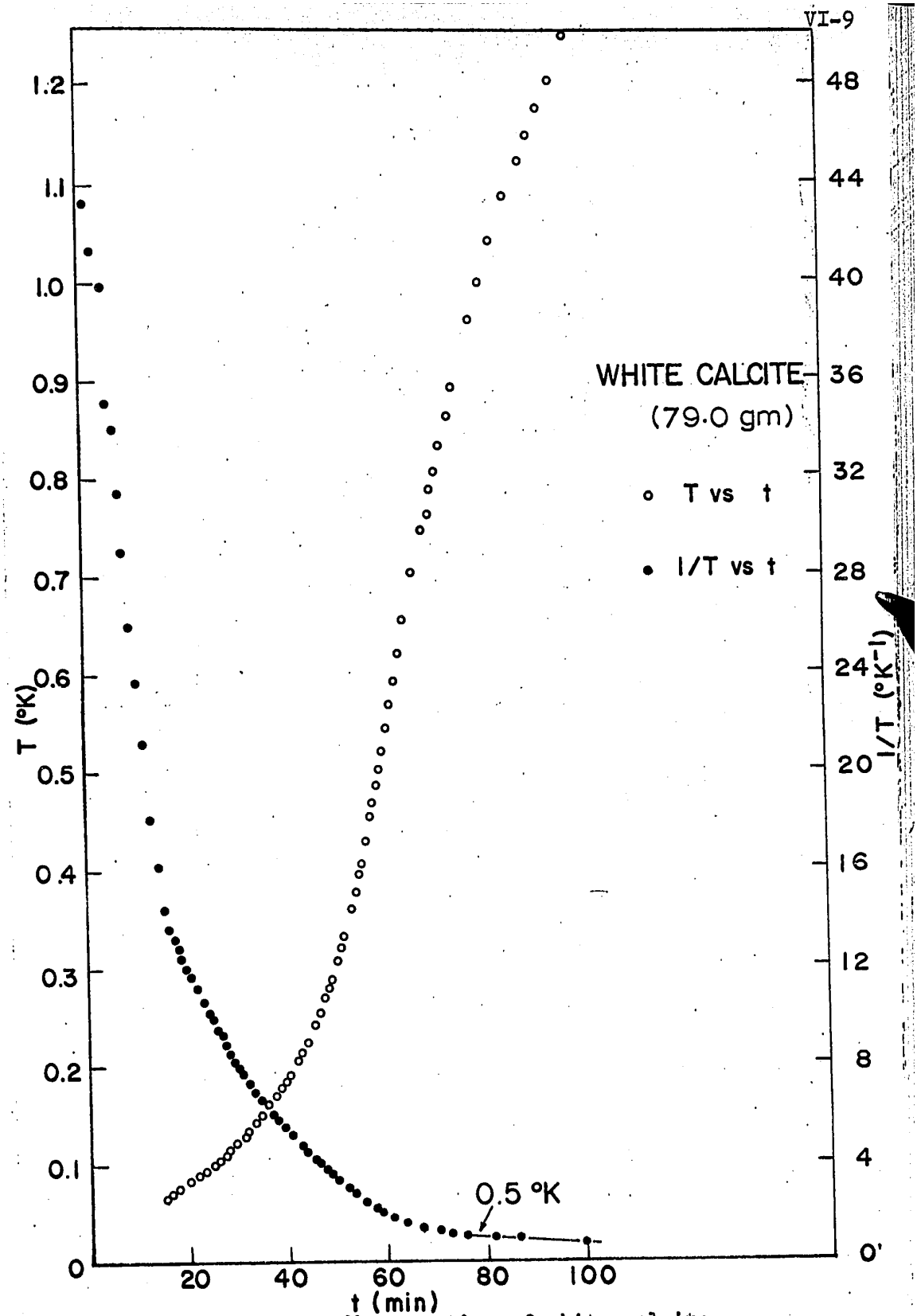

Fig. VI-2. Warm-up time of white calcite.

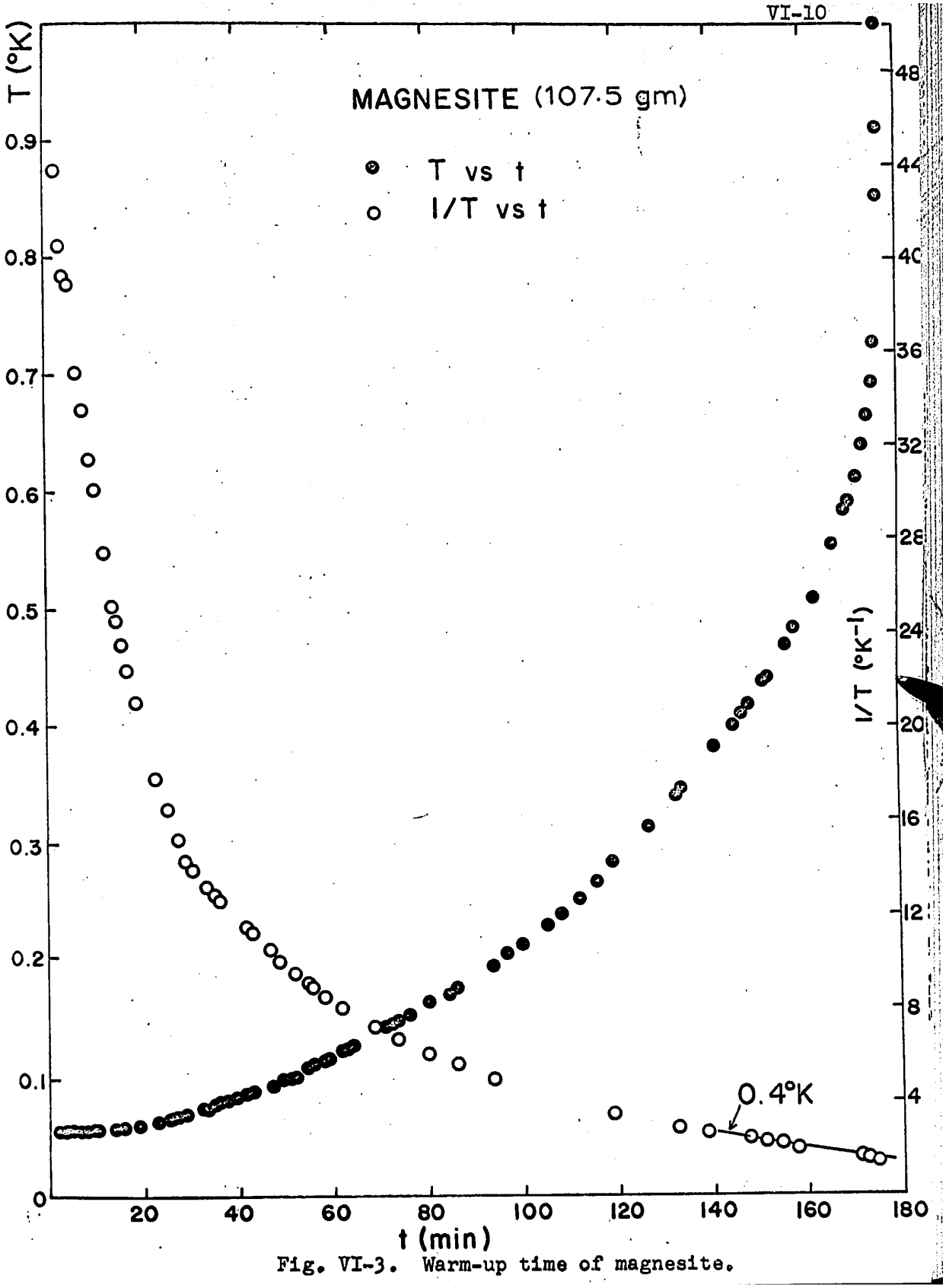

Fig. VI-3. Warm-up time of magnesite.

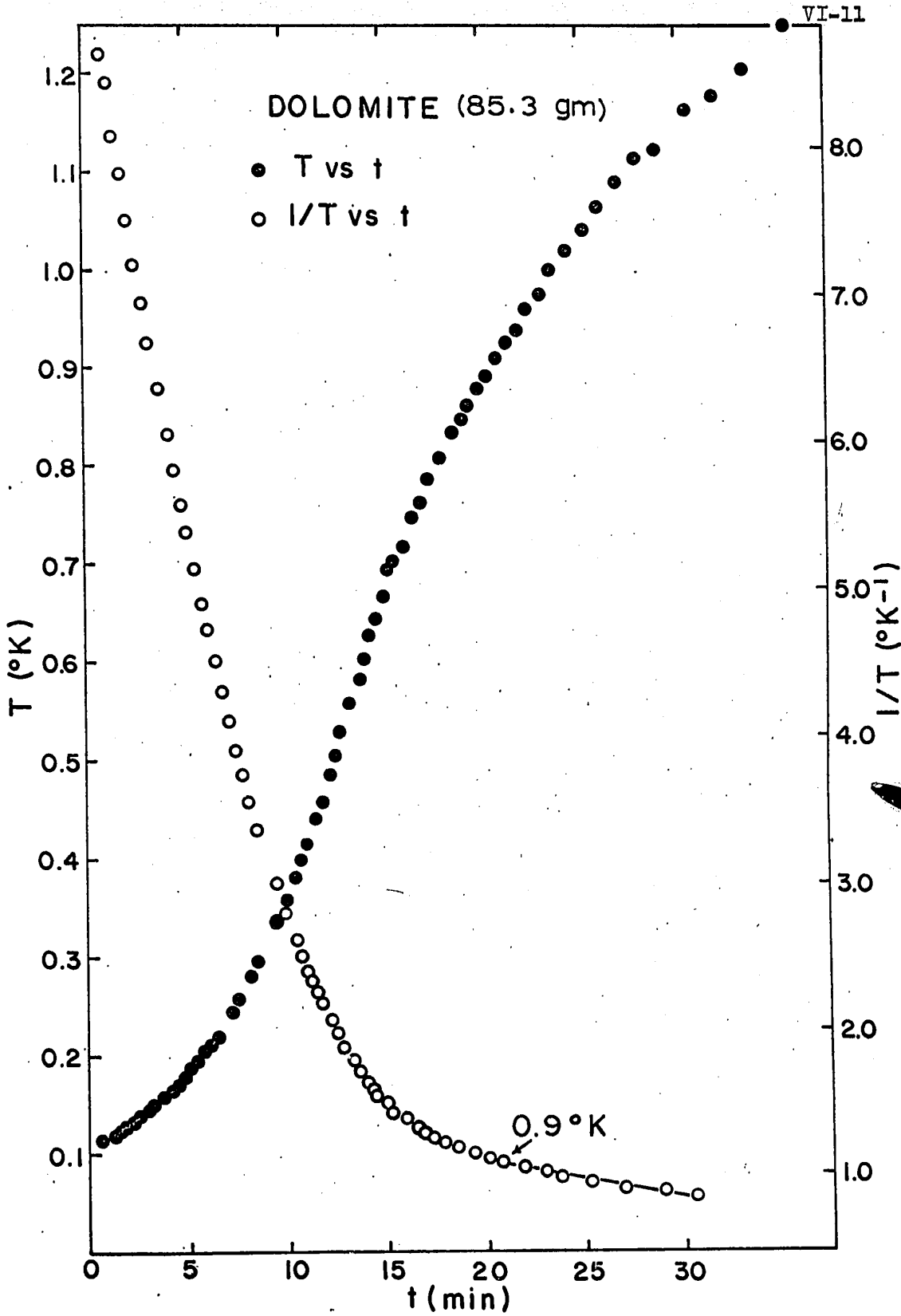

Fig. VI-4. Warm-up time of dolomite.

2) S/R-T Diagram

Figs. VI-5 to 8 show the zero magnetic field entropy S and the magnetic specific heat c as a function of temperature for the pink calcite, the white calcite, the magnesite and the dolomite, respectively. The c/R-T curves in these figures were calculated directly from the S/R-T curves by using the relationship $c = T(dS/dT)$. In these results the lattice and the coil foil entropies were neglected, because the former is assumed to be very small below $1^{\circ}K$ compared to the magnetic entropy and the latter is also very small compared to that of the big amount of the sample. The data were taken in different runs and on different days which are specified in each figure and they were consistent with each other.

The entropies of the pink calcite and the dolomite were lower than those of the white calcite and the magnesite at any temperature. It is indicative of the strong magnetic interactions in the pink calcite and the dolomite. These interactions shall be evaluated in Section 4-(3). The results of c/R-T curves show that the lowest temperatures obtained from these samples are near the anomalous specific heat peaks.

Figs. VI-9 to 12 show the cooling curves of these samples indicating the various final temperatures obtained with various initial conditions. These curves show that

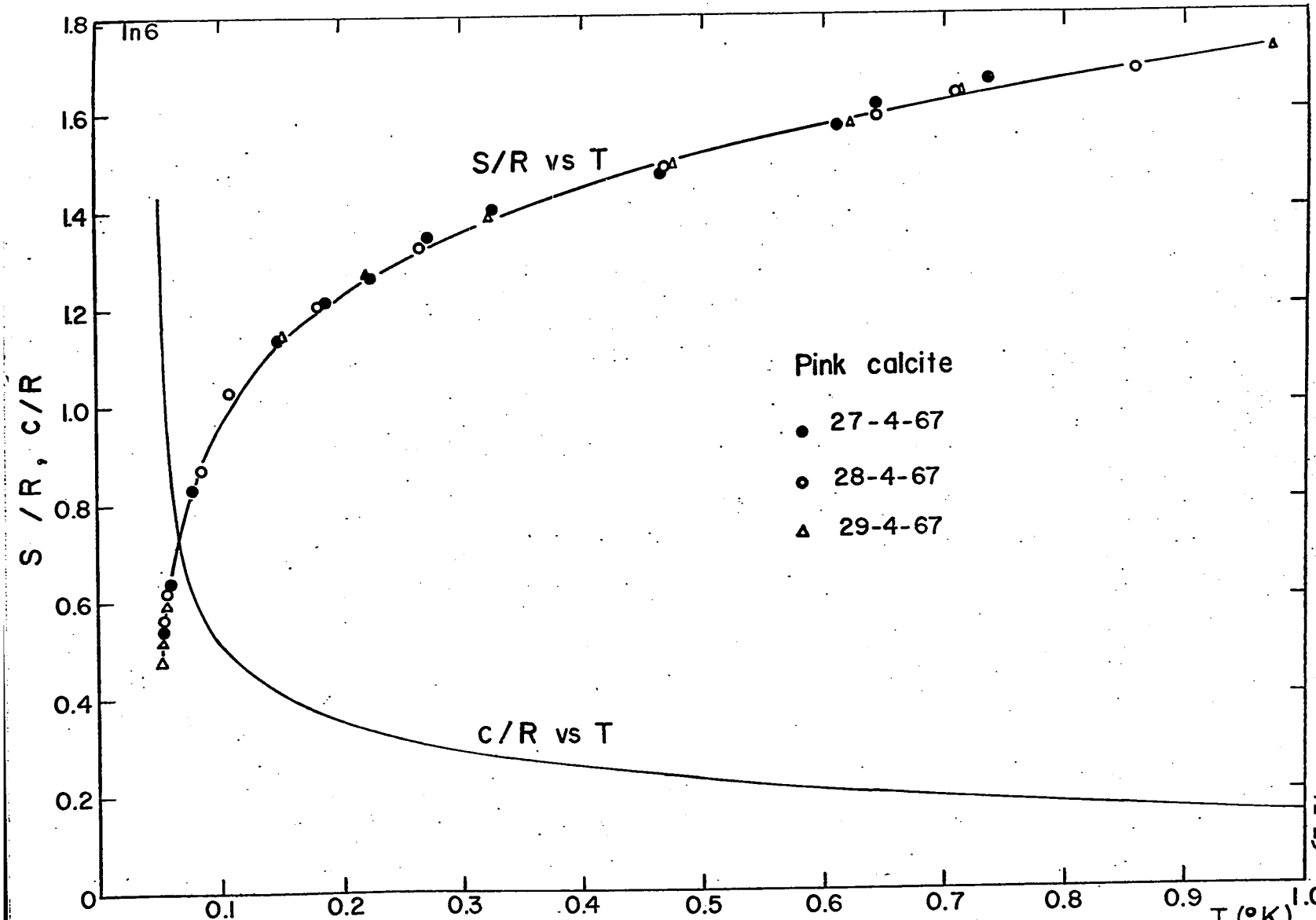

Fig. VI-5. S/R-T and c/R-T diagrams of pink calcite.

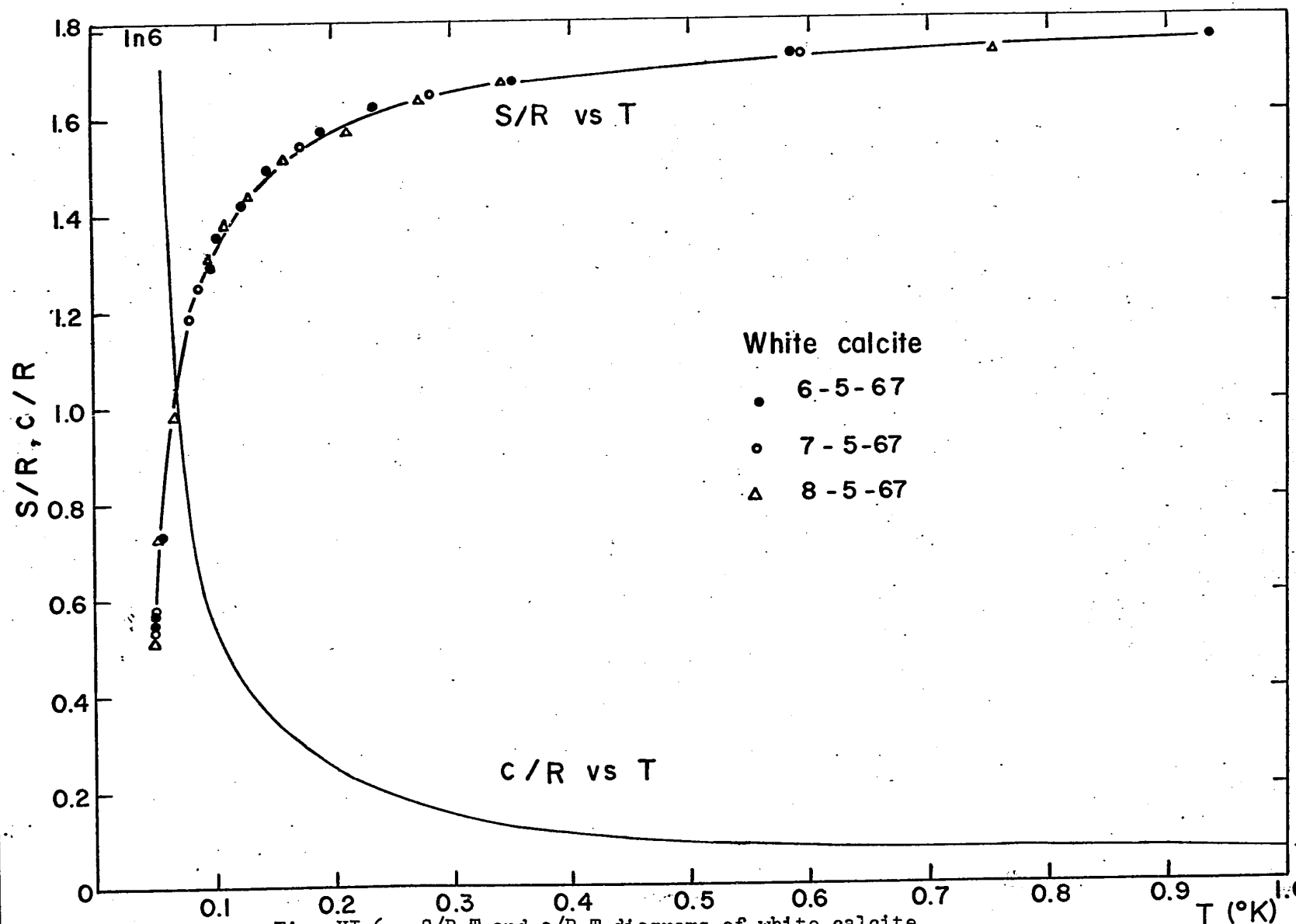

Fig. VI-6. S/R-T and c/R-T diagrams of white calcite.

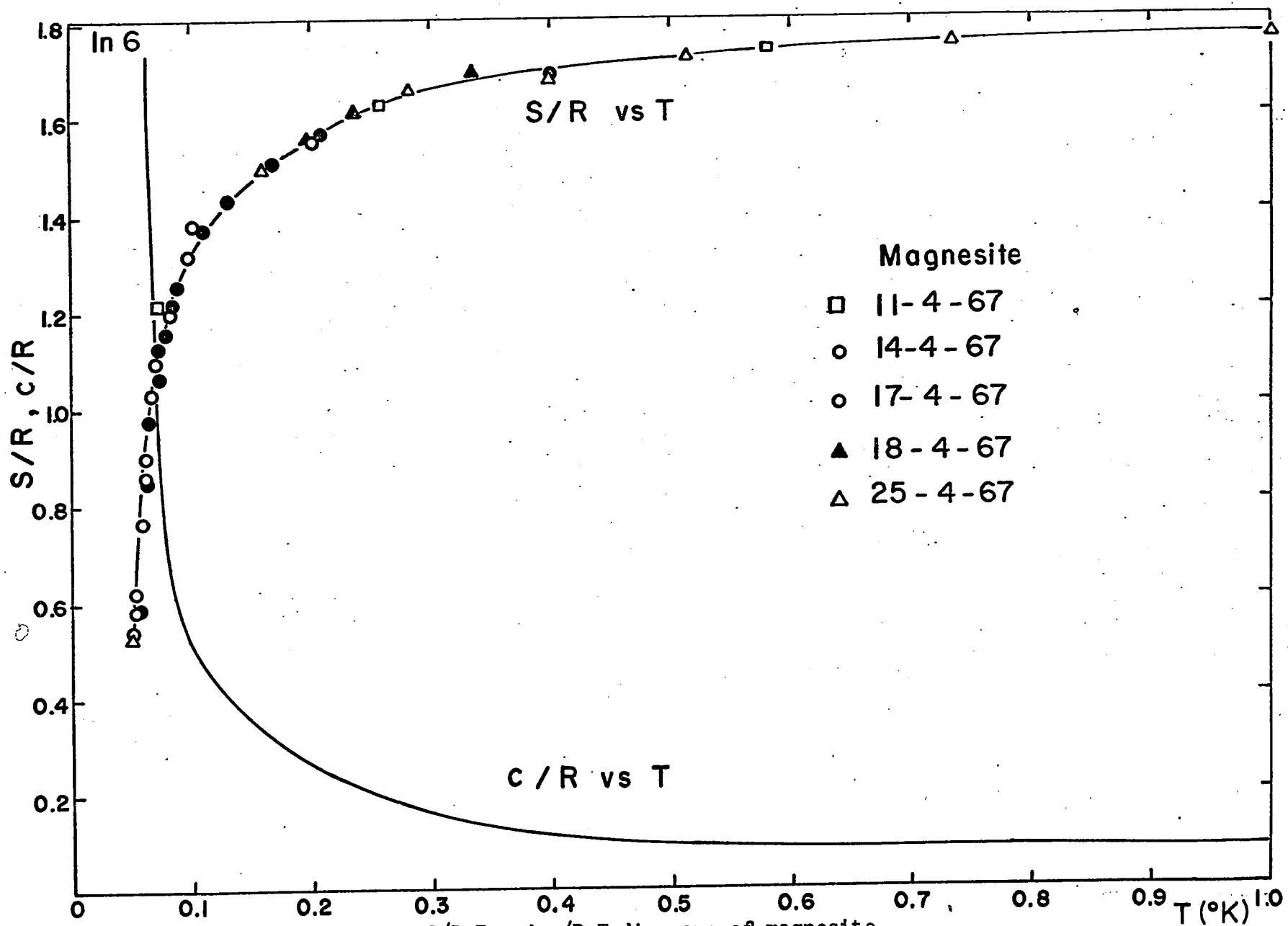

Fig. VI-7. S/R-T and c/R-T diagrams of magnesite.

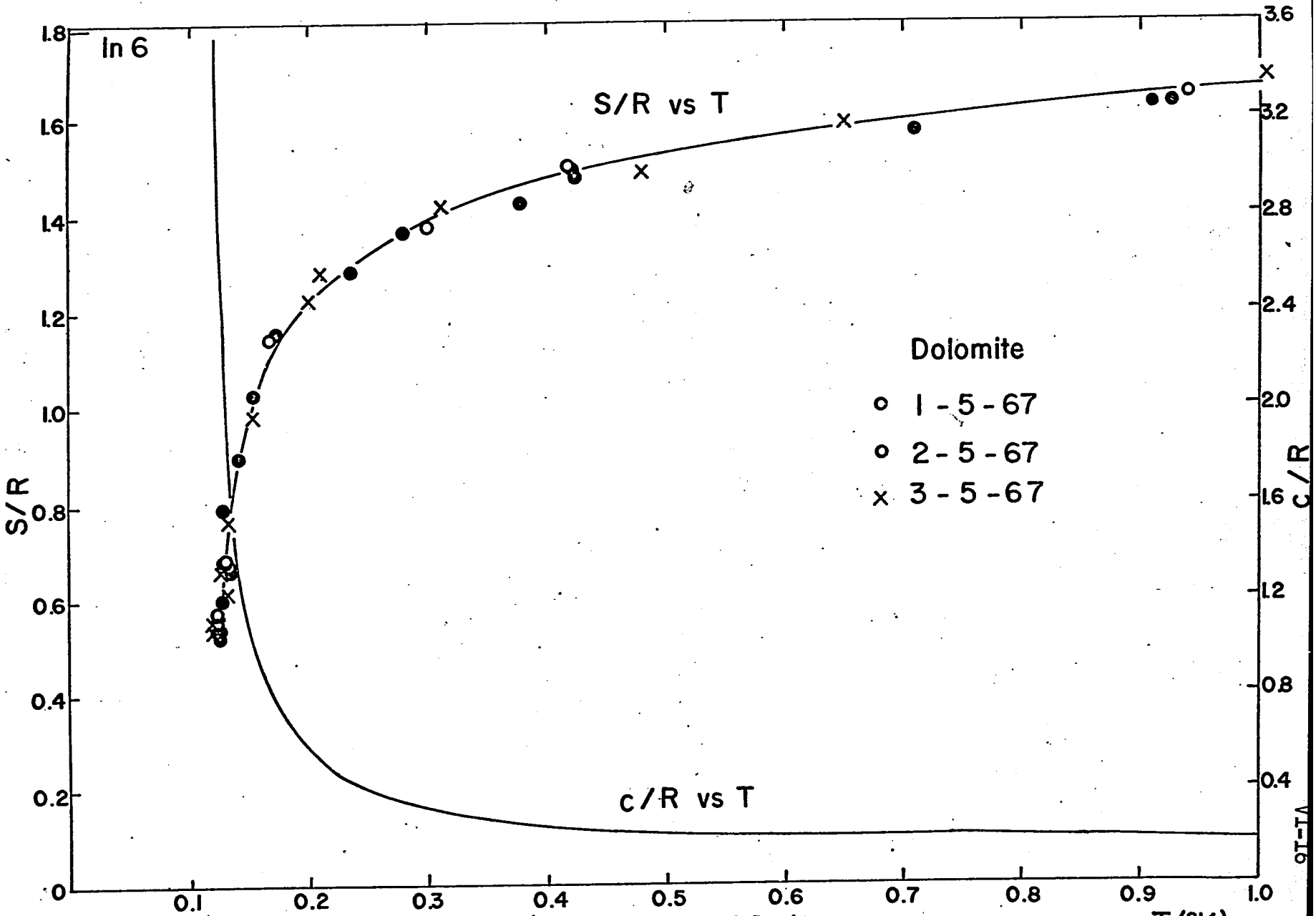

Fig. VI-8. S/R-T and c/R-T diagrams of dolomite.

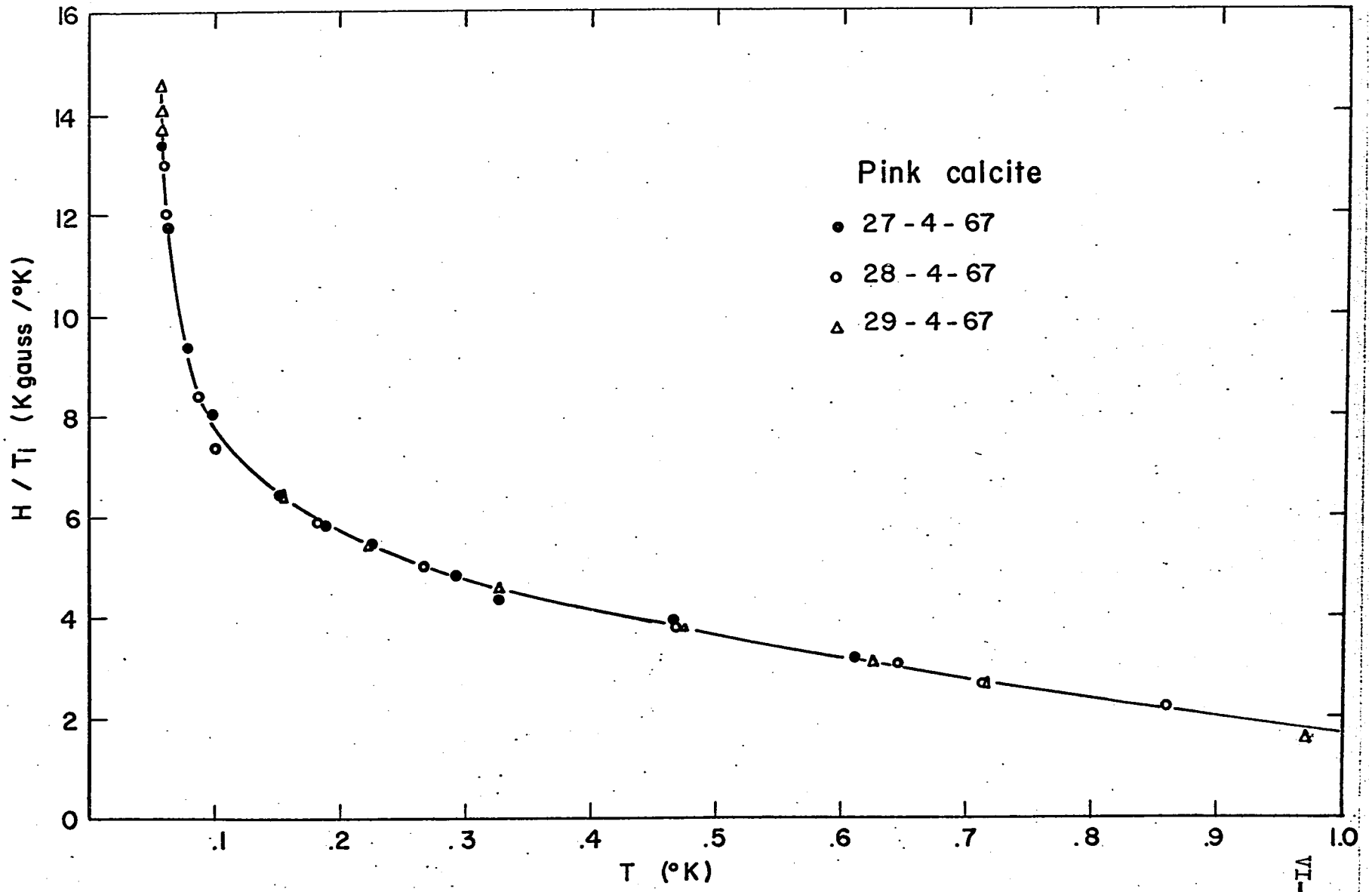

Fig. VI-9. Cooling curve of pink calcite.

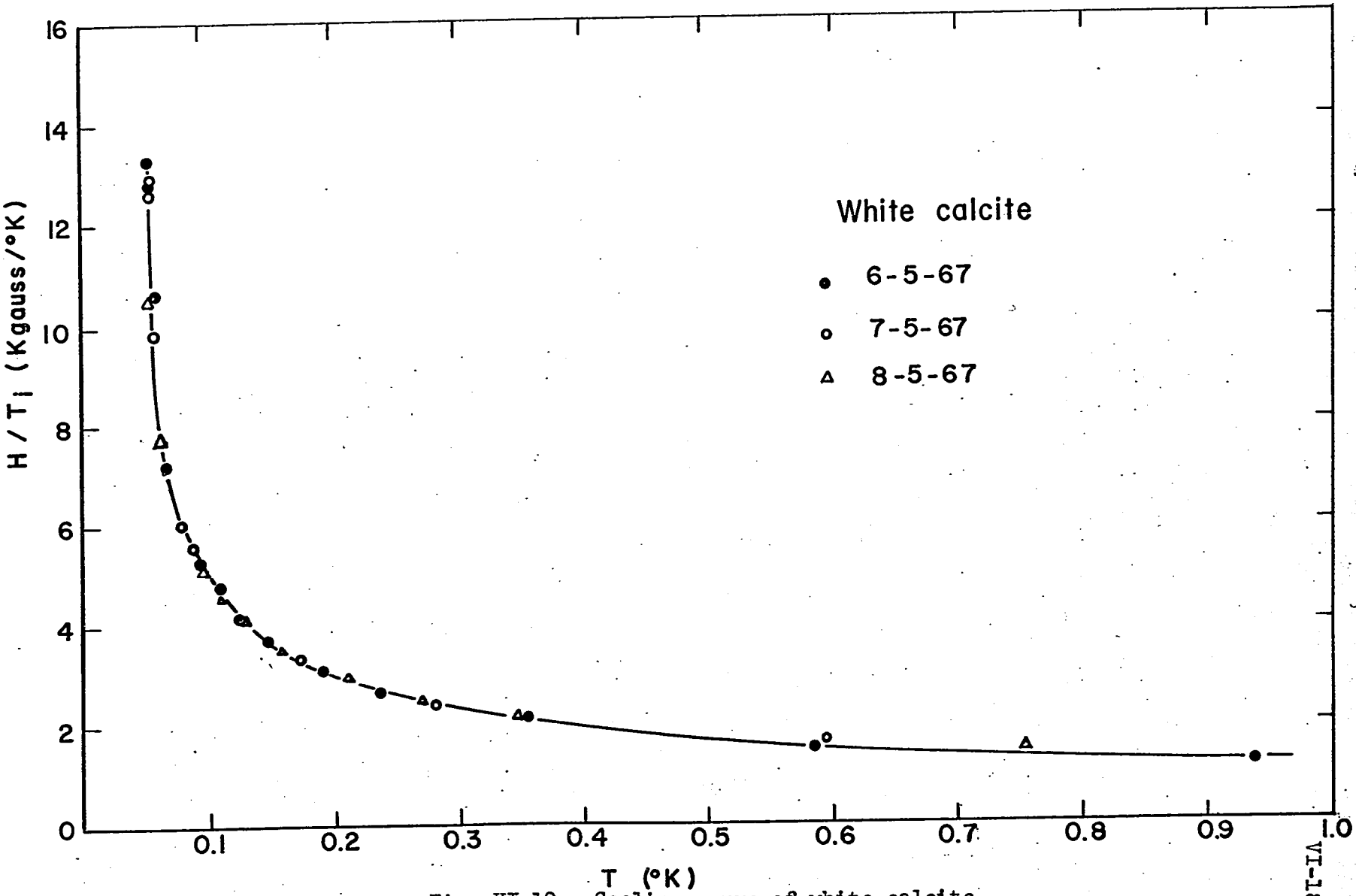

Fig. VI-10. Cooling curve of white calcite.

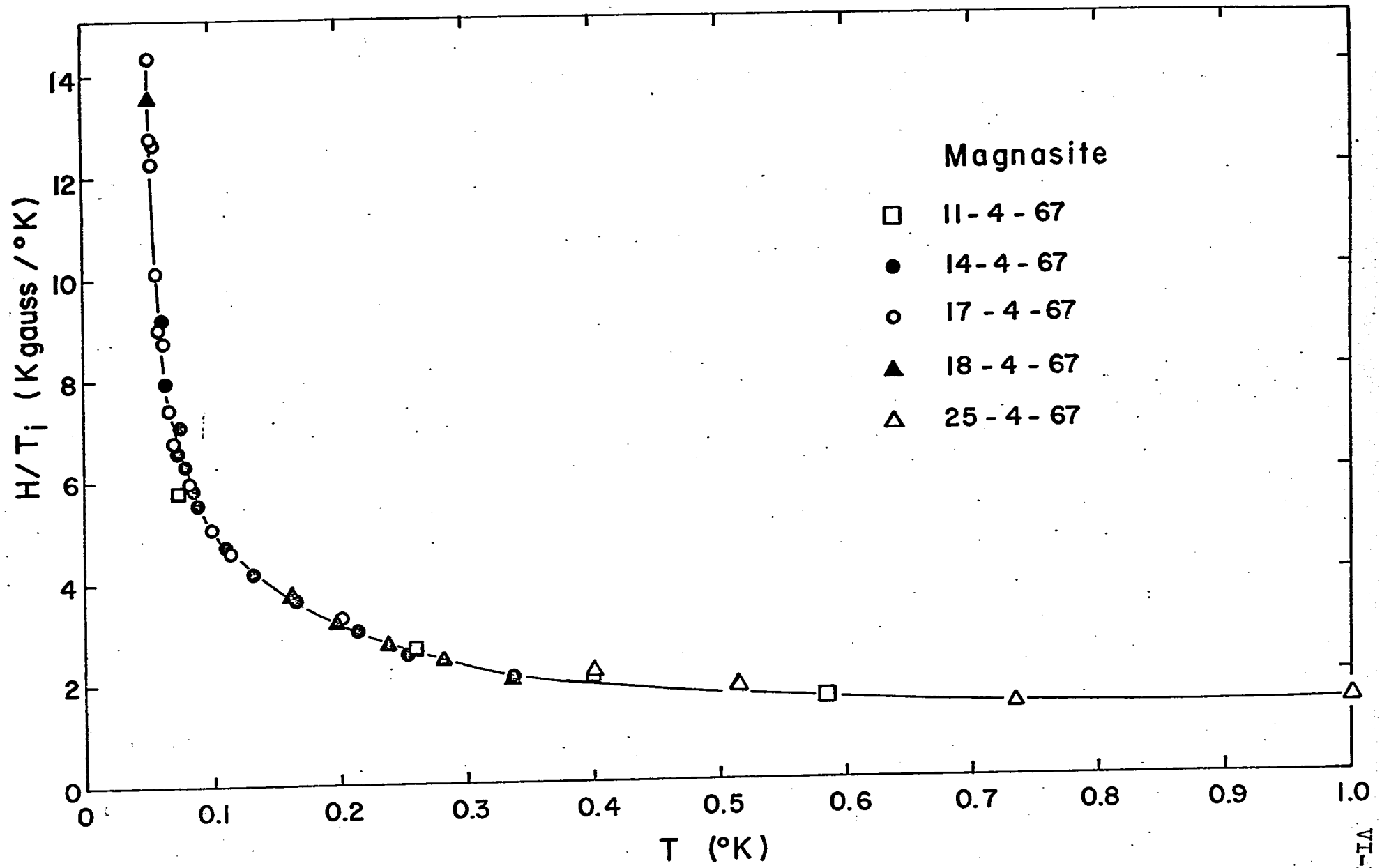

Fig. VI- 11. Cooling curve of magnesite.

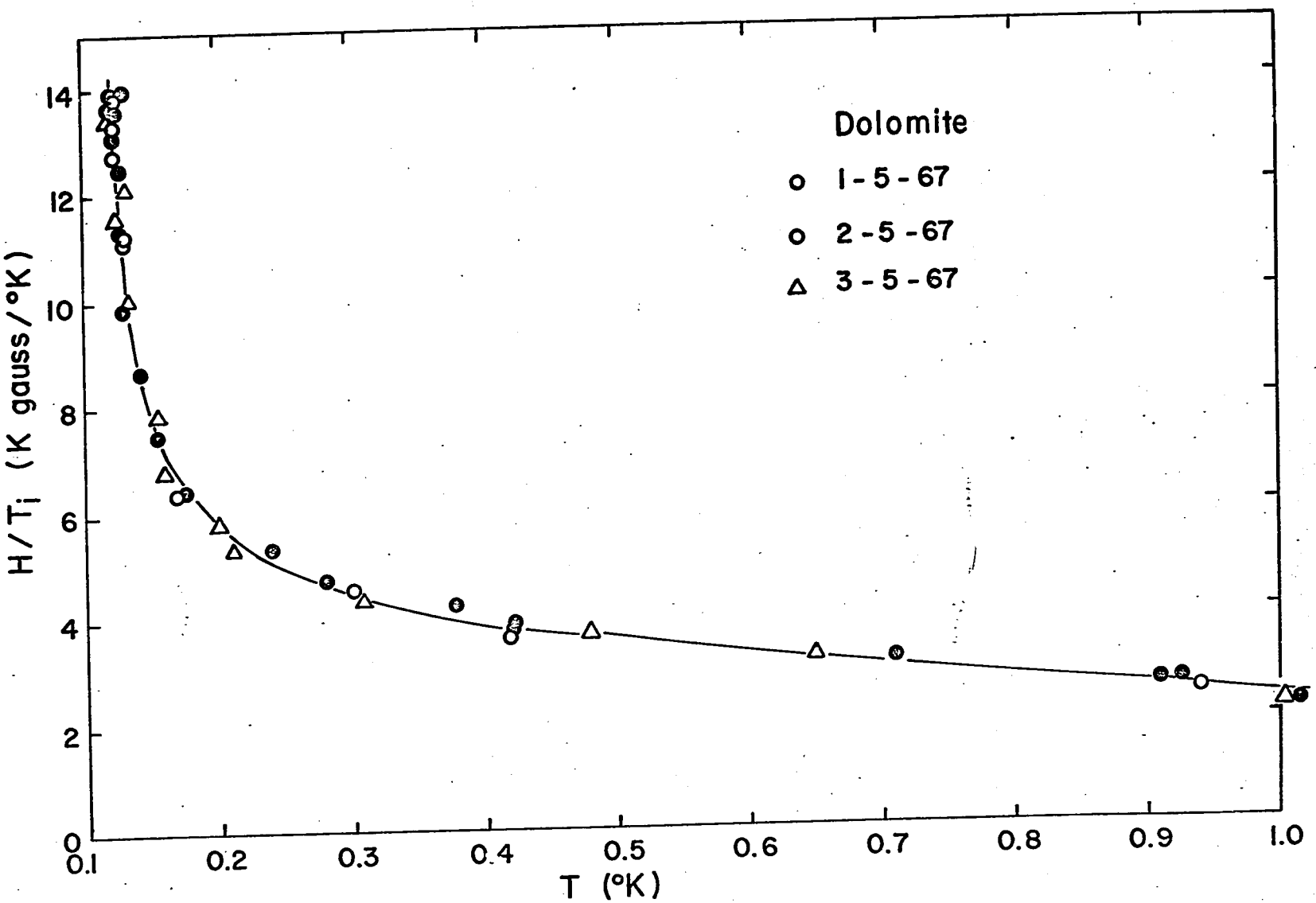

Fig. VI-12. Cooling curve of dolomite.

the white calcite or the magnesite can attain a lower temperature than the pink calcite or the dolomite with a given initial condition. If we extrapolate these curves, we can find that the temperatures would not go much lower even with high values of H/T_i. If H/T_i = 20 kilo-gauss/^oK, the final temperature that can be attained for the pink and the white calcites and the magnesite is about 0.05^oK, but for the dolomite is only about 0.1^oK. From the extrapolation of these curves, one can expect the characteristic temperature ⊛ for the pink calcite, the white calcite, the magnesite to be near 0.05^oK and that for the dolomite to be near 0.1^oK. These values are quite in agreement with the predicted values which were given in Table IV-3.

3) Evaluation of the "High Temperature" Specific Heat Constant

In order to evaluate the "high temperature" specific heat constant b, the reduction of entropy was plotted against $1/T^2$. b is then calculated from the slope using Eq. (VI.5). Figs. VI-13 to 16 show these plots for these samples. It is seen that the (ln6-S/R) vs $1/T^2$ curve for the pink calcite is a straight line down to 0.47^oK, whereas for the white calcite down to 0.5^oK, for the magnesite down to 0.4^oK and for the dolomite down to 0.9^oK. They are in good agreement with the results obtained from the warm-up time curves.

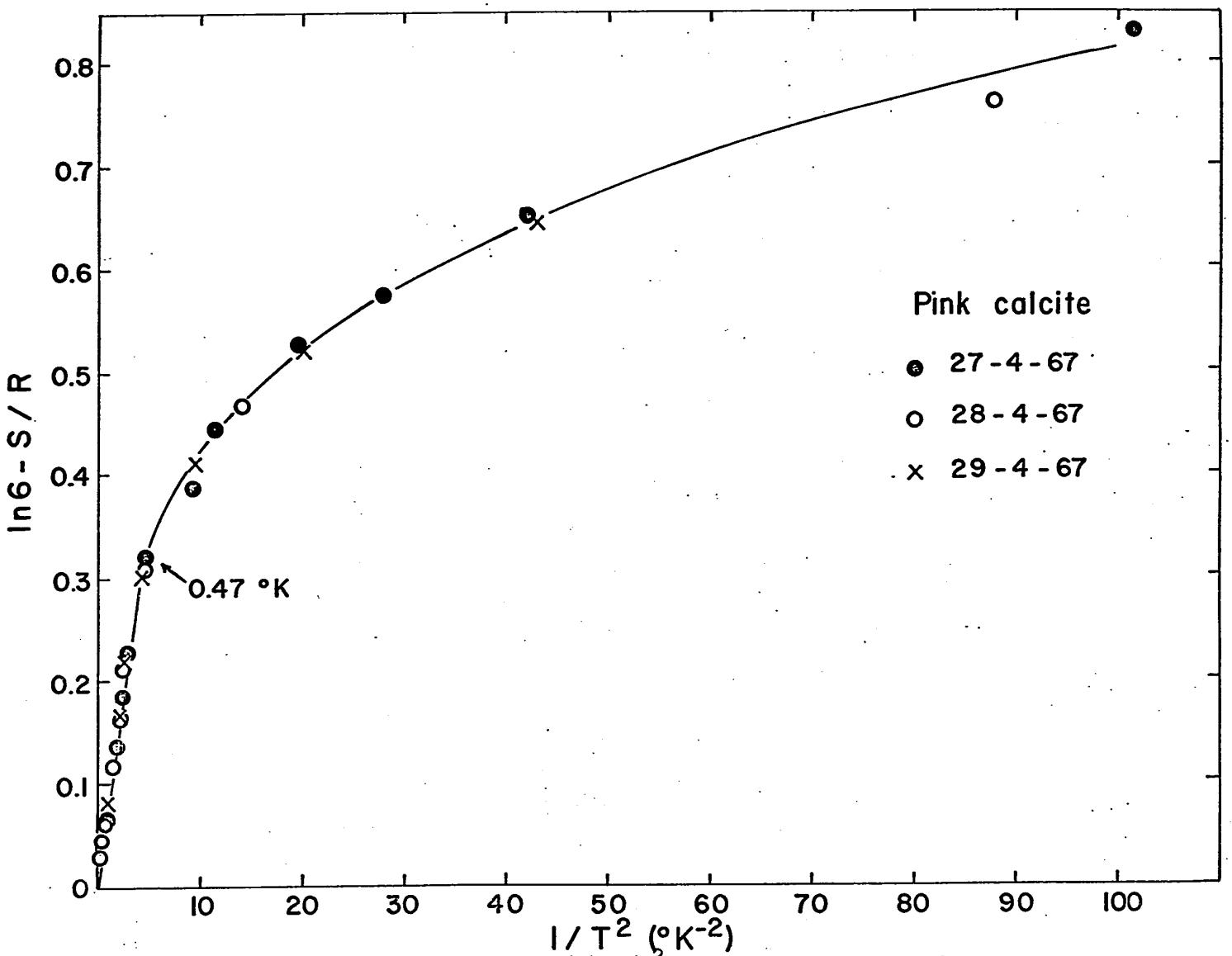

Fig. VI-13. (ln6-S/R)-1/T^2 diagram of pink calcite.

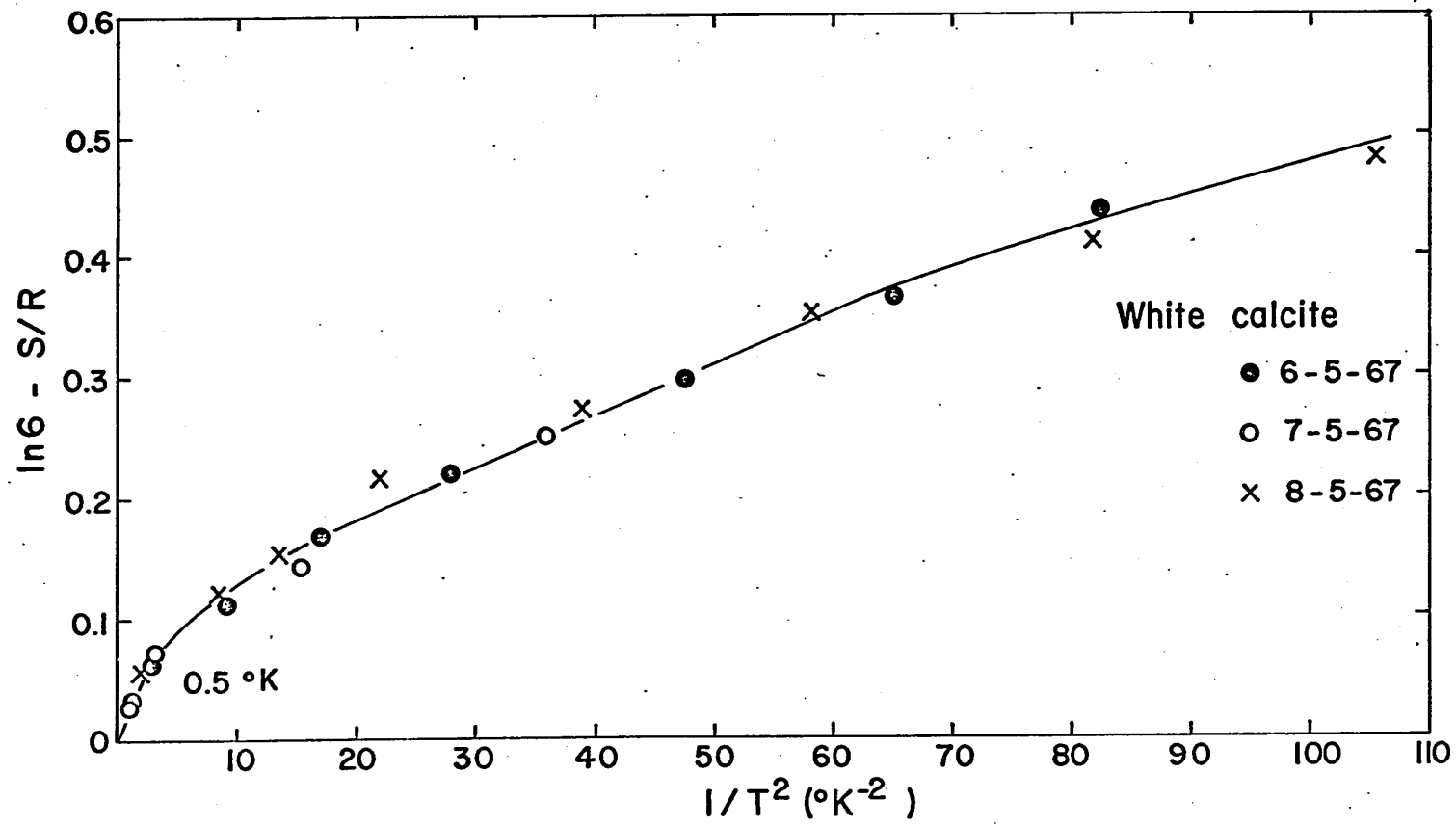

Fig. VI-14. (ln6-S/R) - $1/T^2$ diagram of white calcite.

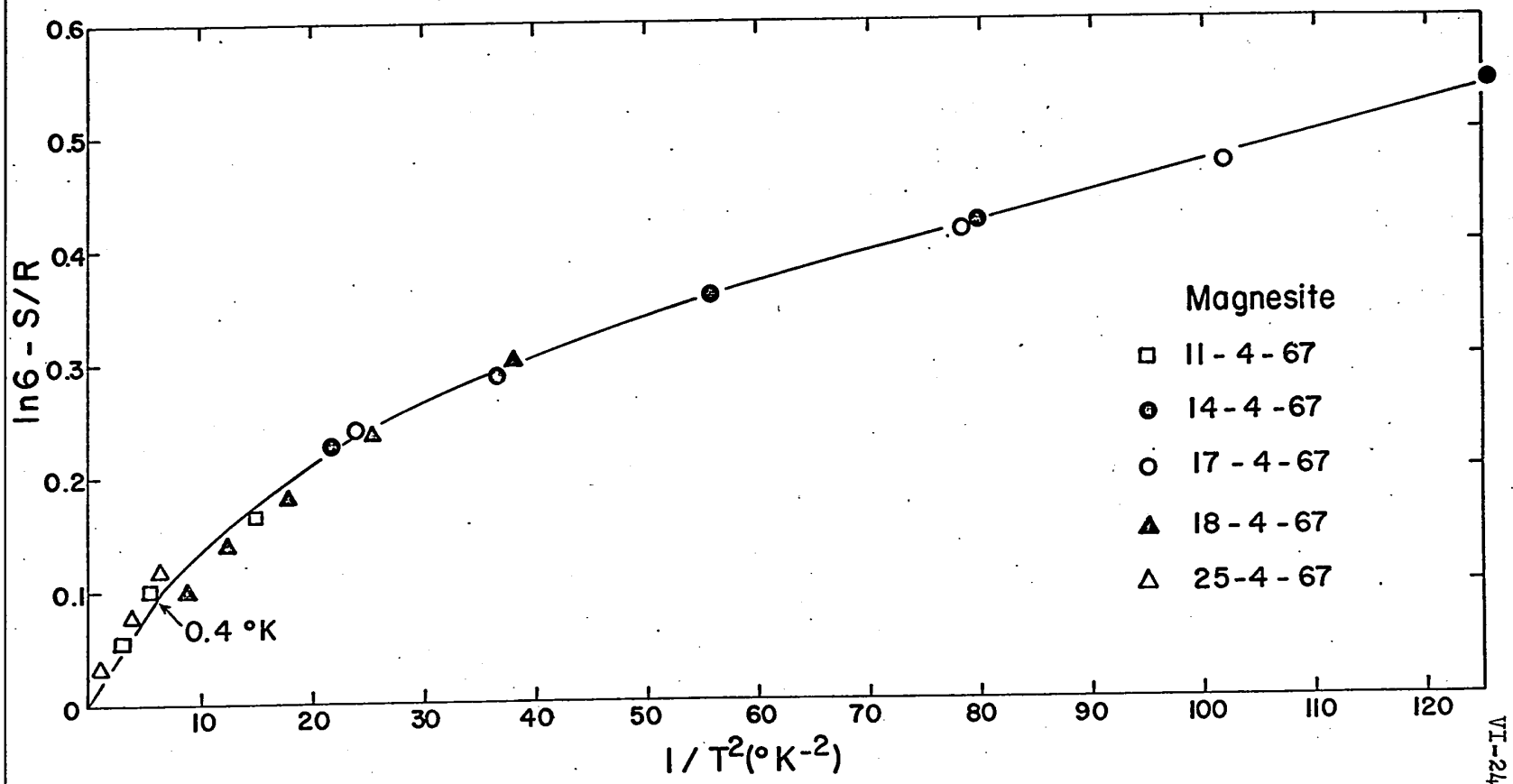

Fig. VI-15. (ln6-S/R) - $1/T^2$ diagram of magnesite.

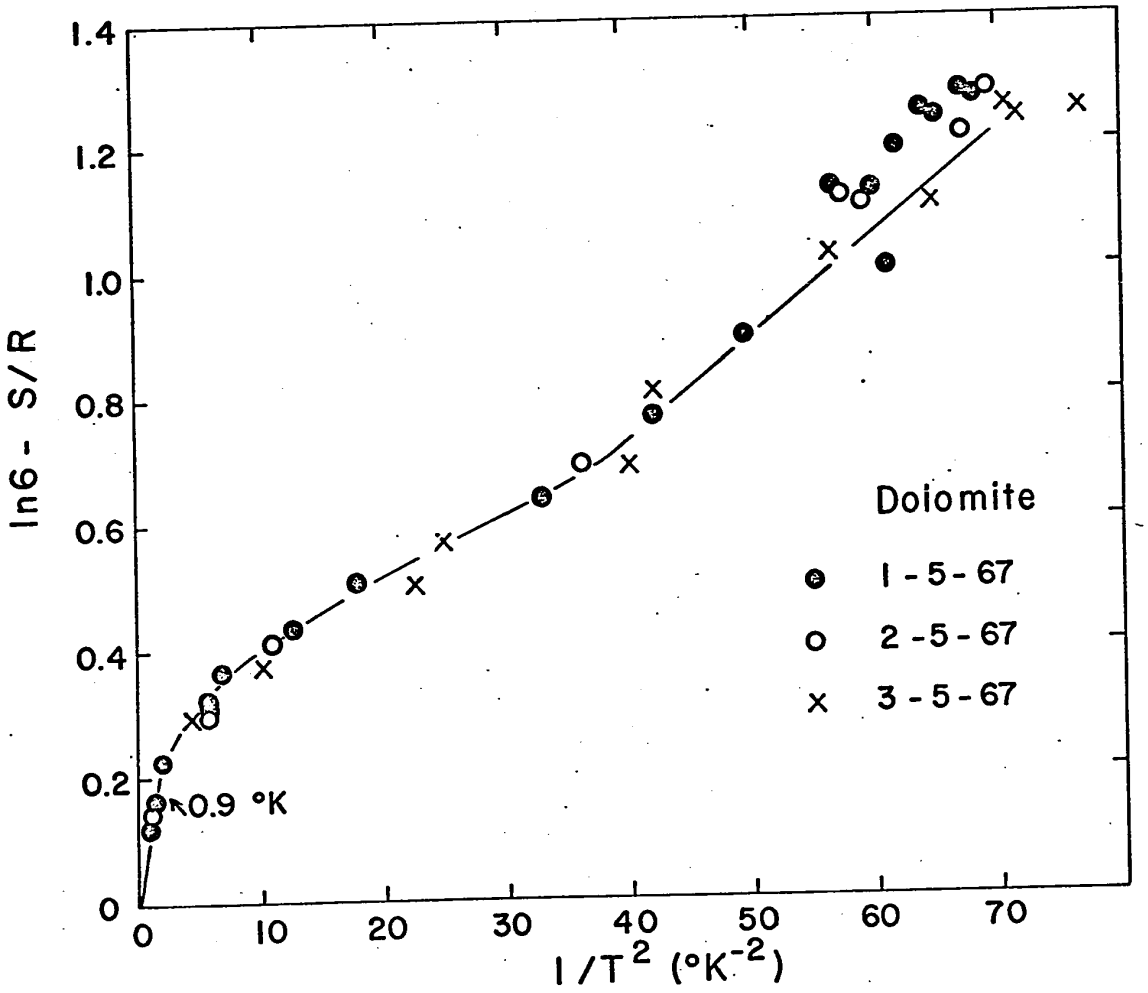

Fig. VI-16. (In6-S/R) - $1/T^2$ diagram of dolomite.

The experimental results for "high temperature" specific heat constant b_{expt} which is further divided into "high" and "low" temperature regions are tabulated in Table VI-1. The reason for this division into two parts is due to the fact that the (ln6 - S/R) vs $1/T^2$ curve for each sample did not show a straight line all the way down to the neighborhood of its specific heat peak, but it shows two significant slopes. The interpretation will be made in the next paragraph. The calculated results, b_{ESR}, obtained from Chapter IV are also listed in Table VI-1 just for comparison.

TABLE VI-1

THE "HIGH TEMPERATURE" SPECIFIC HEAT CONSTANTS

Material	$b_{expt}\{(^oK)^2\}$		b_{ESR} $\{(^oK)^2\}$
	High Temp. Region (above ~0.4°K)	Low Temp. Region (below ~0.4°K)	
Pink Calcite	140×10^{-3}	$\sim6\times10^{-3}$	4.8×10^{-3}
White Calcite	32	~6	4.8
Magnesite	30	~6	4.7
Dolomite	100	~22	6.3

As we know, the crystalline Stark effect, hyperfine structure, dipolar interaction and exchange interactions all contribute a term proportional to $1/T^2$. Thus, their

The experimental results for "high temperature" specific heat constant b_{expt} which is further divided into "high" and "low" temperature regions are tabulated in Table VI-1. The reason for this division into two parts is due to the fact that the (ln6 - S/R) vs $1/T^2$ curve for each sample did not show a straight line all the way down to the neighborhood of its specific heat peak, but it shows two significant slopes. The interpretation will be made in the next paragraph. The calculated results, b_{ESR}, obtained from Chapter IV are also listed in Table VI-1 just for comparison.

TABLE VI-1

THE "HIGH TEMPERATURE" SPECIFIC HEAT CONSTANTS

Material	$b_{expt}\{(^oK)^2\}$		b_{ESR} $\{(^oK)^2\}$
	High Temp. Region (above ~0.4°K)	Low Temp. Region (below ~0.4°K)	
Pink Calcite	140×10^{-3}	$\sim6\times10^{-3}$	4.8×10^{-3}
White Calcite	32	~6	4.8
Magnesite	30	~6	4.7
Dolomite	100	~22	6.3

As we know, the crystalline Stark effect, hyperfine structure, dipolar interaction and exchange interactions all contribute a term proportional to $1/T^2$. Thus, their

contributions except that due to the anisotropic exchange interaction are all additive. It is seen from Table VI-1 that in the "high temperature" region (above $\sim 0.4^{\circ}K$) the experimental result for each sample is due only to Stark effect and hyperfine structure. In the "low temperature" region (below $\sim 0.4^{\circ}K$), b_{expt}-value is close to b_{ESR}-value for each sample. These discrepancies could arise from many sources which are discussed in the following:

a) Lattice specific heats are appreciable in the "high temperature" region

It was mentioned in Section 3(2) about the calculation of entropy S for each point on the assumption that it is the same as it was in the beginning of the demagnetization. But the sample was at a "high temperature" (about $1.3^{\circ}K$) at that point which conceivably broke down the validity of the assumptions for some low-field demagnetizations at a considerably high temperature. The discrepancy is quite evident in Figs. VI-13 to 16 where the points toward the origin deviated from a straight line.

The argument could be examined qualitatively. According to Debye T^3 approximation at low temperatures,

the lattice entropy S_ℓ can be deduced as

$$\frac{S_\ell}{R} \sim 80\left(\frac{T}{\Theta_D}\right)^3 \qquad \text{(VI.10)}$$

where Θ_D is Debye characteristic temperature which ranges from 100 to 1000°K for most of dielectric solids. Then S_ℓ ranges from $2\times10^{-4}R$ to $2\times10^{-7}R$. On the other hand, if S_r represents the reduction in entropy due to the magnetic field H, then S_r is in the order of $10^{-2}R$ when H is up to about 2.4 kilo-gauss. From the concentration of the paramagnetic ions, we know that the host crystal has about 10^3 times more moles/gm than the ions. Therefore, S_ℓ and S_r are comparable. It can be seen from Figs. VI-13 to 16 that S_ℓ can be neglected only below about 0.4°K.

b) Dipole-dipole interaction between Fe^{2+} and Mn^{2+} ions has a contribution to the specific heat.

It is seen from Table VI-1 that the b_{expt}-value of pink calcite is much larger than that of white calcite. We also examine their concentrations of Fe^{2+} and Mn^{2+} from Appendix A which shows that the pink calcite contains about 0.5% of Fe^{2+} and about 0.13% of Mn^{2+} and the white calcite contains about 0.25% of Fe^{2+} and about 0.06% of Mn^{2+}. It was also discussed in Chapter IV that the Mn^{2+} ESR lines in these samples were broadened to a certain extent by a dipolar interaction with Fe^{2+} ions. From these evidences, one might expect that the dipolar interaction between Fe^{2+}

and Mn^{2+} in these samples has a contribution to the specific heat.

c) Fe^{2+} in these carbonates probably contributes to paramagnetism in the high temperature region. Therefore, it contributed to the specific heat.

4) Magnetic Susceptibility

Fig. VI-17 shows the measured magnetic susceptibilities (in units of 0.5 emu/cm^3) plotted against 1/T for the polycrystalline pink calcite, magnesite and dolomite. It is seen that the pink calcite obeys Curie's law down to $\sim 0.8^{\circ}K$, the magnesite to $\sim 0.3^{\circ}K$ and the dolomite to $\sim 0.8^{\circ}K$. Below these temperatures these susceptibilities tend to deviate gradually from 1/T law. From these results also we can see that they are still far from their susceptibility peaks, therefore their Curie or Néel points must be below $0.06^{\circ}K$.

The straight line in each graph is the susceptibility curve for CMN sample which was plotted for comparison. The CMN sample had approximately the same volume as each sample. The Curie constants C for these samples were calculated by comparing their slopes with that of CMN. From these Curie constants concentrations of Mn^{2+} ions were then calculated. The results are given in Table VI-2. This calculation was based on the assumption that Mn^{2+} was the only type of paramagnetic ions in these samples.

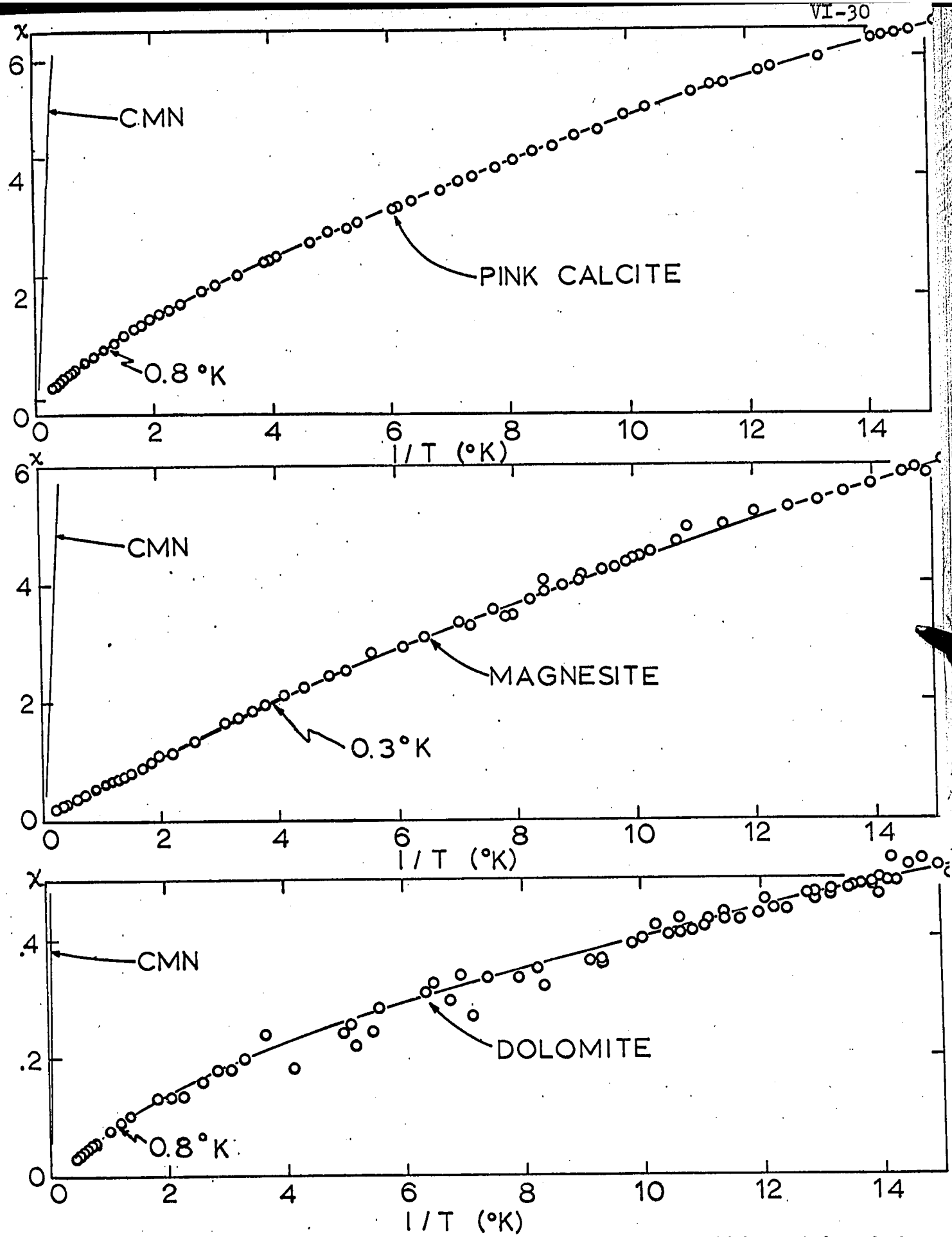

Fig. VI-17. Magnetic susceptibilities of the polycrystalline pink calcite, magnesite and dolomite, in units of (0.5 emu/cm^3).

TABLE VI-2

EXPERIMENTAL VALUES OF CURIE CONSTANTS & CONCENTRATION OF Mn^{2+} IN THE CARBONATES

Material	C (emu/cm^3)	Wt.% Concentration of Mn^{2+}
Pink Calcite	0.44×10^{-3}	0.43
Magnesite	0.27	0.24
Dolomite	0.05	0.04

However, according to these results, one could conclude that the pink calcite and the magnesite contain more than one type of paramagnetic ions which contributed to the paramagnetism. Since the results for Mn^{2+} in the pink calcite and in the magnesite were much larger than the values obtained from the spectrochemical analysis (see Appendix A), it is therefore assumed that Fe^{2+} is still paramagnetic in these samples at temperatures down to around $0.5^{\circ}K$. This interpretation has to be confirmed by performing a further study, such as ESR study at K-band or higher frequencies and at helium temperatures as suggested in Chapter IV.

CHAPTER VII

THERMAL CONDUCTIVITY

1. Introduction

Measurements were made on single crystals of iceland spar (transparent calcite) and white calcite, and polycrystalline pink calcite, magnesite and dolomite in a temperature range which varied with specimen but generally extended from 0.2 to 4°K. The specimens, all except iceland spar, were prepared from the same pieces of minerals which were used for magnetic entropy and susceptibility measurements. The thermal conductivities of iceland spar and white calcite were measured along their cleavage axes [100]. The investigation of iceland spar, with its lower concentration of impurities, was made for the purpose of comparison.

Since the purity of the specimens was poor, no attempt was made to find a suitable model for fitting the results. The thermal conductivities of these samples compare favorably with that of CrK alum and $FeNH_4$ alum which have been reported elsewhere.

In this experiment, a conventional heating method was used and the Ancsin-Lamarche He^4 double heat switch[51] cryostat was employed as a refrigerator. For this purpose, only one of the switches was used to cool the specimen down to helium temperatures. The reason for using heat switch instead of helium exchange gas is that helium gas is very difficult to evacuate completely in the helium temperature range and any helium residual gas would make the experimental results meaningless. In order to improve thermal contact between specimen and carbon thermometers, a new method of mounting samples was developed.

2. Theoretical Aspects

The most important mechanisms of heat transfer in solids are transfer by lattice waves and transfer by the conduction electrons. For non-metallic materials heat transfer is only by lattice waves. Debye[52] assumed that these waves must be anharmonic in spite of the conducting material being a good dielectric, since solids expand upon heating. For a given solid, the thermal resistance may be determined by the following factors:[52-55]

1) umklapp processes (in which the direction of flow of energy is changed after the collision of phonons),

2) scattering of waves by boundaries of solids,

3) scattering of waves by impurities and lattice

imperfections,

4) scattering of waves by amorphous structures, and

5) scattering of waves by isotope effects.

Debye[52] showed that thermal conductivity of an insulator can be represented by

$$K(T) = \frac{1}{3} C_\ell v \lambda \qquad \text{(VII-1)}$$

where $K(T)$ is the thermal conductivity of the solid at $T^{o}K$, C_ℓ the lattice specific heat of the substance per unit volume at constant volume, v the average phonon velocity in the material, and λ the phonon mean free path which is a measure of the distance of travel of a wave required to attenuate its intensity by a factor e. At low temperatures the umklapp process becomes ineffective in limiting the thermal conductivity, and the size effect becomes dominant. de Haas and Biermasz[55] discovered that the mean free path λ is limited by the width or diameter d of the specimen, when λ becomes comparable with d, at low temperatures. This effect was interpreted by Peierls and Casimir[54]. According to Casimir's calculation, $\lambda \approx 1.12d$ for the specimen with square cross section. At low temperatures C_ℓ and v are given with high accuracy by the Debye model of the lattice specific heat; i.e., $C_\ell = \gamma T^3$ where γ is a constant, and v is a constant also. Thus,

$$K(T) = \alpha T^3 \qquad \text{(VII-2)}$$

where $\alpha = 1.12 dv\gamma/3$. For amorphous and polycrystalline dielectric solids, the lattice specific heat might not be exactly proportional to the cube of the absolute temperature. Therefore Eq. (VII.2) can be approximately written in a general form:

$$K(T) = \alpha T^n \qquad \text{(VII-3)}$$

The thermal conductivity of a dielectric crystal has a maximum usually around 10 to 20°K in which the isotope effect becomes dominant[56] and the conductivity below that maximum is determined by crystal impurities and imperfections. At low temperatures the presence of impurities or lattice defects will increase the thermal resistance. The resistance due to impurities is proportional to the temperature and therefore dies away much more slowly than that due to umklapp process. It decreases exponentially with T in the low temperature region. Thus, boundary scattering alone is important only at very low temperatures.

In polycrystalline dielectric solids the phonon mean free path is limited by scattering at the crystalline boundaries at sufficiently low temperatures. Thus the mean free path in the polycrystalline material is of the order of the size of the crystallites[57-59]. In an amorphous solid, such as glasses, however, the mean free path is restricted by the disordered structure to a length of the order of the

interatomic distance and Debye assumed that it would be independent of temperature. Therefore in both polycrystalline and amorphous dielectric solids the thermal conductivity should be proportional to the lattice specific heat at very low temperatures.

The contribution of the spins in a paramagnetic salt to thermal conductivity was treated theoretically by Fröhlich and Heitler[60] and by Akhieser and Pomeranchuk[61]. They estimated that this contribution would be equal to the phonon conductivity, but no effect was found experimentally[62]. According to recent reports[63-66], the electron spins of paramagnetic ions are important when they are in a magnetic field.

3. Literature Survey

1) Thermal conductivity measurements were made by Kurti, Rollin and Simon (KRS)[67] on cylindrical samples, 7 mm in diameter, of $FeNH_4$ alum (23 mm long) and CrK alum (30 mm long). Both samples were cut from a single crystal. Few cracks in the samples were evident. The experimental method employed was to measure a mean conductivity by observing the rate of temperature equalization of the ends of samples demagnetized from inhomogeneous fields. An average magnetic susceptibility was measured for each end of the sample, from which an average T^* (magnetic temperature) was derived and hence an average T. The results for K

(in W cm^{-1} $^oK^{-1}$) were obtained as follows: for the $FeNH_4$ alum, K = 2.52×10^{-5} at T = 0.020°K and 7.56×10^{-5} at 0.055°K; for the CrK alum K = 9.66×10^{-5} at T = 0.165°K.

2) The thermal conductivity of CrK alum was also measured by Bijl[68] and by Garrett[62]. Bijl used a conventional heating method and determined the temperature gradient by the susceptibility method. The measurements were made between 1.4 and 3.9°K and in this region K was found to be proportional to a power of the absolute temperature of about 2.3. It was also found that the conductivity depended on the rate at which the sample was cooled below 70°K, an effect which has not yet been fully explained[69]. Garrett investigated the same salt between 0.16 and 0.29°K by a method similar to that of KRS[67], but a temperature gradient was produced in the crystal by magnetizing the sample non-uniformly after the adiabatic demagnetization. In this region K was found to be proportional to the cube of the temperature within the experimental accuracy and seemed to fit on to an extrapolation of the "slow cooling" curve of Bijl, as shown in Fig. VII-2.

3) Hudson[58] obtained some mean conductivity values between 0.1 and 0.22°K for a compressed powder of $FeNH_4$ alum of nearly single crystal density. The sample consisted of crystallites which were estimated to be between 10^{-3} and 10^{-2} cm in size. At 0.05°K the conductivity was about fifty

times less than the single crystal value of KRS[67]. In this case, the thermal conductivity could have been several times less which could be estimated according to those small size of crystallites, but the discrepancy was attributed to an increase of the phonon mean free path above the size of the crystallites because of a good thermal contact among the crystallites.

4) Measurement of the thermal conductivity at low temperatures is very sensitive to the crystal imperfections. The high values of thermal conductivity are always seriously reduced by anything which disturbs the lattice vibrations. Thus small amounts of chemical or structural disorder in the lattice will decrease the conductivity. Berman[70] has shown experimentally that the low temperature conductivity of quartz crystals can be greatly reduced by neutron irradiation. The thermal conductivity of potassuim chloride is also sensitive to small amounts of impurity. For example[71], a large pure crystal of KCl had a conductivity of about 250 w cm^{-1} $^{o}K^{-1}$ at 10^{o}K; it would take only 4 parts per million of calcium to reduce this conductivity by 10%. At 5^{o}K the sensitivity to impurities would still be higher. According to a recent investigation[72], in single crystals (KCl & KBr) containing lithium the thermal conductivity was greatly reduced.

4. Experimental

1) Experimental Arrangement

A cryostat with a "double mechanical heat switch" was employed for the thermal conductivity measurement. Since this cryostat has been described in detail before by Ancsin[10] and Ancsin and Lamarche[51], only the modification to the apparatus will be discussed here. For this purpose, only one of the switches, helium bath to salt heat switch (HS2), was used. The specimen holder and pull rod for the other switch (HS1) were removed and hence the end of the copper link from the pill to HS1 was available for the cold end of the heat sink. The samples were normally made about 8 cm long and 1 cm square and were mounted by clamping them tightly with the aid of four strips of coil foil to the end of the copper link with brass clamps. Apiezon N grease covered all the surfaces to improve thermal contact. The end of the copper link was U-shaped and allowed the specimen to be fitted in place. The other end of the sample was free; but the whole mounting was rigid.

Fig. VII-1 shows a sketch of the two Speer carbon thermometers (R_2 and R_3 in Chapter V), four coil foils and the heater mounting. To assure having a proper thermal contact between the specimen and the thermometers, two types of arrangement were made. The arrangement shown in Fig. VII-1(a) is for polycrystalline pink calcite,

4. Experimental

1) Experimental Arrangement

A cryostat with a "double mechanical heat switch" was employed for the thermal conductivity measurement. Since this cryostat has been described in detail before by Ancsin[10] and Ancsin and Lamarche[51], only the modification to the apparatus will be discussed here. For this purpose, only one of the switches, helium bath to salt heat switch (HS2), was used. The specimen holder and pull rod for the other switch (HS1) were removed and hence the end of the copper link from the pill to HS1 was available for the cold end of the heat sink. The samples were normally made about 8 cm long and 1 cm square and were mounted by clamping them tightly with the aid of four strips of coil foil to the end of the copper link with brass clamps. Apiezon N grease covered all the surfaces to improve thermal contact. The end of the copper link was U-shaped and allowed the specimen to be fitted in place. The other end of the sample was free; but the whole mounting was rigid.

Fig. VII-1 shows a sketch of the two Speer carbon thermometers (R_2 and R_3 in Chapter V), four coil foils and the heater mounting. To assure having a proper thermal contact between the specimen and the thermometers, two types of arrangement were made. The arrangement shown in Fig. VII-1(a) is for polycrystalline pink calcite,

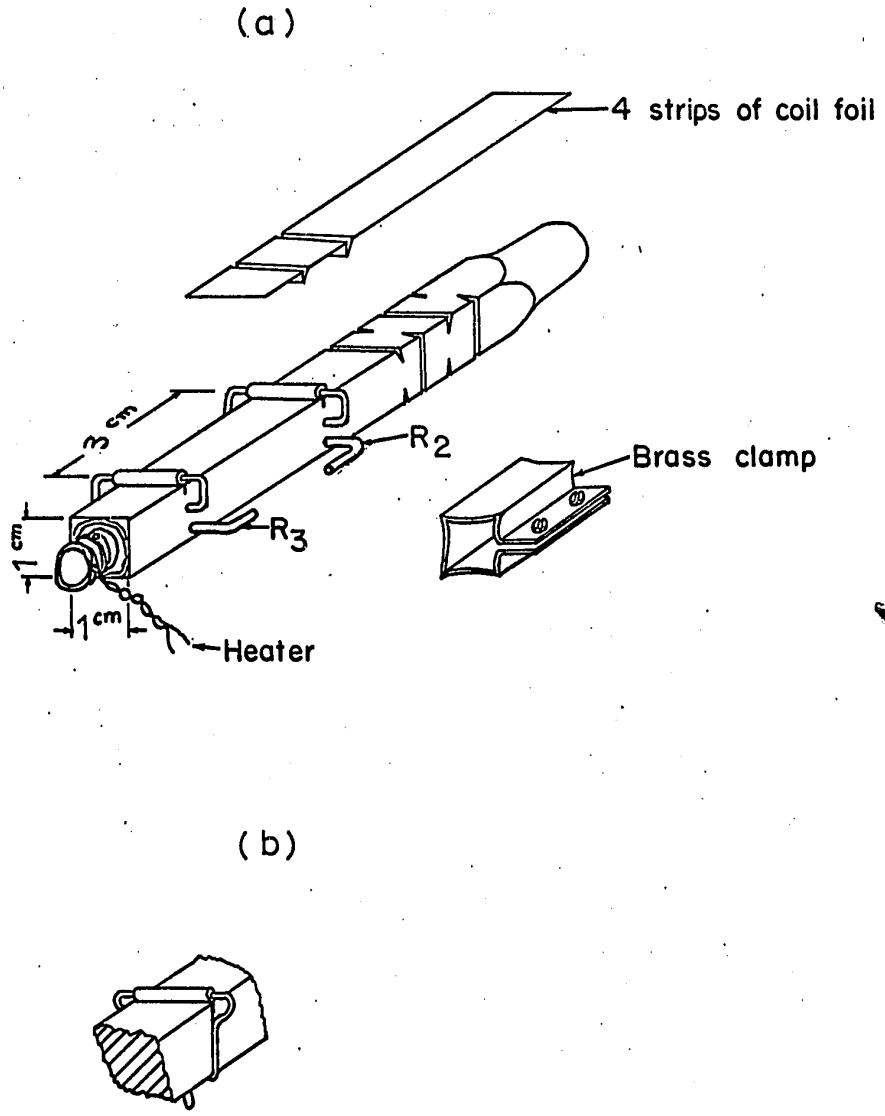

Fig. VII-1. Experimental arrangements for thermal conductivity measurement.

magnesite and dolomite. Holes could easily be drilled in these specimens. The other arrangement shown in Fig. VII-1-(b) is for the single crystals of white calcite and iceland spar. These on the other hand cracked readily when drilling was attempted. A $\frac{1}{32}$" solid carbide high helix straight shank drill #1757* was used to drill holes on polycrystalline specimens and the holes were reamed with a 0.035" ordinary drill in order to pass through the 0.033" resistor leads with ease. Apiezon N grease was applied on the contact areas before assembly. The heater was a 100 Ω No. 42 manganin enamelled wire (43 Ω/ft) wound bifilarly onto one end of the specimen. For polycrystalline specimen, this end of the specimen was shaped and two holes were drilled in such a way that the manganin wire was easily wound on and remained secured when pumping. For iceland spar and white calcite, polycrystalline ends were glued on their ends with Lepage's epoxy†, so that holes could be easily drilled also to secure the heater wire.

Lead coated and insulated No. 42 manganin wires were used as leads in the experimental chamber. They were attached with a piece of masking tape against the copper wall of the pill container before being brought out to a

---

*A product of the Cleveland Twist Drill Co., U. S. A.

†A product of Lepage's Ltd., Montreal, Canada. Size No. 350.

terminal block which was in thermal contact with liquid helium bath on the top of the chamber. At the terminal block, pairs of leads were shunted by 1,000 pF silver-mica capacitors to reduce stray rf energy.

The heater current was supplied from either a dry battery or a 2 volts storage battery and the power determined by measuring the potential across the heater and across a 100 Ω standard resistor (± 0.05%) with a portable potentiometer Type 3184D*. The resistances of carbon thermometers were measured with the same Wheatstone bridge and Philip recorder which were used for calibrating the thermometers. All the circuits were connected only when readings were being taken.

2) Experimental Procedure

a) Measurement Below 1°K

The runs were started by precooling to about liquid nitrogen temperature with 1 atm of nitrogen exchange gas in the vacuum chamber. When the sample attained thermal equilibrium, the exchange gas was evacuated for a period of about six hours in order to minimize residual gas. Then the heat switch was closed and liquid helium was transferred. Two or three helium transfers were required before the sample attained 4.2°K. As soon as the last transfer was

---

*A product of Tinsley Instruments, Smith Falls, Ontario, Canada.

completed, the pill was magnetized with a magnetic field of 18 kilo-gauss. Subsequent pumping reduced sample temperature to about 1.5°K, in a period of about 3 hours. The pill was demagnetized, immediately after the heat switch was opened. The demagnetization time was about 20 minutes. The lowest temperature achieved was about 0.06°K.

Within 50 minutes, the sample came to equilibrium with salt pill and then the heater was switched on. Due to the boundary resistance between sample and the pill, the entire sample warmed up slightly when a heater current was applied. Measurement was taken after thermal equilibrium was established. Then the heater was disconnected and sufficient time was allowed for removal of temperature gradient across sample. Subsequent to this the heater was switched on again, thermal equilibrium established and another measurement was made. Thus the entire temperature range was covered.

The performance of the double-heat switch cryostat was excellent.

b) Measurement at Helium-4 Temperatures

Upon finishing measurements below 1°K, the heat switch was closed and a thermal connection was established between helium bath and sample. As soon as the specimen came to equilibrium, measurements were made using the same technique as that for temperature below 1°K. For the white

calcite and the iceland spar, which have a higher thermal conductivity than the polycrystalline samples, a special arrangement was made to reduce boundary thermal resistances. These occured between the bath and the heat switch and also between the heat switch and the sample. In this arrangement, four pieces of coil foil were thermally connected to the top of the heat switch and the cold end of the sample. With this arrangement measurements were made possible up to $4^{\circ}K$.

On the following day after the specimen warmed up to room temperature, another run was started especially for the measurement between 1 and $4^{\circ}K$. The same procedure was adopted as that for measurement below $1^{\circ}K$.

5. Results and Discussion

The results of the measurements for the five materials are shown in Fig. VII-2. The thermal conductivity K(T) was calculated by means of the relation,

$$K(T) = \frac{\dot{Q}F}{\Delta T},$$

where $\dot{Q}$ is the heat power input to the specimen, ΔT the temperature difference it produced between the carbon thermometers, T is the arithmetic average of the temperatures of the carbon thermometers and F the form factor ℓ/A; ℓ is the distance between the thermometers and A the cross-sectional area of the specimen. The values of ΔT varied from 0.01 to $0.26^{\circ}K$, $\dot{Q}$ from 2×10^{-6} to 8×10^{-3} watt, whereas

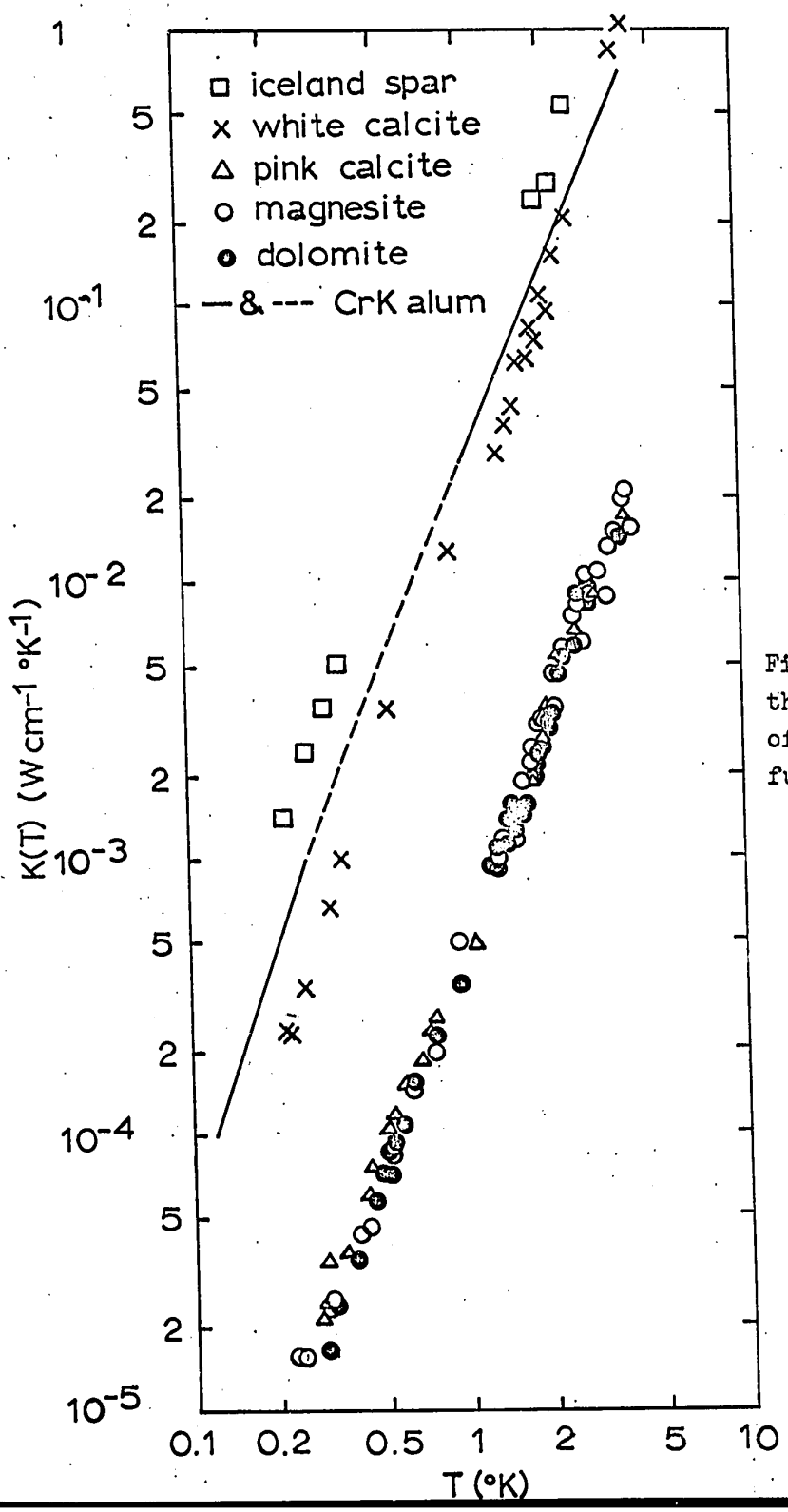

Fig. VII-2. The thermal conductivities of three carbonates as function of temperature.

the maximum heat generated in the carbon resistor was about 10^{-10} watt, a negligible quantity with respect to main heater power. Great care was taken to minimize heat leak losses. The leads attached to the sample were made of No. 42 lead coated manganin wires; each wire was about $7\frac{1}{2}$" long. They were attached to the wall of the salt pill. The pressure in the experimental chamber was less than 10^{-7} mm Hg and actually no helium exchange gas was used for the duration of experiment. The correction for the heat leak due to residual gas therefore was negligible. The heat leak due to radiation from the cryostat wall was less than 3×10^{-8} watt at $4^{\circ}K$ and less than 10^{-10} watt at $1^{\circ}K$. The heat leak due to vibration was also negligible, because a vibration-free-suspension system was used. The temperature could be determined with an accuracy of better than 2% with respect to the calibrated resistors. The values plotted in Fig. VII-2 are expected to be in error by $\sim$ 5% at helium temperatures, because the carbon thermometer is less sensitive in this range, and by $\sim$ 3% at temperatures below $1^{\circ}K$. Most of the error arose from a systematic deviation in temperature calibration.

With this apparatus, we could measure thermal conductivity down to about $0.2^{\circ}K$. Below $0.2^{\circ}K$, measurements were not reproducible. Although the lowest temperature achieved was around $0.06^{\circ}K$, the sample and the salt pill

warmed up immediately to about 0.1°K due to the large amount of metal present (copper container and brass clamp). At least two runs were performed on each sample.

Thermal conductivities of single crystals of ice-land spar and white calcite vary as T^3 at temperatures approximately below 1°K within the experimental error. They deviate from T^3 law above 1°K. This is probably mostly due to the high concentration of impurities and partly due to the crystal defects. The thermal conductivities of the three polycrystals are substantially lower and they vary as $\sim T^{2.6}$ which is similar to that of some amorphous dielectric solids measured by Anderson et al.[73] The values of α for all specimens were calculated and they are compared in Table VII-1 with those of a number of substances useful in cryogenic design.

For the purpose of comparison, the K(T)-T curve of CrK alum was transferred directly from Garrett's paper[62] to Fig. VII-2. This conductivity was measured on a sample having 6.5x1.5 cm^2 cross-section and $\alpha = 57.87 \times 10^{-3}$ watt $cm^{-1}\ {}^{o}K^{-4}$ was calculated from this graph. According to Casimir's theory with regard to size effect, the value of α would be reduced by factor of ~ 5 for the cross-section of 1x1 cm^2. If this value is compared with those of the ice-land spar and the white calcite, then the latter are respectively ~ 15 and ~ 2 times higher than that of the

TABLE VII-1

THE THERMAL CONDUCTIVITIES OF SOME CARBONATE MINERALS AND A NUMBER OF SUBSTANCES USEFUL IN CRYOGENIC DESIGN

Material	σ †	n	Temp. Range (^{o}K)	Ref.
Iceland Spar	166.18×10^{-3}	3	0.35-0.22	*
White Calcite	18.75	3	0.92-0.23	*
Pink Calcite	0.5	2.5	1.8 -0.28	*
Magnesite	0.5	2.6	4.0 -2.4	*
Dolomite	0.44	2.65	3.7 -0.3	*
CrK Alum	57.87	3	0.29-0.16	62
Teflon	0.038	2.4	0.7 -0.3	73
Epibond 104	0.1	2.6	0.75-0.2	73
Nylon	0.026	1.75	0.8 -0.2	73
Kel-F	0.066	2.0	0.8 -0.2	73
Epibond 100A	0.285	1.95	0.8 -0.1	73
Pyrex	0.153	1.75	0.8 -0.18	73
Hard Rubber	0.39	1.85	0.6 -0.14	73
70-30 Cupro-Nickel	0.93	1.23	4 -0.3	74
Superconducting Lead	4.5	3	0.75-0.23	75
Manganin	0.555	1	- - -	73

†In units of [watt cm^{-1} $^{o}K^{-(n+1)}$]; the thermal conductivity is presented in the form $K(T) = \sigma T^{n}$. All the samples except the last three were prepared with a cross-section of ~ 1x1 cm^2 but the CrK alum with 6.5x1.5 cm^2.

*The present work.

former.

According to the result for the thermal conductivity of ferric ammonium alum obtained by KRS[67], it is probably greater than that of the iceland spar.

CHAPTER VIII

DISCUSSION & CONCLUSIONS

The experiments were made primarily to secure information as to the suitability of the investigated materials as cooling agents for magnetic cooling below $1^{o}K$. From the results obtained a conclusion could be drawn that these substances containing diluted Mn^{2+} ions have the required properties for this purpose. Particularly, calcite and magnesite containing about 0.1% Mn^{2+} are suited for the cooling process in reaching a lowest temperature of below $0.06^{o}K$.

The information that was obtained from the susceptibility experiments on the magnetic structure of these materials is rather limited, since the measurements on polycrystalline materials are not so valuable in this respect and for the calcite single crystals available, the magnitude of the susceptibility is too small. Owing to the small susceptibility of calcite single crystals, it is not useful to make a measurement on this. On the other hand, since large single crystals of magnesite and dolomite are not

available, no attempt could be made. However, a few remarkable results from the susceptibility measurements were obtained. These are:

1) the values of Curie constant which can be used as a reference for evaluation of cooling power and the concentration of Mn^{2+} ions in these substances,

2) the magnesite follows Curie's law down to about $0.3^{\circ}K$,

3) the ordering temperature of each material is still much less than $0.06^{\circ}K$. This is advantageous if we compare it with the available manganous salts, manganous ammonium sulphate and manganese fluosilicate, which have high ordering temperatures (above $0.1^{\circ}K$, see Table VIII-1).

The measurements of magnetic entropy and ESR linewidth indicate that strong extra interactions exist in these substances due to magnetic ions. It is conclusive that clean samples would be desirable for further studies.

Not much detailed information is available with regard to the thermal conductivity of paramagnetic substances below $1^{\circ}K$. One exception is that of CrK alum. The present investigation has at least the advantage of putting us in a position to make some constructive suggestions as to the problem of securing a high thermal conductivity in these non-hydrated substances.

To summarize all the information on these carbonates

or minerals, we can say that they meet most of the requirements as a cooling agent. That is, they are physically and chemically stable; they are quite hard; they have a high magnetic entropy; they probably have a high Debye characteristic temperature; they have a relatively high heat capacity at very low temperatures; and they follow Curie's or the form of Curie-Weiss law down to the 10^{-2} ^{o}K range. Unfortunately, they have a quite low Curie constant.

It is obvious that a high value of the Curie constant is desirable for a coolant. With increasing value of the Curie constant, the demagnetization power will rise. Although a high value of Curie constant generally leads to high efficiencies in cooling, a high magnetic ordering temperature is allied. Suppose we recall all the results we obtained and informations on these carbonate minerals, we can make a favorable suggestion or conclusion. Accordingly, we can say that calcite and magnesite would be very good materials for cooling below $1^{o}K$ if they are synthetic single crystals doped with about 0.4% Mn^{2+} ions. With this concentration, they would have a large heat capacity and they still have about the same order of the value of thermal conductivity as that of the white calcite. Besides, their Curie constants would increase to the order of that of CrK alum.

The present results are summarized and compared in

Table VIII-1 with those of the hydrated salts commonly used in cryogenics and manganous salts.

Suggestion for Further Work

For further work we suggest that two materials, $MgO:Cr^{3+}$ and $ZnS:Mn^{2+}$, would probably be suitable as working substances for attaining temperatures below $0.04^{o}K$ using the initial condition of about 14 kilo-gauss/^{o}K. Since they have a cubic crystalline field symmetry, they may obey Curie's law below $0.1^{o}K$ and they may constitute a good magnetic thermometer. However, their thermal conductivities and other properties should be investigated further.

1) $MgO:Cr^{3+}$

A single crystal of MgO doped with about 0.3 wt. % or higher of Cr^{3+} would be considered favorable if the local symmetry at Cr^{3+} sites remains cubic.

It was reported[76] that Cr^{3+} in the high purity of MgO divalent lattice behaved as if it were surrounded by a cubic crystalline field to a very high approximation. The energy levels of this Cr^{3+} in MgO have been given by Low[76]. It is seen that only the lowest energy level with four-fold degeneracy would be populated at room temperature. An external or internal magnetic field caused by the nuclear magnetic moment can remove this degeneracy. At high magnetic fields the four energy levels diverge linearly. In this case, most of the magnetic entropy would be removed at

TABLE VIII-1

EXAMPLES FOR COMPARING TO THE PRESENT RESULTS

Substance	Density (gm/cm^3)	Ground State Paramagnetic ion	Curie Constant $\left[\frac{emu-{}^oK}{cm^3}\right]$	Ordering Temp. (^oK)	High Temp. Sp. Ht. Constant b_{expt} $(^oK)^2$	High Temp. Sp. Ht. Constant b_{ESR} $(^oK)^2$	Reference
White Calcite:0.06%Mn^{2+}	2.9	$^6S_{5/2}$ (Mn^{2+})			6×10^{-3}	4.8×10^{-3}	This Work
Pink Calcite:0.13%Mn^{2+}	3.0	$^6S_{5/2}$ (Mn^{2+})	0.44×10^{-3}	< 0.06	6	4.8	This Work
Magnesite:0.1%Mn^{2+}	3.1	$^6S_{5/2}$ (Mn^{2+})	0.27	< 0.06	6	4.7	This Work
Dolomite:0.04%Mn^{2+}	3.0	$^6S_{5/2}$ (Mn^{2+})	0.05	< 0.06	22	6.3	This Work
$Ce_2Mg_3(NO_3)_{12} \cdot 24H_2O$	2.07	$^2F_{5/2}$ (Ce^{3+})	0.83	< 0.002	0.00576		77
$FeNH_4(SO_4)_2 \cdot 12H_2O$	1.71	$^6S_{5/2}$ (Fe^{3+})	15.5	~ 0.04	12.3		78
$Cr^{3}(SO_4)_2 \cdot 12H_2O$	1.83	$^4F_{3/2}$ (Cr^{3+})	6.71	~ 0.01	16.0		79
$Mn(NH_4)_2(SO_4)_2 \cdot 6H_2O$	1.83	$^6S_{5/2}$ (Mn^{2+})	11.0	0.14	30.7	15.4	78,84
$MnSiF_6 \cdot 6H_2O$	1.90	$^6S_{5/2}$ (Mn^{2+})		0.1		6.6	80,84
MgO:0.183%Mn^{2+}	3.6	$^6S_{5/2}$ (Mn^{2+})			6	3.4	9,76,10

temperatures around 1°K. Therefore, a very low temperature could be obtained when demagnetizing adiabatically.

Actually, the energy levels are complicated by the fact that there is a stable isotope of about 9.5% abundance with nuclear spin of 3/2. This would result in an effect on the temperature attainable. However, this effect is very small, since the value of the hyperfine splitting constant is only 17.6 gauss[81] and hence the energy level splittings due to the hyperfine structures are small.

2) Cubic ZnS:Mn^{2+}

Mn^{2+} in cubic ZnS influenced by a crystalline electric field of cubic symmetry has been studied by Matarrese and Kikuchi[82]. Their published ESR parameters give: a = - 1.39 gauss, A = - 68.4 gauss and g = 2.0025. These values are compared to the values obtained from MgO:Mn^{2+} (a = + 19.96 gauss, A = - 86.8 gauss)[83], indicating that the former could attain lower temperature than the latter. In the former case, the value of cubic field splitting constant a is negative. This means the four-fold degenerate level lies lower than the two-fold degenerate one. Besides, its value of hyperfine constant A is appreciably smaller. All of these are advantageous in providing lower temperatures than would be attainable with MgO:Mn^{2+}.

The concentration of Mn^{2+} ions in cubic ZnS should be at least 0.3 wt. %. As long as the cubic crystalline

field symmetry is not distorted, a higher concentration of Mn^{2+} ions is desirable.

APPENDIX A

CHEMICAL ANALYSES & SOURCES OF SAMPLES

1. Sources of Samples

Iceland spar: Mexico clear; Filer's; Loma Linda, Calif., U.S.A.

White calcite: Orford Tp., Quebec, Canada

Pink calcite: Cantley, Quebec, Canada

Magnesite: Kilwar, Quebec, Canada

Dolomite: Portage du Fort, Quebec, Canada

Fluorite: Portage du Fort, Quebec, Canada

Apatite(brown): Huddersfield Tp., Quebec, Canada

Apatite(green & brown): Cantley, Quebec, Canada

Beryl: Lyndock Tp. Ontario, Canada

MgO(brown & yellow): Norton Co., Canada

2. Results of Spectrochemical Quantitative Analyses

Substance	Ca	Mg
Iceland Spar	40.8 wt.%	0.035 wt.%
White Calcite	39.4	0.08
Pink Calcite	38.0	1.02
Magnesite	3.14	26.2
Dolomite	21.1	12.9

50% is the maximum for each element.

3. Results of Spectrochemical Semi-Quantitative Analysis

Substance	Sample	Ca	Mg	Mn	Fe	Cu	Ni	Al	Pb	Si	Ti	Ag	Sr	Co	Be	Mo
Iceland Spar (Transparent Calcite)	1	PC	.04	.009	.03	.004		.04								
White Calcite	1	PC	.10	.06	.02	.03		.01		.01	.05					
	2	PC	.15	.12	.25	.04		.004								
Pink Calcite	1	PC	PC	.10	.47	.005	.009	.007				.002				
	2	PC	.60	.13	.50	.04		.006	.02				.84			
Magnesite	1	PC	PC	.10	.36	.001						.0004				
	2	1.06	PC	.04	.23											
Dolomite	1	PC	PC	.06	.14	.03				.12				.09		
	2	PC	PC	.04	.57	.04										
Fluorite	1	PC	.03	.05	.24									.09		
Apatite(brown)	1	PC	.45	.18	1.50	.17		.62		1.17			.40		.02(Zr)	
Apatite(green & brown)	1	PC	.52	.12	.84	.22		.65		1.59			.30			
Beryl	1	.23	1.49	.07	.99	.04	.007	PC		PC	.002		.72(Na)		PC	.13
MgO:0.183%Mn^{2+}(Brown)	1		PC	.10	.02			.02				.0007				
MgO:Mn^{2+}& Fe^{3+}(yellow)	1	.16	PC	.02	.12	.003	.009					.0008				

Remark: All the values are in wt. %. PC represents "principal constituent".
The accuracy of this analysis is about ±50%.

APPENDIX B

WORKING DRAWING OF GONIOMETER TYPE OF SAMPLE HOLDER FOR ESR X-BAND MICROWAVE CYLINDRICAL CAVITY

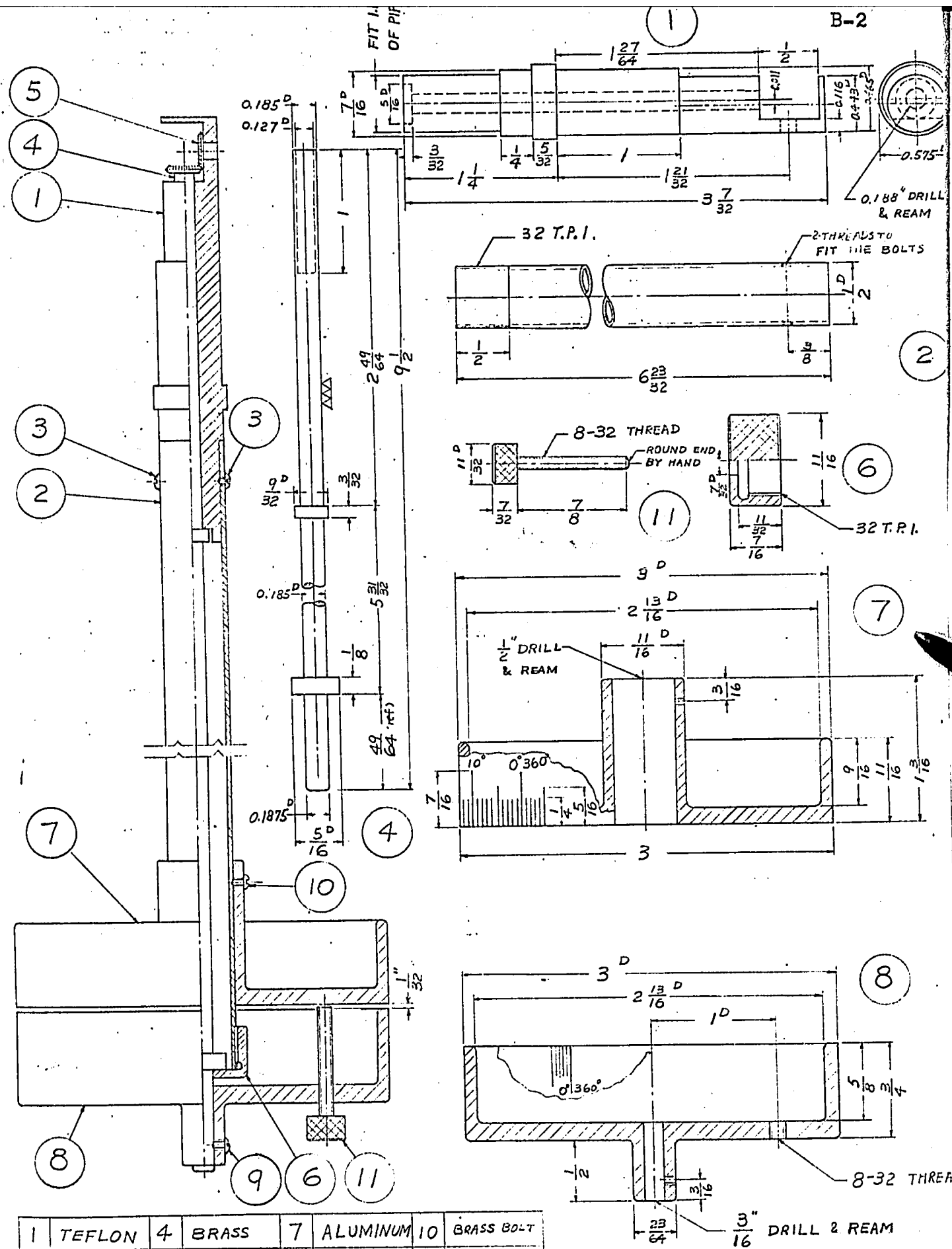

1	TEFLON	4	BRASS	7	ALUMINUM	10	BRASS BOLT
2	1/2" BRASS PIPE	5	TEFLON	8	ALUMINUM	11	BRASS
3	TWO BRASS BOLTS	6	BRASS	9	BRASS BOLT		

SCALE : 1 : 1

UNIT : INCH

APPENDIX C

A STUDY ON GALVANOMETER "DOUBLE-KICK"

A mutual inductor was constructed by winding both the primary and the secondary coils on a bakelite frame. A sketch of this inductor is shown in Fig. C-1. The whole assembly can be moved easily along the experimental chamber. The gap is about 0.0035" between the bakelite and the chamber. The susceptibility measurements were made with this inductor on a CMN sample (the same CMN sphere used in Chapter V) which was placed in various positions in the chamber. The results are given in Fig. C-2 where T is the temperature at which the CMN started to follow Curie's law. The shaded area is the "double-kick" region in which χ of the CMN did not vary as 1/T. When the CMN was at d = 129 cm, a copper disk (2.87 cm in diameter and 0.67 cm in height) was placed at the bottom of the stainless steel support (see Fig. V-1), then $T = T_1 = 2.42^{\circ}K$. With two and three identical disks, then $T_2 = 2.65^{\circ}K$ and $T_3 = 3.0^{\circ}K$ respectively.

From these results, we can conclude that T depends on the position where a paramagnetic sample is placed in

a metallic chamber. If the amount of metal is distributed approximately equally on both sides of the sample, then no galvanometer "double-kick" would be experienced.

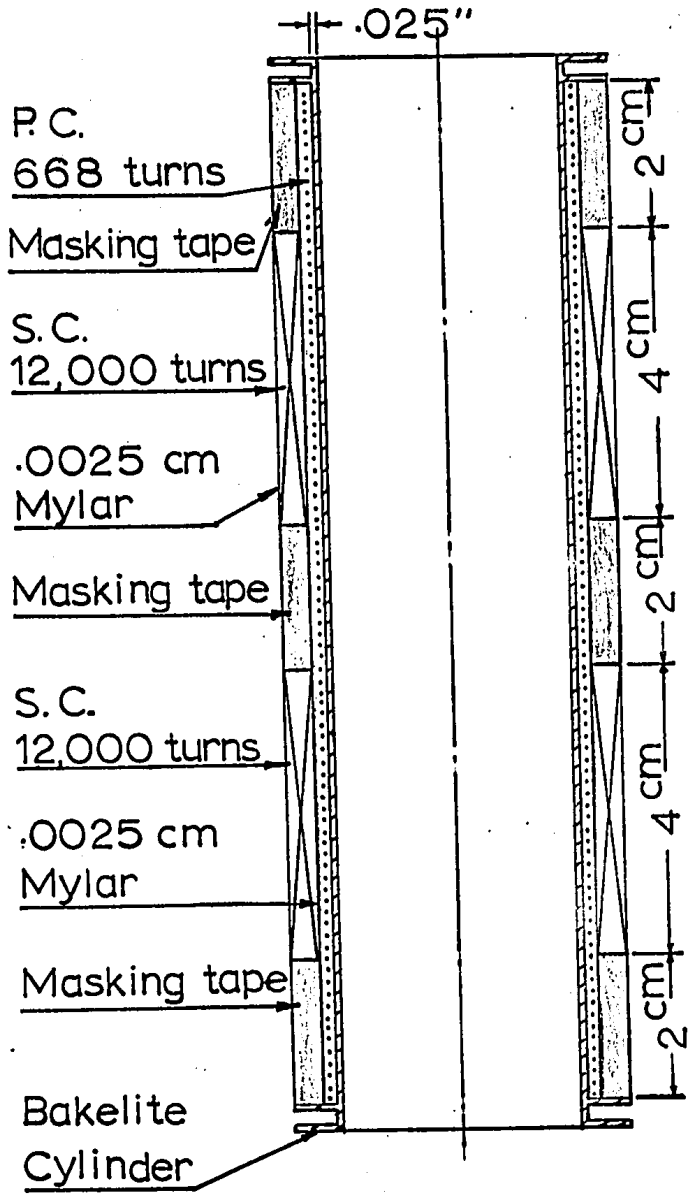

Fig. C-1. The sliding mutual inductor for magnetic susceptibility measurement.

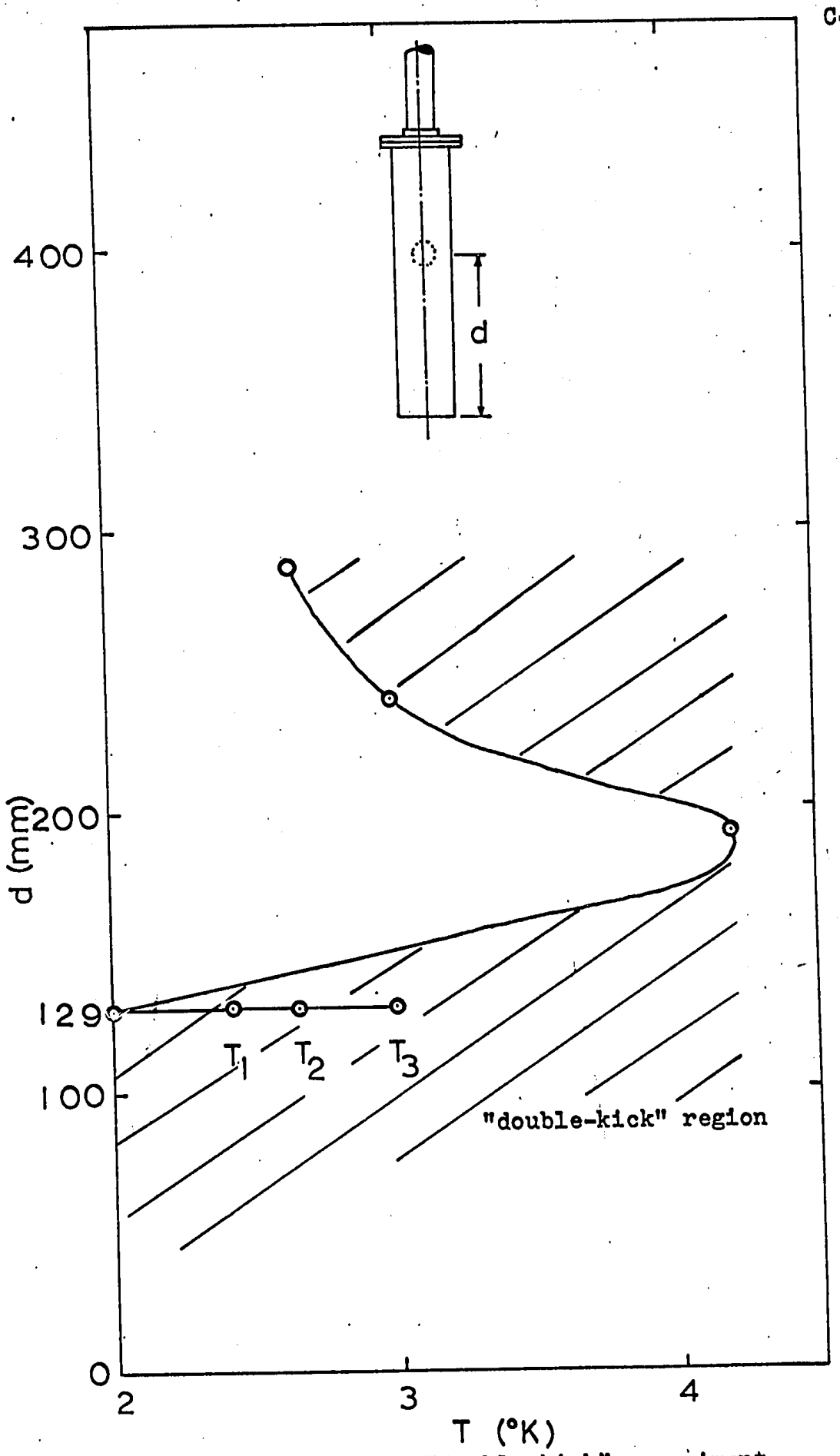

Fig. C-2. Results of "double-kick" experiment.

REFERENCES

1. P. Debye, Ann. Phys., Lpz., 81, 1154 (1926).
2. W. F. Giauque, J. Am. Chem. Soc. 49, 1864 (1927).
3. W. F. Giauque & D. P. McDougall, Phys. Rev. 43, 768 (1933).
4. J. G. Daunt & W. L. Pillinger, Supp. Bull. Int. Inst. Refrig., Annexe 3, 158 (1955).
5. E. Ambler & R. P. Hudson, Phys. Rev. 102, 916 (1956).
6. J. G. Daunt & K. Brugger, Z. Phys. Chem. 16, 203 (1958); J. G. Daunt, D. O. Edwards, M. Kreitman, R. C. Pandore & J. W. Snider, Proc. 7th Interna. Low Temp. Conf., Toronto, Paper 5-3.
7. R. D. Parks & W. A. Little, Phys. Lett. 6, 539 (1961).
8. R. Yee, G. O. Zimmerman, L. Meyers, R. P. Guertin & R. D. Parks, Bull. Am. Phys. Soc. 12, 135 (1967).
9. D. Walsh, M.Sc. Thesis, Dept. of Phys., Univ. of Ottawa (1964).
10. J. Ancsin, Ph.D. Thesis, Dept. of Phys., Univ. of Ottawa (1965).
11. J. G. Daunt & D. O. Edwards, Temp. Its Measurements & Control 3, 133 (1962).

12. W. H. Dennen, Principles of Mineralogy, (The Ronald Press Co., New York, 1959).

13. L. G. Berry & Brian Mason, Mineralogy, (W. H. Freeman & Co., San Francisco, 1959).

14. C. Palache, H. Berman & Clifford, Dana's System of Mineralogy, (John Wiley & Sons, Inc., New York, 1951).

15. W. A. Deer, R. A. Howi & J. Zussman, Rock-Forming Minerals, (Longmans, London, 1962), Vol. 5.

16. R. W. G. Wykoff, Crystal Structures, (Interscience Publishers, Inc., New York, 1960), Vol. III.

17. C. Palache, H. Berman & C. Frondel, The System of Mineralogy of J. D. Dana & E. S. Dana, (John Wiley & Sons, Inc., New York, 1953), 7th Ed.

18. S. St. J. Warne, J. Sed. Pet. 32, 29 (1962).

19. F. K. Hurd, M. Sachs & W. D. Hershberger, Phys. Rev. 93, 373 (1954).

20. M. M. Zaripov, Sh. F. Murtazin & V. G. Stepanov, Optics & Spectroscopy (U.S.A.) 14, 224 (1963) also Optik i Spektrosk. (USSR) 14, 421 (1963).

21. C. Kikuchi, Phys. Rev. 100, 1243 (1955).

22. H. M. McConnell, J. Chem. Phys. 24, 904 (1956).

23. See Fig. III-1.

24. C. Kikuchi, R. Ager & L. M. Matarrese, Bull. Am. Phys. Soc. 3, 135 (1958).

25. C. Kikuchi & L. M. Matarrese, J. Chem. Phys. 33, 601

(1960).

26. L. M. Matarrese, J. Chem. Phs. 34, 336 (1961).

27. I. Ursu, V. Lupei & A. Lupei, Rev. Roum. Phys. 11, 875 (1966).

28. V. M. Vinokurov, M. M. Zaripov & V. G. Stepanov, Soviet Phys. - Crystallography 6, 83 (1961), see also Soviet Phys. - JETP 12, 1081 (1961).

29. B. Bleaney & D. J. E. Ingram, Proc. Roy. Soc. (London) A205, 336 (1951).

30. B. Bleaney & R. S. Trenan, Proc. Roy. Soc. (London), A223, (1954).

31. S. A. Marshall & A. R. Reinberg, Phys. Rev. 132, 134 (1963).

32. J. E. Wertz, P. Auzins, J. H. E. Griffiths & J. W. Orton, Disc. Faraday Soc. 26, 66 (1958).

33. D. M. S. Baguley, B. Bleaney, J. H. E. Griffths, R. P. Penrose & B. I. Plumpton, Proc. Phys. Soc. 61, 551 (1948).

34. H. Kumagai, K. Ōno & I. Hayashi, Phys. Rev. 87, 374 (1952).

35. I. Hayashi & K. Ōno, J. Phys. Soc. Japan 8, 270 (1953).

36. B. Bleaney, Phys. Rev. 78, 214 (1950).

37. I. Kimura & N. Uryû, J. Phys. Soc. Japan 23, 1204 (1967).

38. R. P. Hudson & R. S. Kaeser, Physics 3, 95 (1967).

39. H. van Dijk, M. Durieux, J. R. Clement & J. K. Logan, The "1958 He^4 Scale of Temperatures", (U. S. Department of Commerce, National Bureau of Standards, Washington, D. C.), NBS Monograph 10.

40. W. R. Abel, A. C. Anderson & J. C. Wheatley, Rev. Sci. Instr. 35, 444 (1967).

41. A. C. Anderson, G. L. Sallinger & J. C. Wheatley, Rev. Sci. Instr. 32, 1110 (1961).

42. J. C. Wheatley, D. F. Griffing & T. L. Estle, Rev. Sci. Instr. 27, 1070 (1956).

43. J. P. Harrison, Rev. Sci. Instr. 39, 145 (1968).

44. J. H. Van Vleck, J. Chem. Phys. 5, 320 (1937).

45. J. M. Daniels, Proc. Phys. Soc. A66, 673 (1953).

46. D. de Klerk, Encyclopedia of Physics XV, 38 (1956).

47. M. H. Hebb & E. M. Purcell, J. Chem. Phys. 5, 338 (1937).

48. J. H. Van Vleck & W. G. Penney, Phil. Mag. 17, 961 (1934).

49. B. Bleaney, Phys. Rev. 78, 214 (1950).

50. J. R. & R. A. Hull, J. Chem. Phys. 9, 465 (1941).

51. J. Ancsin & J. L. G. Lamarche, Rev. Sci. Instr. 38, 368 (1967).

52. P. Debye, Vorträge über die Kinetische Theorie der Materie und der Elektrizität, (Teubner, Berlin, 1914).

53. R. Peierls, Ann. Physik 3, 1055 (1929).

54. H. B. G. Casimir, Physica 5, 495 (1938).

55. W. J. de Haas & T. Biermasz, Physica 2, 673 (1935); ibid. 4, 752 (1937); ibid. 5, 47, 320, 619 (1938).

56. R. Berman, Cryogenics 5, 297 (1965).

57. H. van Dijk & W. H. Keeson, Physica 7, 970 (1940).

58. R. P. Hudson, Thesis, University of Oxford (1949).

59. R. Berman, Proc. Phys. Soc. (London) A65, 1029 (1952).

60. H. Fröhlich & W. Heitler, Proc. Roy. Soc. (Lodon) A155, 640 (1936).

61. A. Akhieser & I. Pomeranchuk, J. Phys. (USSR) 8, 216 (1944).

62. C. G. B. Garrett, Phil. Mag. 41, 621 (1950).

63. E. D. Tucker, Phys. Rev. Lett. 6, 183 (1961).

64. D. I. Bolef & R. B. Gosser, Proc. Phys. Soc. (London) 79, 442 (1962).

65. I. P. Morton & H. M. Rosenber, Phys. Rev. Lett. 8, 200 (1962).

66. R. Orbach, Proc. Roy. Soc. (London) A264, 458 (1961).

67. N. Kürti, B. V. Rollin & F. Simon, Physica 3, 266 (1936).

68. D. Bijl, Physica 14, 684 (1949).

69. J. Eisenstein, Rev. Mod. Phys. 24, 74 (1952).

70. R. Berman, Proc. Roy. Phys. Soc. (London) A208, 90 (1951).

71. G. A. Slack, Phys. Rev. 105, 832 (1957).

72. F. C. Bauman, J. P. Harrison, R. O. Pohl & W. D. Seward, Phys. Rev. 159, 691 (1967).

73. A. C. Anderson, W. Reese & J. C. Wheatley, Rev. Sci. Instr. 34, 1386 (1963).

74. H. A. Fairbank & D. M. Lee, Rev. Sci. Instr. 31, 660 (1960).

75. W. Reese & W. A. Steyert, Rev.Sci. Instr. 33, 43 (1962).

76. W. Low, Phys. Rev. 105, 801 (1957).

77. R. P. Hudson & R. S. Kaeser, Physics 3, 95 (1967).

78. A. H. Cooke, H. Meyer & W. P. Wolf, Proc. Roy. Soc. (London) 237, 395 (1956).

79. B. Bleaney, Proc. Roy. Soc. (London) A204, 216 (1951).

80. A. Ohtsubo, T. Haseda & E. Kanda, Physica 24, S161 (1958).

81. A. Manoogian & D. J. I. Fry, Colloque Ampère XIV, (North-Holland Publ. Co., Amsterdam, 1967), P. 156.

82. L. M. Matarrese & C. Kikuchi, J. Phys. Chem. Solids, 1, 117 (1956).

83. W. Low, Phys. Rev. 105, 793 (1957).

84. B. Bleaney & D. J. E. Ingram, Proc. Roy. Soc. (London) A205, 336 (1950).

85. J. G. Daunt, Proc. Phys. Soc. (London) B70, 641 (1957).